

Order and Transport in Disordered Type-II Superconductors

Inaugural-Dissertation
zur
Erlangung des Doktorgrades
der Mathematisch-Naturwissenschaftlichen Fakultät
der Universität zu Köln

vorgelegt von
Aleksandra Petković
aus Kragujevac, Serbien

Köln 2009

Berichterstatter: Prof. Dr. Thomas Nattermann
Prof. Dr. Joachim Krug

Tag der mündlichen Prüfung: 26.06.2009

Contents

Contents	iii
1 Introduction	1
1.1 Flux lines in type-II superconductors	1
1.2 Luttinger liquids	4
2 Order and creep in flux lattices pinned by planar defects	9
2.1 Introduction	9
2.2 Bragg glass phase	11
2.3 Single defect	16
2.3.1 Model	16
2.3.2 Renormalization group analysis	18
2.3.3 Effective Hamiltonian	20
2.3.4 Density oscillations	22
2.4 Finite density of weak defects	24
2.4.1 Model	24
2.4.2 Functional renormalization group approach	27
2.4.3 Properties of the planar glass	30
2.4.4 Stability of the Bragg glass and the weakly pinned Bose glass	32
2.5 Finite density of strong defects	34
2.6 Flux line creep	37
2.6.1 Single defect	38
2.6.2 Finite density of weak defects	42
2.6.3 Finite density of strong defects	44
2.7 Dislocations	47
2.8 Conclusions	49
2.A Replica Hamiltonian for the defect free system	51
2.B Effective Hamiltonian on the defect plane	52
2.C Density oscillations for an irrelevant defect plane	54
2.D Density oscillations for a relevant defect plane	55
2.E Sample-to-sample fluctuations of the magnetic susceptibility	57
2.F Positional correlation function	59

2.G	List of recurrent symbols	61
3	Voltage-current characteristics in thin superconducting films	65
3.1	Introduction	65
3.2	Model	66
3.3	BKT transition	68
3.4	Transport	69
3.5	Discussions and conclusions	75
4	The effect of randomness on the Mott state	77
4.1	Introduction	77
4.2	Model	79
4.3	Rigidities and ac conductivity	81
4.3.1	Generalized rigidities	81
4.3.2	Ac conductivity	83
4.4	Phase diagram	84
4.5	Discussions and conclusions	88
	Bibliography	91
	Acknowledgements	99
	Abstract	101
	Zusammenfassung	103
	Erklärung	105
	Curriculum vitae	107

Introduction

Understanding the role of disorder, such as impurities or other structural inhomogeneities, is of fundamental interest in condensed matter physics, since disorder is unavoidable in real materials and in experimental samples. Even weak quenched impurities can drastically affect the properties of a system. For example, they give rise to very strong effects in one and two space dimensions, such as the Anderson localization of noninteracting free electrons. Then, instead of a metallic state an insulating state appears. Inhomogeneities are also intimately involved in many other spectacular effects as the integer quantum Hall effect and pinning of flux lines in type-II superconductors.

1.1 Flux lines in type-II superconductors

The Bronze Age began when metallurgist realized that by adding a small concentration of tin to copper some stronger material is produced. In a pure soft metal, dislocation lines move under an applied stress deforming the material. Differently, in a doped metal the motion of dislocations and plastic deformations are precluded by the impurities that pin dislocations in place. Today, similar problems arise in type-II superconductors exposed to an external magnetic field, as will be explained below. In order to set the stage for an analysis conveyed in the main part of this thesis, we briefly summarize some important properties of type-II superconductors. For more detailed explanations see the book of Tinkham [1] and for an extensive summary of results see the reviews by Blatter et al. [2] and by Nattermann and Scheidl [3].

Opposite to type-I superconductors, where from the superconducting Meissner phase there is a direct first order phase transition to the normal phase, type-II superconductors exhibit so-called mixed phase or Schubnikov phase. Above the lower critical field H_{c1} an external magnetic field penetrates the sample in the form of flux (vortex) lines. They are made of a normal core filament of radius roughly given by the superconductor coherence length ξ and surrounded by supercurrent that screens the external magnetic field over a radius determined by the penetration depth λ . Each flux line carries

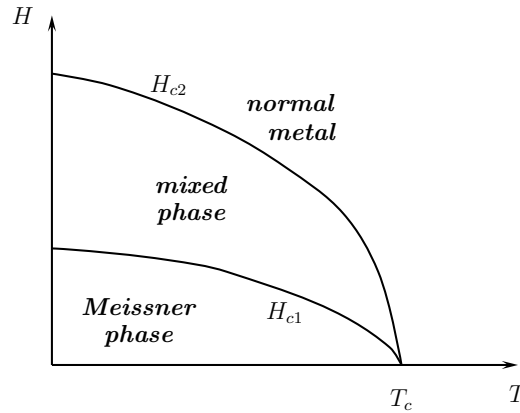


Figure 1.1: The naive phase diagram of a type-II superconductor in the mean field approach of the Ginzburg-Landau theory. A normal metallic phase is separated by the upper critical line $H_{c2}(T)$ from the mixed or Schubnikov phase. Below the lower critical field $H_{c1}(T)$ the Meissner phase exists.

a magnetic flux quantum $\phi_0 = hc/(2e)$. The flux lines repel each other due to the supercurrents, making a regular triangular Abrikosov lattice of lines aligned with the external magnetic field. Increasing the field, the flux lines density is increased, and at the upper critical field H_{c2} the flux lines start to overlap. Beyond H_{c2} the normal metallic state occurs, see Fig. 1.1.

The phase diagram shown in Fig. 1.1 was accepted for more than three decades. In 1986, the discovery of high-temperature superconductors by Bednorz and Müller initiated a burst of investigations and reexaminations of existing theories. Soon it was realized that thermal fluctuations melt the Abrikosov lattice into a flux liquid around the lower and the upper critical field as shown in Fig. 1.2. Near H_{c2} thermally induced fluctuations of flux lines positions are large enough to melt the Abrikosov lattice, while near H_{c1} the flux lines are dilute, with the spacing greater than the penetration depth λ , and the interaction between them is small. As a consequence, the lattice becomes "soft", characterized by a very small shear modulus, and the melting line develops a reentrant behavior.

Next, we briefly discuss the transport properties of type-II superconductors. A transport current originates a Lorentz force and the flux lines in a pure superconductor start to move as dislocations move in a pure soft metal under an applied stress. The flux line motion generates an electric field in the direction of the current and, as a result, the system dissipates energy. The material becomes non-superconducting, having a linear resistivity $\rho = \rho_n B/H_{c2}$, where ρ_n is the resistivity of the normal state and B denotes the magnetic induction [4]. Therefore, in a pure superconductor only the Meissner phase is superconducting. Since superconducting wires are ex-

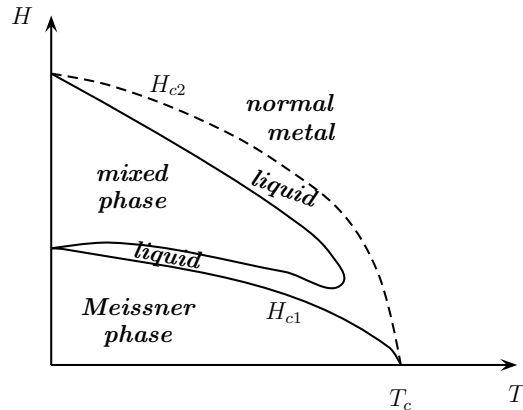


Figure 1.2: Schematic phase diagram of a pure type-II superconductor. Thermal fluctuations melt the Abrikosov lattice into a flux liquid over the indicated part of the phase diagram.

posed to high magnetic fields in many applications, as in high-field magnets in magnetic resonance imagers or in superconducting motors, it is of great technological interest to prevent the flux line motion and to sustain superconductivity. Like the motion of dislocations in a soft metal is prevented by impurities, a similar mechanism takes place in superconductors. There are many different pinning sources for flux lines. One example are point impurities, such as vacancies and interstitials. Another example are columnar defects artificially produced by a heavy ion radiation, as well as planar defects in the form of twin boundaries. The competition between a pinning force and the Lorentz force determines the critical current density J_c . For current densities $J > J_c$ the Lorentz force wins, the flux lines are deppined and the system dissipates energy. Even for $J < J_c$, a finite resistivity appears at finite temperatures. This happens due to hopping of thermally activated flux lines over the pinning barriers. Such motion is called flux line creep [5, 6]. However, the effect of disorder on the mixed phase and on the flux liquid differs drastically. Quenched pinning sites drive the Abrikosov lattice into a glassy phase with diverging pinning barriers for asymptotically small currents. Then, the system regains superconductivity in the sense that the linear resistivity vanishes. On the other hand, even in the presence of disorder the flux liquid state remains characterized by a finite linear resistivity.

In high- T_c materials point impurities are almost always present due to a non-stoichiometric composition of most materials. The generic phase diagram of type-II superconductors in the presence of point impurities is shown in Fig. 1.3. Generally, above H_{c1} two different glassy phases appear: the

high-field amorphous glass and the low field Bragg glass phase. The order of the flux line lattice was a puzzle for a long time. In 1970 Larkin concluded that randomly distributed point impurities destroy the long-range order of the Abrikosov lattice [7]. In 1990's, it was realized that the effect of impurities is weaker, resulting in a power law decay of the translational order of the flux lines in the Bragg glass phase [8, 9, 10, 11, 12, 13]. By increasing the disorder strength dislocations appear and the Bragg glass phase "melts" into the amorphous glass [14, 15]. An increase of the magnetic field effectively increases the disorder strength, as shown in Fig. 1.3. Some peculiarities regarding the phase diagram for specific materials are discussed, e.g., in Refs. [16, 17].

We summarize the characteristics of the Bragg glass phase in more detail in Chapter 2 of this thesis, where we study the influence of planar defects on the stability of the Bragg glass phase. Chapter 2 focuses mainly on static and dynamic properties of flux line lattices in the presence of planar defects. We use an elastic description of the flux lines, ignoring microscopic details of the superconducting state, but capturing the most important physics for a macroscopic characterization of the flux lattice lines, i.e., for transport and order. A flux line is treated as an elastic object having a displacement vector that is measured with respect to its equilibrium position in the Abrikosov lattice. The repulsive flux line interaction mimics the elastic forces that tend to prevent distortions induced by disorder and by thermal fluctuations. Therefore, some of the results of Chapter 2 also apply to a wide class of other systems that can be described in this way, including a stack of membranes under tension, charge density waves [18] and domain walls in magnets and in incommensurate systems [19].

Note that the above review of results applies to three-dimensional superconductors, while the physics of superconducting films is different, as will be discussed in Chapter 3. In two-dimensional systems the effects of thermal fluctuations are more pronounced than in analogous systems in three dimensions. Moreover, the interaction between vortices is changed. Thus the resulting phase diagrams are different than those discussed above. In Chapter 3 we summarize some known results in equilibrium and study the transport properties of thin superconducting films in the absence of an external magnetic field.

1.2 Luttinger liquids

In Chapter 4, we deal with a one-dimensional interacting electron system. The low energy physics of that system is described by the Luttinger liquid

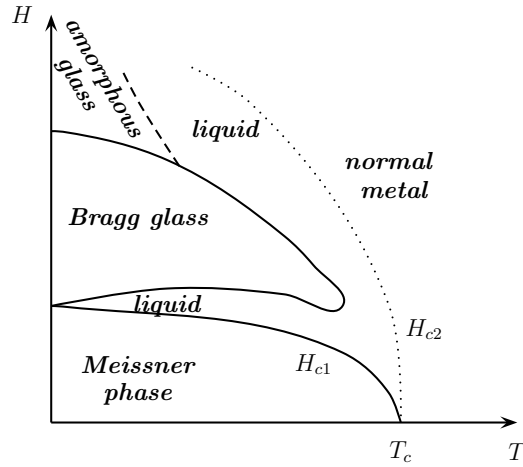


Figure 1.3: Schematic phase diagram of a type-II superconductor in the presence of point impurities. The Bragg glass melts due to thermal fluctuations into a flux liquid and due to disorder induced fluctuations into the amorphous glass.

theory [20, 21]. This theory is usually formulated using the bosonization technique [20, 21]. Loosely speaking, the bosonization translates interacting one-dimensional fermions into free bosons by representing fermion operators in terms of boson operators. In the following, we consider spinless electrons with a short-range interaction. Within the classical physics, electrons at zero temperature would form an ideal lattice due to repulsive interactions. However, their quantum-mechanical nature prohibits that. The electrons are described by the Euclidean quadratic action which depends on the two-dimensional electron displacement field $\varphi(x, \tau)$, measured with respect to the classical positions. Here the (imaginary) time-dependence τ accounts for the effects of quantum fluctuations.

Although, at first glance, classical flux line lattices and quantum Luttinger liquids are very different, many similarities arise on the theoretical level. Using the bosonized description, a Luttinger liquid can be mapped onto flux lines confined in a plane, where the time direction stands for the direction of the magnetic field and electron space-time displacement field can be viewed as the displacement field of flux lines. The role of thermal fluctuations in flux line lattices is played by quantum fluctuations in Luttinger liquids. Moreover, the influence of disorder on a Luttinger liquid can be treated in a similar manner as in flux line lattices. The problem of quenched point impurities in a Luttinger liquid can be mapped onto in-plane flux lines with quenched columnar defects. However, an important difference is that in the latter case disorder acts constructively, sustaining superconductivity, while in the former case it has a destructive role and diminishes conductivity.

It is worthwhile to point out some other similarities between flux lattices and Luttinger liquids arising from completely different reasons than the above mentioned mapping. Both, the three-dimensional Bragg glass phase and the Luttinger liquid are at their critical dimensions, and therefore characterized by a power law decay of the translational order parameter. In the former, translational long-range order is partially destroyed by point impurities, while in the latter by quantum fluctuations. As a result, striking similarities appear between the Bragg glass phase with a single planar defect and a Luttinger liquid with a single frozen impurity, as will be shown in Chapter 2.

Next, we briefly recall the main characteristics of Luttinger liquids. For more details see the book of Giamarchi [21]. Two- and three-dimensional interacting fermionic system are nicely explained by Landau's Fermi liquid theory [22]. The impressive result of this theory is that an interacting system can be described in terms of nearly free quasiparticles. In one-dimensional electron systems, the Fermi liquid theory breaks down and the low energy physics is described by the Luttinger liquid theory. A fundamental difference between one- and higher-dimensional fermionic interacting systems is that an individual electron has to push other electrons in order to move in one dimension. Examples of one-dimensional systems are carbon nanotubes [23, 24], polydiacetylen [25], quantum Hall edge states [26], semiconductor cleaved edge quantum wires [27] and ultracold gases [28].

A Luttinger liquid is characterized by non-universal power law decay of the translational order with an interaction-dependent exponent, the Luttinger liquid parameter K . For the noninteracting electrons $K = 1$, while $K < 1$ ($K > 1$) corresponds to repulsive (attractive) interaction. Effectively, by changing the interaction, one changes the amount of quantum fluctuations. By decreasing K the influence of quantum fluctuations decreases and $K = 0$ denotes the purely classical case. Apart from K , the Luttinger liquid theory depends on one more parameter, on the velocity of excitations v .

An ideal Luttinger liquid state has the electric conductance $G = e^2/h$ and an infinite dc conductivity. However, this is not the realistic result since the effects of point impurities, that almost always present, are very pronounced. Even a single weak quenched impurity strongly suppresses conductivity at low temperatures and makes the system insulating at zero temperature in the case of repulsive interactions [29, 30, 31]. For sufficiently weak and dense impurities, such that the effect of a single impurity is negligible, the physics is dominated by collective pinning. Then, the system is always turned into an insulator at zero temperature, the Anderson insulator, except for sufficiently attractive interactions, $K > 3/2$ [32]. Another type of insulating state that will be studied in this thesis, arises from completely different reasons and in a completely different way, namely, due to interactions. In the

continuum, electron-electron interactions conserve momentum, while in the presence of an underlying crystal lattice only the momentum modulo a vector of the reciprocal lattice has to be conserved. These processes that do not conserve the momentum are called umklapp processes and they can lead to an insulating state. As a consequence of the Fermi surface reduction in one-dimension, umklapp processes can affect the low energy behavior of a Luttinger liquid only if a certain commensurate electron filling is realized in the system. Otherwise, they are irrelevant. At zero temperature, for sufficiently small quantum fluctuations $K < K_c$, where K_c depends on the order of the commensurability, the strength of an umklapp process flows to strong coupling, leading to the appearance of the Mott insulating state [33]. The properties of the Anderson and Mott insulating states are discussed in Chapter 4, where we study the simultaneous effect of randomly distributed point impurities and umklapp scattering processes in the Luttinger liquid.

Order and creep in flux lattices pinned by planar defects

2.1 Introduction

The technologically most interesting property of type-II superconductors is their ability to carry a transport current with as little dissipation as possible. The transport current leads to a motion of the flux lines (FLs) in disorder-free samples and hence gives rise to dissipation [1]. In order to recover the desired property of a dissipation-free current flow in type-II superconductors, FLs have to be pinned. Point defects are one type of pinning source that leads to a zero linear resistivity [2]. However, thermal fluctuations allow for FL creep, resulting in a nonzero nonlinear resistivity of the form $\rho(J) \sim \exp[-(J_P/J)^\mu]$ for $J \ll J_P$, where the creep exponent is $\mu = 1/2$ for point impurities [8]. J denotes the current density. The parameter J_P depends on the magnetic induction B , the temperature T , and the concentration and strength of the pinning centers. Moreover, it depends on properties of the material through the superconductor coherence length ξ and the penetration depth λ . This response of the system to an external current is closely related to a power law decay of translational order of the flux line lattice (FLL) in the Bragg glass phase [8, 9, 10, 11, 12, 13].

More effective pinning sources can further suppress the nonlinear resistivity. One example are columnar defects that have been considered by Nelson and Vinokur [34, 35]. These authors mapped the physics of FLs onto the problem of the localization of bosons in two dimensions where world lines of the bosons play the role of FLs. A similar approach was proposed also by Lyuksyutov [36]. At low temperatures they found strongly localized FLs at the columnar defects, forming a "Bose glass" phase [34, 35]. Thermally activated hopping of noninteracting FLs in the limit $J \rightarrow 0$ leads to the creep exponent $\mu = 1/3$, while FL interactions yield the increased creep exponent $\mu = 1$ [2]. The transport in this regime closely resembles the variable range hopping of electrons in two-dimensional disordered semiconductors. This picture is expected to be valid for weak enough applied magnetic fields,

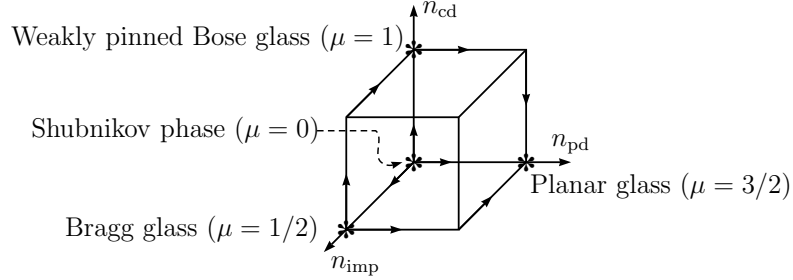


Figure 2.1: Schematic phase diagram of disordered flux line lattices resulting from impurities, columnar and planar defects with a concentration n_{imp} , n_{cd} and n_{pd} , respectively. The stability of the phases with respect to different kinds of disorder is indicated by arrows. μ denotes the creep exponent.

such that the density of defects is bigger than the FL density. For a larger magnetic field, Radzihovsky [37] argued that the Bose glass coexists with a resistive liquid of interstitial FLs which upon cooling freezes into a weakly pinned Bose glass. For asymptotically weak currents, the creep of FL bundles determines the nonlinear resistivity and $\mu = 1$ is the creep exponent [2].

In this chapter of the thesis we consider planar defects, like twin boundaries, from which even stronger pinning can be expected. Twin boundaries are ubiquitous in superconducting $\text{YBa}_2\text{Cu}_3\text{O}_{7-x}$ and La_2CuO_4 where they are needed to accommodate strains arising from tetragonal to orthorhombic transition as a result of oxygen vacancy ordering and due to rotation of the CuO_6 octahedra, respectively [38]. Twin boundaries occur frequently with the same orientation [39, 40, 41] or in orthogonal families of lamellas ("colonies") [38, 42]. They can be regularly distributed with rather fixed spacing or with large variations in the spacing [43]. The mean distance ℓ_D of the defect planes varies between 10 nm [39, 40, 42] and $1\mu\text{m}$ [41, 44].

The common feature of all of the above mentioned defects is that they lead to FL pinning, but what distinguishes them is the nature of the pinned phase. In contrast to point disorder, which promotes FL wandering, planar defects inhibit wandering and promote localization. Pinning of individual FLs by columnar as well as planar defects in presence of bulk point disorder has been investigated in the past [45, 46, 47, 48]. The competition between a planar defect and point impurities in three-dimensional systems, for a single FL, leads to localization of the FL at all temperatures [45, 46, 47]. The influence of many parallel defect planes on the creep of a single FL perpendicular to the planes has been studied at low temperatures when the FL spacing exceeds the average spacing between the planes [43].

The main focus of this chapter is correlated disorder in the form of planar defects. First, we discuss the influence of a single planar defect on the

stability of the Bragg glass phase and then we explore the effect of many defect planes on the FLL. Results on a single defect plane have been published in Refs. [49, 50], and results on many defect planes have been published in Refs. [50, 51]. This chapter is organized as follows. In Sec. 2.2, we introduce a model for interacting FLs that couple to weak point impurities and briefly review known results of this model. In Sec. 2.3, we consider a single defect plane as a perturbation to the Bragg glass phase and study the FL order using the a renormalization group analysis. A finite density of randomly distributed defects is explored in Sec. 2.4, where a new phase planar glass is found and characterized. Functional renormalization group equations are derived in $d = 6 - \epsilon$ dimensions. The response to tilt and shear deformations is discussed as well as sample to sample fluctuations of the longitudinal magnetic susceptibility. The positional correlation functions are computed and the stability of planar glass with respect to point and columnar disorder is studied. In Sec. 2.5, we consider the limit of strong planar defect potentials. In Sec. 2.6, we consider the FL dynamics for small currents by investigating FL creep in the presence of a single defect plane, both with and without point impurities, and in the presence of a finite density of planes. Finally, in Sec. 2.7 we discuss a model with a vector displacement field. The conclusions of this chapter are summarized in Sec. 2.8. Technical details and a list of recurrent symbols are relegated to Sec. 2.8.

2.2 Bragg glass phase

In this section we summarize some known results on pinning effects due to randomly distributed point impurities for interacting FLs. We use elasticity theory to describe a dislocation free array of FLs (for a review see, e.g., Blatter et al. [2]). Undistorted FLs are exactly parallel to the z -axis which we assume to be the direction of the applied magnetic field. The FLs form a triangular Abrikosov FLL in the xy -plane with a lattice constant a . In order to describe distortions of the FLs from the perfect lattice positions \mathbf{R}_ν , we use a two-component vector displacement field $\mathbf{u}_\nu(z)$. Since we are interested in the behavior on large length scales, it is appropriate to describe the interacting FLs in terms of a continuum elastic approximation with a continuous displacement field $\mathbf{u}_\nu(z) \rightarrow \mathbf{u}(\mathbf{r})$.

The Hamiltonian

$$\mathcal{H} = \mathcal{H}_0 + \mathcal{H}_P \tag{2.1}$$

consists of the elastic energy of the FLL, \mathcal{H}_0 , and pinning energy of point impurities, \mathcal{H}_P . In the following $\tilde{A}(\mathbf{q})$ denotes Fourier transform of a quantity

$A(\mathbf{r})$. The elastic energy of the dislocations free FLL reads

$$\mathcal{H}_0 = \frac{1}{2} \int \frac{d^2 \mathbf{q}_\perp dq_z}{(2\pi)^3} \tilde{\mathbf{u}}(\mathbf{q}) \left(\tilde{\mathcal{G}}_L^{-1} \mathbf{P}_L + \tilde{\mathcal{G}}_T^{-1} \mathbf{P}_T \right) \tilde{\mathbf{u}}(-\mathbf{q}), \quad (2.2)$$

where $\mathbf{q}_\perp = q_x \hat{\mathbf{x}} + q_y \hat{\mathbf{y}}$. $\mathbf{P}_L^{ij} = q_i q_j / q_\perp^2$ and $\mathbf{P}_T^{ij} = \delta_{ij} - q_i q_j / q_\perp^2$ are projectors onto the longitudinal and transversal modes, respectively, with propagators

$$\tilde{\mathcal{G}}_L^{-1} = c_{11} \mathbf{q}_\perp^2 + c_{44} q_z^2, \quad (2.3)$$

$$\tilde{\mathcal{G}}_T^{-1} = c_{66} \mathbf{q}_\perp^2 + c_{44} q_z^2. \quad (2.4)$$

In general, the compression (c_{11}) and the tilt (c_{44}) moduli are non-local on length scales smaller than the penetration depth λ but the shear modulus c_{66} is always local. However, the dispersion of c_{11} and c_{44} on small length scales is negligible for the present problem, since we are interested in asymptotic properties at large length scales and small currents. Hence, in the following we introduce a cutoff in momentum space given by $\Lambda \approx 2\pi/\lambda$ and neglect the non-locality of the elastic moduli. The elastic Hamiltonian of Eq. (2.2) can be obtained from symmetry arguments [52]. The ideal FLL is isotropic in xy -plane and has D_{6h} symmetry group.

The pinning energy of randomly distributed point impurities is modeled by the coupling

$$\mathcal{H}_P = \int d^3 \mathbf{r} \rho(\mathbf{r}, \mathbf{u}) V_P(\mathbf{r}), \quad (2.5)$$

of the local FL density $\rho(\mathbf{r}, \mathbf{u}) = \sum_\nu \delta(\mathbf{x} - \mathbf{R}_\nu - \mathbf{u}_\nu(z))$ to the pinning potential $V_P(\mathbf{r})$, where $\mathbf{x} = (x, y)$. From this definition and the Poisson summation formula [10, 11] the density can be also written as

$$\rho(\mathbf{r}, \mathbf{u}(\mathbf{r})) = \rho_0 + \rho_0 \left\{ -\nabla_{\mathbf{x}} \mathbf{u}(\mathbf{r}) + \sum_{\mathbf{G} \neq 0} e^{i\mathbf{G}[\mathbf{x} - \mathbf{u}(\mathbf{r})]} \right\} \quad (2.6)$$

where $\rho_0 = 2/(\sqrt{3}a^2)$, and \mathbf{G} is a vector of the reciprocal lattice. $V_P = -v_p \sum_i \delta_\xi(\mathbf{x} - \mathbf{x}_i) \delta(z - z_i)$ represents the pinning potential due to randomly distributed point impurities. The δ -functions are considered to have a finite width of the order of the superconductor coherence length ξ . For simplicity we subtract the average of the random potential and look at fluctuations around the average value. The pinning potential then satisfies

$$\overline{V_P(\mathbf{r})} = 0, \quad \overline{V_P(\mathbf{r}) V_P(\mathbf{r}')} = n_{\text{imp}} v_p^2 \delta_\xi(\mathbf{x} - \mathbf{x}') \delta(z - z'). \quad (2.7)$$

The strength of the disorder is characterized by $v_p^2 n_{\text{imp}}$, where n_{imp} denotes the density of point impurities. Higher order correlations of the (unrenormalized) pinning potential are nonzero, but for weak disorder can be neglected. The restriction to two-point correlations of V_P leads to the same replica Hamiltonian one obtains when V_P would be Gaussian distributed.

The model given by Eqs. (2.1)–(2.7) has been studied in detail using perturbation theory [7], Flory-type arguments [8, 53], a Gaussian variational ansatz [9, 10, 54] and functional renormalization group method [9, 10, 11, 12]. The correlations of the FLL fluctuations change with length scale and are characterized by three different regimes: the Larkin or random force regime, the random manifold regime and the Bragg glass phase. These regimes are distinguished by the scaling behavior of

$$\overline{\langle (\mathbf{u}(\mathbf{r}) - \mathbf{u}(\mathbf{0}))^2 \rangle} \propto |\mathbf{r}|^{2\zeta}, \quad (2.8)$$

which defines the roughness exponent ζ . Here $\langle \dots \rangle$ denotes a thermal and $\overline{\dots}$ a disorder average.

(i) In the Larkin regime [7] the displacements are sufficiently small so that the FLs stay within one minimum of the disorder potential $V_P(\mathbf{r})$ and perturbation theory can be applied. The effect of the disorder potential on the FLL is properly described by a random force $\mathbf{F}_P(\mathbf{R}_\nu, z) = -\nabla_{\mathbf{x}} V_P(\mathbf{R}_\nu, z)$. The roughness exponent is $\zeta_{RF} = (4 - d)/2$, where d denotes dimension of the system, so that the positional correlation function

$$S_{\mathbf{G}}(\mathbf{r}) = \overline{\langle e^{i\mathbf{G}\mathbf{u}(\mathbf{r})} e^{-i\mathbf{G}\mathbf{u}(\mathbf{0})} \rangle} \quad (2.9)$$

decays exponentially fast in $d = 3$. The Fourier transform of $S_{\mathbf{G}}(\mathbf{r})$ is the structure factor which can be directly measured in diffraction experiments. The Larkin lengths L_ξ^z and L_ξ^x are defined as the crossover length scales where the conditions

$$\begin{aligned} \overline{\langle (\mathbf{u}(\mathbf{0}, z = L_\xi^z) - \mathbf{u}(\mathbf{0}))^2 \rangle} &\propto \xi^2, \\ \overline{\langle (\mathbf{u}(|\mathbf{x}| = L_\xi^x, 0) - \mathbf{u}(\mathbf{0}))^2 \rangle} &\propto \xi^2 \end{aligned} \quad (2.10)$$

are satisfied. This leads to

$$\begin{aligned} L_\xi^z &\simeq \frac{\phi_0 \xi^6}{B v_p^2 n_{\text{imp}}} \frac{c_{44} c_{66}}{1 + \kappa} \\ L_\xi^x &\simeq \frac{\phi_0 \xi^6}{B v_p^2 n_{\text{imp}}} \frac{c_{44}^{1/2} c_{66}^{3/2}}{1 + \kappa^{3/2}}, \end{aligned} \quad (2.11)$$

where $\phi_0 = hc/(2e) = 2.07 \cdot 10^{-7} \text{G cm}^2$ is the flux quantum and $\kappa = c_{66}/c_{11}$. The length L_ξ increases with decreasing disorder strength. An increase in

the magnetic induction B effectively increases the disorder strength so that L_ξ shrinks.

(ii) On scales greater than the Larkin length, a description in terms of random forces become inapplicable and the random manifold regime applies. In the random manifold regime FLs explore many minima of the disorder potential but the typical displacement is still smaller than the FL spacing a . Hence the FLs do not compete with neighboring FL for identical pinning centers. A Flory-type argument [55, 56] yields the roughness exponent $\zeta_{RM} = (4 - d)/6$ but in Ref. [11] it was shown within an $\epsilon = 4 - d$ expansion that ζ_{RM} depends on the ratio $\kappa = c_{66}/c_{11}$ and varies between 0.1737ϵ and 0.1763ϵ . The positional order decays according to a stretched exponential,

$$S_{\mathbf{G}}(\mathbf{r}) \sim \exp \left[-\frac{G^2 r^{2\zeta_{RM}}}{2} \right]. \quad (2.12)$$

(iii) On length scales larger than the positional correlation length L_a the random manifold regime becomes inapplicable. $L_a^{z,\mathbf{x}} \approx L_\xi^{z,\mathbf{x}} (a/\xi)^{1/\zeta_{RM}}$ is defined as the scale at which the mean square displacement of FLs is of the order a . Therefore, it is crucial to keep the periodicity $\mathbf{u} \rightarrow \mathbf{u} + \mathbf{R}_\nu$ of the interaction between FLs and point disorder [8]. This leads to a much slower logarithmic increase ($\zeta_{BG} = 0$) of the elastic displacement of the FLs than in the Larkin and random manifold regime. It was shown [8, 9, 10, 11, 12, 54] that thermal fluctuations are irrelevant and that the pinned FLL exhibits a power law decay of positional correlations,

$$S_{\mathbf{G}}(\mathbf{x}, 0) \sim |\mathbf{x}|^{-\eta_{\mathbf{G}}}, \quad (2.13)$$

where $\eta_{\mathbf{G}} = \eta(G/G_0)^2$ and $G_0 = 4\pi/(\sqrt{3}a)$. This result resembles the correlations in pure two-dimensional crystals at finite temperatures. A functional renormalization group analysis in $d = 4 - \epsilon$ dimensions yields a non-universal exponent η that varies with the elastic constants of the FLL [11, 12]. Extrapolating to $d = 3$, one finds only a very weak variation with $1.143 < \eta < 1.159$ [11, 12]. Despite of the glassy nature of the phase algebraically divergent Bragg peaks still exist which motivated the name Bragg glass [9, 10]. The existence of the Bragg glass phase has been experimentally confirmed [13, 57].

After this summary of the scaling regimes, we briefly review the replica theory for the Hamiltonian of Eq. (2.1). Using the replica method, we average over point impurities (see App. 2.A) and obtain the replica Hamiltonian

$$\mathcal{H}_P^n = \sum_{\alpha=1}^n \mathcal{H}_0(\mathbf{u}^\alpha) - \frac{1}{2T} \sum_{\alpha,\beta=1}^n \int d^3\mathbf{r} R_P[\mathbf{u}^\alpha(\mathbf{r}) - \mathbf{u}^\beta(\mathbf{r})], \quad (2.14)$$

$$R_P(\mathbf{u}) = (v_p \rho_0)^2 n_{\text{imp}} \sum_{\mathbf{G} \neq 0} e^{i\mathbf{G}\mathbf{u}} \delta_{\xi^{-1}}(\mathbf{G}), \quad (2.15)$$

where $\delta_{\xi^{-1}}(\mathbf{G})$ is the delta function smeared out over a region of size ξ^{-1} . The correlation functions C_T and C_D that describe thermal fluctuations and disorder induced fluctuations, respectively, can be written as

$$\begin{aligned} C_T &= \overline{\langle \tilde{\mathbf{u}}(\mathbf{q}) \tilde{\mathbf{u}}(-\mathbf{q}) \rangle} - \overline{\langle \tilde{\mathbf{u}}(\mathbf{q}) \rangle \langle \tilde{\mathbf{u}}(-\mathbf{q}) \rangle} \\ &= (2\pi)^d T \{ \tilde{\mathcal{G}}_L(\mathbf{q}) + \tilde{\mathcal{G}}_T(\mathbf{q}) \} \\ C_D &= \overline{\langle \tilde{\mathbf{u}}(\mathbf{q}) \rangle \langle \tilde{\mathbf{u}}(-\mathbf{q}) \rangle} = (2\pi)^d \Delta(\mathbf{q}) \{ \tilde{\mathcal{G}}_L^2(\mathbf{q}) + \tilde{\mathcal{G}}_T^2(\mathbf{q}) \}, \end{aligned} \quad (2.16)$$

where the last equation defines $\Delta(\mathbf{q})$, which we shall obtain in harmonic approximation below.

In the next section we study the interplay between point impurities and a planar defect. This is a difficult problem since we have to deal with two nonlinear terms. We consider the planar defect as a perturbation to the Bragg glass fixed point and examine the stability of the Bragg glass phase. Also we explore the effects of the defect on the order of the FLL. In the following we will use an effective quadratic Hamiltonian that reproduces the displacement correlations of Eq. (2.8) of the full nonlinear disordered model Eq. (2.14). A systematic analysis must be based on $\epsilon = 4 - d$ expansion, and a functional renormalization group analysis shows that displacements obey Gaussian statistics to lowest order in ϵ [58]. It should be noted that the effective Hamiltonian does not capture all physics, in particular, it cannot describe correctly the FL dynamics since it cannot reproduce the energy barriers for FL motion [59]. An effective quadratic Hamiltonian has been also used for a model with a uniaxial displacement to study a dislocation mediated transition of the FLL [16].

The effective quadratic replica Hamiltonian in d dimensions reads [11, 12]

$$\mathcal{H}_0^n = \frac{1}{2} \sum_{\alpha, \beta=1}^n (2\pi)^{-d} \int d^d \mathbf{q} \tilde{\mathbf{u}}^\alpha(\mathbf{q}) \tilde{\mathcal{G}}_{\alpha, \beta}^{-1}(\mathbf{q}) \tilde{\mathbf{u}}^\beta(-\mathbf{q}), \quad (2.17)$$

where

$$\tilde{\mathcal{G}}_{\alpha, \beta}^{-1}(\mathbf{q}) = \delta_{\alpha, \beta} \left(\tilde{\mathcal{G}}_L^{-1}(\mathbf{q}) \mathbf{P}_L + \tilde{\mathcal{G}}_T^{-1}(\mathbf{q}) \mathbf{P}_T + n \frac{\Delta(\mathbf{q})}{T} \mathbf{1} \right) - \frac{\Delta(\mathbf{q})}{T} \mathbf{1}. \quad (2.18)$$

It yields the correlation functions of Eq. (2.16), where $\Delta(\mathbf{q})$ describes the behavior of $\Delta = -\partial_{u_x}^2 R_P(\mathbf{0}) = -\partial_{u_y}^2 R_P(\mathbf{0})$ on different length scales. Using a functional renormalization group in $d = 4 - \epsilon$ dimensions, it has been shown

that to lowest order in ϵ [11, 12]

$$\Delta(\mathbf{q}) \sim \begin{cases} 1, & \frac{1}{L_\xi} \lesssim q \lesssim \Lambda \\ q^{\epsilon-2\zeta_{RM}}, & \frac{1}{L_a} \lesssim q \lesssim \frac{1}{L_\xi} \\ \epsilon q^\epsilon, & q \lesssim \frac{1}{L_a}. \end{cases} \quad (2.19)$$

The function $\Delta(\mathbf{q})$ reaches the fixed point form $q^\epsilon \Delta^*(\kappa) c_{44} c_{66} a^2$ in the Bragg glass phase, where $\Delta^*(\kappa) \sim \epsilon/(1 + \kappa)$ depends only on elastic constants but not on the disorder strength. We note that Emig et al. [11, 12] have obtained their results by calculating the integrals, needed for the renormalization group equations, systematically for $d = 4$ with a two-dimensional vector \mathbf{z} . The results are then extended to three dimensions by setting $\epsilon = 1$ in $\Delta^*(\kappa)$. This approach does not influence the main physics (like the logarithmic roughness of FL in the Bragg glass phase), but may influence the dependence of exponents η and ζ_{RM} on the elastic constants. In this way the dimensionality of z "axis" and the contribution of the term $c_{44} \mathbf{q}_z^2$ in the propagators are more weighted than the other axes and other terms $\sim c_{66}, c_{11}$, respectively. In the following, in order to not overestimate the effect of a planar defect that is parallel to the z axis, we will calculate all the integrals in $d = 3$ if not stated otherwise. If the numerical values of η and ζ_{RM} are important for our conclusions, we will comment on a possible influence that the use of results found by Emig et al. [11, 12] can have.

2.3 Single defect

In this section the influence of a single planar defect on the Bragg glass order of the FLL is studied. In some parts of this section, when examining FLs density oscillations around the defect, we will study the isotropic limit with $c_{11} = c_{44} = c_{66} = c$ in order to focus on the important physics. In this limit the propagators read $\tilde{\mathcal{G}}_L^{-1}(\mathbf{q}) = \tilde{\mathcal{G}}_T^{-1}(\mathbf{q}) = cq^2$. By this assumption, only the weak dependence of η and ζ_{RM} on the elastic constants is ignored.

2.3.1 Model

The pinning energy of a planar defect can be written in the form

$$\mathcal{H}_D = \int d^3\mathbf{r} \rho(\mathbf{r}, \mathbf{u}) V_D(\mathbf{r} \cdot \mathbf{n}_D - \delta), \quad (2.20)$$

where $V_D(\mathbf{r} \cdot \mathbf{n}_D - \delta)$ is the potential of the defect plane. \mathbf{n}_D and δ denote the unit vector perpendicular to the defect plane and its distance (along

\mathbf{n}_D) from the origin of the coordinate system, respectively. The Bragg glass order that we are interested in is dominated by disorder fluctuations on large length scales where microscopic details become irrelevant. Therefore we may approximate the defect potential by a smeared out δ -function, $V_D(x) \approx -v\delta_\xi(x)$. Since the superconducting order is reduced in the defect plane, it is plausible to assume $v > 0$ (for more details, see Section IX of Blatter et al. [2]). When we assume that FLs gain condensation energy when they overlap with the defect plane, a rough estimate for the defect strength is $v \approx H_c^2 \xi^3$ with H_c the thermodynamic critical field.

In order to integrate over the delta function of the defect potential, it is convenient to introduce an explicit parametrization for the position vector \mathbf{r}_D of the defect plane which obeys $\mathbf{r}_D \cdot \mathbf{n}_D = \delta$. With the parametrization

$$\begin{aligned} \mathbf{r}_D &= (\mathbf{x}_D, z_D) + \delta \mathbf{n}_D, \quad z_D = t \cos \beta, \\ \mathbf{x}_D &= (s \sin \alpha - t \cos \alpha \sin \beta, s \cos \alpha + t \sin \alpha \sin \beta), \\ \mathbf{n}_D &= (\cos \beta \cos \alpha, -\cos \beta \sin \alpha, \sin \beta), \end{aligned} \quad (2.21)$$

we introduce in-plane coordinates s , t , and the two angles α and β which determine the rotation of the plane with respect to the y - and z -axis, respectively (see Fig. 2.2). The defect energy now reads

$$\begin{aligned} \mathcal{H}_D = v\rho_0 \int dt ds dr_\perp \delta_\xi(r_\perp - \delta) \left\{ \nabla_{\mathbf{x}} \mathbf{u}(t, s, r_\perp) \right. \\ \left. - \sum_{\mathbf{G} \neq \mathbf{0}} e^{i\mathbf{G}[r_\perp \mathbf{n}_D + \mathbf{x}_D - \mathbf{u}(t, s, r_\perp)]} \right\}, \end{aligned} \quad (2.22)$$

where $r_\perp = \mathbf{r} \cdot \mathbf{n}_D$. Since the displacement field \mathbf{u} varies slowly on the scale of the FLL constant a , the integrals over s and t vanish for all \mathbf{G} with the exception of those for which the oscillatory factor $e^{i\mathbf{G}\mathbf{x}_D}$ is unity (for all s , t). This condition can be satisfied only if $\sin \beta = 0$, i.e., if the defect plane is parallel to the applied magnetic field. There remains a second condition for the angle α which results from the constraint that $\mathbf{G} = m\mathbf{b}_1 + n\mathbf{b}_2$, with integer m and n , has to be perpendicular to \mathbf{x}_D . Expressing the defect plane (for $\sin \beta = 0$) as $\mathbf{x}_D = (c_1\mathbf{a}_1 - c_2\mathbf{a}_2)s$ where $\mathbf{a}_i \cdot \mathbf{b}_j = 2\pi\delta_{ij}$, one sees that the second condition is equivalent to the condition $m/n = c_2/c_1$. Hence if c_1/c_2 is irrational, the effect of the defect plane is always averaged to zero. On the other hand, for rational c_2/c_1 we may choose m_D, n_D to be the smallest coprime pair with $c_2/c_1 = m_D/n_D$. Then m_D, n_D are the Miller indices of the defect plane and only those \mathbf{G} which are integer multiples of $\mathbf{G}_D = m_D\mathbf{b}_1 + n_D\mathbf{b}_2$ contribute in Eq. (2.22). In the following, we will concentrate on the contribution from these \mathbf{G} -vectors only. The FLL planes

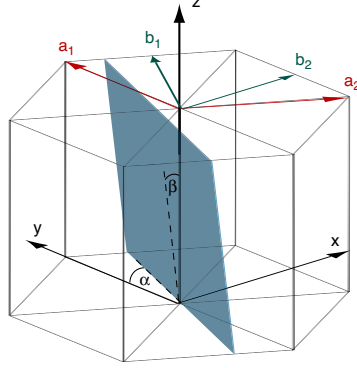


Figure 2.2: (Color online) Vectors of the triangular flux line lattice (\mathbf{a}_1 , \mathbf{a}_2) and of its reciprocal lattice (\mathbf{b}_1 , \mathbf{b}_2), and the angles α , β that define the orientation of the defect plane.

(of the ideal lattice) that are parallel to a defect plane with Miller indices m_D , n_D have a separation of $\ell = \frac{\sqrt{3}}{2}a/\sqrt{m_D^2 + m_D n_D + n_D^2}$ and hence $G_D = 2\pi/\ell$.

For the defect plane aligned to the magnetic field we take the x -axis to be perpendicular to the defect (i.e., $\alpha = \beta = 0$), and hence the defect Hamiltonian becomes

$$\mathcal{H}_D = \rho_0 v \int dy dz \left\{ \nabla_{\mathbf{x}} \mathbf{u}(\mathbf{r}_D) - \sum_{k>0}^{[\ell/\xi]_G} 2 \cos [k G_D (\delta - u_x)] \right\}, \quad (2.23)$$

where $\mathbf{r}_D = (\delta, y, z)$. Here u_x denotes the component of the displacement field that is perpendicular to the defect plane and $[x]_G$ is the integer number that is closest to x .

2.3.2 Renormalization group analysis

In this subsection we discuss the influence of the planar defect on the stability of the Bragg glass phase using a renormalization group analysis. We employ a sharp-cutoff scheme by integrating out the displacement field $\tilde{\mathbf{u}}^>(\mathbf{q})$, with wave vectors \mathbf{q} in an infinitesimal momentum shell below the cutoff $\Lambda > |\mathbf{q}| > \Lambda/b = \Lambda e^{-l}$ and subsequently rescale lengths and momenta according to

$$\mathbf{q}' = \mathbf{q}b, \quad (2.24)$$

$$\mathbf{r}' = \frac{\mathbf{r}}{b}. \quad (2.25)$$

We split the displacement field into weakly varying modes $\mathbf{u}^<(\mathbf{r})$ and strongly varying modes $\mathbf{u}^>(\mathbf{r})$ that include Fourier components out of and in the

momentum shell, respectively. We choose to not rescale the field $\mathbf{u}'(\mathbf{r}') = \mathbf{u}^<(\mathbf{r})$ which implies a rescaling of its Fourier transform, $\tilde{\mathbf{u}}'(\mathbf{q}') = \tilde{\mathbf{u}}^<(\mathbf{q})/b^3$.

The defect plane is considered as a perturbation to the Hamiltonian of Eq. (2.17). The gradient term of Eq. (2.23) scales as $\sim L$ if the defect size is $\sim L^2$. Since the elastic energy of Eq. (2.2) scales in the same way, the gradient term is a marginal perturbation. It can be also eliminated by the transformation

$$u'_x(\mathbf{r}) = u_x(\mathbf{r}) + \frac{v\rho_0}{2c_{11}} \text{sgn}(x - \delta), \quad (2.26)$$

where $\text{sgn}(0) = 0$. This transformation does neither change the terms $\sim c_{66}$, c_{44} of Eq. (2.2) nor the pinning energy due to point impurities in Eq. (2.14) since all replica fields are transformed in the same way. The gradient term of the defect pinning energy tends to increase the FL density at the defect as can be seen from the transformation above.

In order to account for different renormalization of the harmonic components of the defect pinning energy, we introduce the variables v_k for the strengths of the harmonics of order k . A cumulant expansion yields to first order in v the renormalization

$$\begin{aligned} \frac{v_k(l)}{T(l)} &= \frac{v}{T} e^{2l} \langle \cos [kG_D u_x^{\alpha,>}(\mathbf{r}_D)] \rangle \\ &= \frac{v}{T} e^{2l} e^{-\frac{1}{2}(kG_D)^2 \langle [u_x^{\alpha,>}(\mathbf{r}_D)]^2 \rangle} \\ &= \frac{v}{T} e^{(2-k^2g)l}, \quad g = \frac{3}{8}\eta \left(\frac{a}{\ell}\right)^2, \end{aligned} \quad (2.27)$$

where the factor e^{2l} is due to a rescaling of lengths. $\langle [u_x^{\alpha,>}(\mathbf{r}_D)]^2 \rangle$ is obtained at the Bragg glass fixed point to linear order in l . Due to the irrelevance of thermal fluctuations, we have neglected contributions that come from the thermal part of the propagator of Eq. (2.18). We have chosen to rescale temperature instead of elastic constants in order to organize the renormalization group analysis of the zero temperature Bragg glass fixed point. It is important to note that Eq. (2.27) holds only on length scales larger than the positional correlation length L_a .

In the random manifold regime $\overline{\langle e^{i\mathbf{G}\mathbf{u}(\mathbf{r})} \rangle}$ decays with the system size as a stretched exponential and the effect of the defect plane is reduced by disorder fluctuations on intermediate length scales. Hence, the renormalized and rescaled value of the defect strength is reduced to

$$v_k \approx v(L_a/a)^2 e^{-\mathcal{C}(G_D k a)^2} \quad (2.28)$$

on the scale $L = L_a$, where \mathcal{C} is a positive constant. This value is the initial defect strength $v_k(l=0)$ to be used in Eq. (2.27).

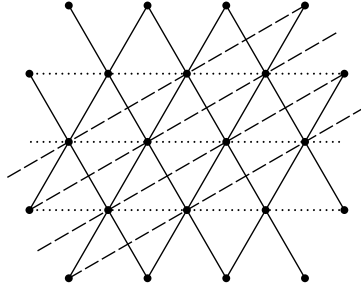


Figure 2.3: Two possible orientations of defect planes relative to the flux line lattice, corresponding to $g = \eta/2$ (dotted lines) and $3\eta/2$ (dashed lines).

The renormalization group flow equations in the Bragg glass regime now read

$$\frac{dT}{dl} = -T, \quad (2.29)$$

$$\frac{dv_k}{dl} = v_k(1 - k^2 g). \quad (2.30)$$

Hence v_1 is a relevant perturbation provided $g < 1$, i.e., if

$$\eta(m_D^2 + m_D n_D + n_D^2) < 2 \quad \text{or} \quad \ell > \sqrt{\frac{3\eta}{8}} a \approx 0.66 a, \quad (2.31)$$

which is compatible only with $\ell = \sqrt{3}a/2 \approx 0.87a$. A relevant defect plane must be oriented parallel to one of the three main crystallographic planes of the FLL (i.e., $\cos 2\beta = \cos 6\alpha = 1$). When ℓ increases (g decreases) more FLs can gain energy from the defect plane and hence render it more relevant.

Emig et al. [11, 12] have calculated η in a one-loop functional renormalization group expansion in $4 - \epsilon$ dimensions. Higher loops as well as the fact that all integrals are evaluated in $d = 4$ with \mathbf{z} being a two-dimensional vector, may influence the actual numerical value of the coefficient η in $d = 3$. However, we argue that this higher order correction does not affect our conclusion that a single defect is relevant only if it is parallel to the main crystallographic planes, since $g = \eta(m_D^2 + m_D n_D + n_D^2)/2$ can change only in finite steps ($\eta/2$, $3\eta/2$, $7\eta/2$, ...) when rotating the defect plane (see Fig. 2.3).

2.3.3 Effective Hamiltonian

In this section we discuss whether higher order cumulants in v can lead to a renormalization of the parameter g and hence can influence the condition for the relevance of a defect that was derived in the previous section. The

renormalization described by Eq. (2.30) does not occur in the bulk but on the defect plane. Hence it is possible to develop an effective theory that is defined on the defect plane only. Since the defect couples only to the displacement u_x on the defect plane, we integrate out u_x outside the defect and u_y across the entire sample. This integration is facilitated by employing the effective Gaussian theory for the Bragg glass phase of the previous section. At $T = 0$ we are interested in the ground state and hence we solve the Euler–Lagrange equation for $\mathbf{u}(\mathbf{r})$ with the condition $u_x(\mathbf{r}_D) = \varphi(\mathbf{r}_D)$ at the defect plane, where $\varphi(\mathbf{r}_D)$ is an arbitrary function. An equivalent functional integral approach is presented in App. 2.B. The effective replica Hamiltonian on the defect plane reads

$$\begin{aligned} \mathcal{H}_{\text{eff}}^n = & - \sum_{\alpha} \sum_{k>0} 2v_k \rho_0 \int d\mathbf{r}_D \cos \{kG_D[\delta - \varphi^{\alpha}(\mathbf{r}_D)]\} \\ & + \frac{1}{2} \sum_{\alpha, \beta} \frac{1}{(2\pi)^{d-1}} \int d^{d-1} \mathbf{q} \tilde{\varphi}^{\alpha}(\mathbf{q}) \tilde{\mathcal{Q}}_{\alpha, \beta}^{-1}(\mathbf{q}) \tilde{\varphi}^{\beta}(-\mathbf{q}), \end{aligned} \quad (2.32)$$

where \mathbf{q} is the in-plane momentum,

$$\langle \tilde{u}_x^{\alpha}(x, \mathbf{q}) \tilde{u}_x^{\beta}(x, \mathbf{q}') \rangle = T(2\pi)^d \delta(\mathbf{q} + \mathbf{q}') \tilde{\mathcal{Q}}^{\alpha, \beta}(\mathbf{q}), \quad (2.33)$$

and v_k are renormalized parameters on the scale of the positional correlation length. In order to avoid technical complications, we consider the limit of isotropic elasticity. In line with an ϵ expansion, we evaluate the integrals in $d = 4$ and then set $\epsilon = 1$ in the expression for fixed point value $\Delta^*(\kappa)$. This approach does not affect our conclusion and leads to a clearer result. On scales larger than L_a we get

$$\begin{aligned} \mathcal{Q}_{\alpha, \beta}^{-1}(\mathbf{q}) = & 2\sqrt{\frac{cn\Delta_{BG}}{T} + (qc)^2 \delta_{\alpha, \beta}} \\ & - \frac{2c\Delta_{BG}}{T} \left(cq + \sqrt{\frac{cn\Delta_{BG}}{T} + (qc)^2} \right)^{-1}, \end{aligned} \quad (2.34)$$

where c is the elastic constant and $\Delta_{BG} = c^2 a^2 \Lambda \Delta^*(1)$. The same procedure can be performed also in the random force and random manifold regimes using the corresponding quadratic Hamiltonian in d dimensions. The effective Hamiltonian in $d - 1$ dimensions has a long-ranged elasticity (term $\sim q$ in the limit $\Delta_{BG} \rightarrow 0$) that results from the local bulk elasticity. A renormalization group analysis of the effective Hamiltonian of Eq. (2.32) shows that neither Δ_{BG} nor the elastic constants are renormalized, and hence g is not renormalized. From this we conclude that a weak defect is a relevant perturbation only for $g < 1$.

2.3.4 Density oscillations

Next, we study the order of the FLs next to a defect plane. We consider separately the case of a relevant and an irrelevant planar defect. For simplicity, we assume isotropic elasticity and choose to place the origin of the coordinate system on the defect plane, i.e., we set $\delta = 0$. In the absence of a planar defect, FL density fluctuations due to point impurities obey $\overline{\langle \rho(\mathbf{r}) - \rho_0 \rangle} = 0$. The defect plane pins FLs and yields a long-ranged restoration of the translational order parameter $e^{i\mathbf{G}\mathbf{u}(\mathbf{r})}$. We find Friedel-like oscillations of the FL density with an amplitude that decays as a power law with an exponent that depends on if the defect is relevant or irrelevant in the renormalization group sense.

Irrelevant defect

First, we consider an irrelevant defect parallel to the magnetic field. The irrelevance of the defect potential for $g > 1$ allows us to compute the thermal and disorder average of FL density perturbatively in the defect strength,

$$\overline{\langle \delta\rho(\mathbf{r}, \mathbf{u}(\mathbf{r})) \rangle} = \lim_{n \rightarrow 0} \prod_{\alpha=1}^n \int \mathcal{D}\mathbf{u}^\alpha \delta\rho(\mathbf{r}, \mathbf{u}^\alpha(\mathbf{r})) e^{-\beta\mathcal{H}^n}, \quad (2.35)$$

where $\delta\rho(\mathbf{r}, \mathbf{u}) = \rho(\mathbf{r}, \mathbf{u}) - \rho_0$, γ is an arbitrary replica index and

$$\mathcal{H}^n = \mathcal{H}_0^n + \sum_{\alpha=1}^n \mathcal{H}_D(\mathbf{u}^\alpha). \quad (2.36)$$

To the zeroth order in the defect strength we get

$$\overline{\langle \delta\rho(\mathbf{r}, \mathbf{u}(\mathbf{r})) \rangle} = \lim_{n \rightarrow 0} \langle \delta\rho(\mathbf{r}, \mathbf{u}^\gamma(\mathbf{r})) \rangle = 0. \quad (2.37)$$

Even if the defect is irrelevant in the renormalization group sense, it breaks the translational symmetry perpendicular to the defect and hence modifies the FL density locally. To correctly describe this effect we need to compute the average change in the FL density to first order in v :

$$\overline{\langle \delta\rho(\mathbf{r}, \mathbf{u}(\mathbf{r})) \rangle} = -\beta \lim_{n \rightarrow 0} \sum_{\alpha=1}^n \langle \delta\rho(\mathbf{r}, \mathbf{u}^\alpha(\mathbf{r})) \mathcal{H}_D(\mathbf{u}^\alpha) \rangle. \quad (2.38)$$

We find that in the limit $T \rightarrow 0$ this result can be expressed as

$$\overline{\langle \delta\rho(\mathbf{r}, \mathbf{u}(\mathbf{r})) \rangle} \approx \frac{v_1 \rho_0^2 G_D^2 L_a}{c(2g-1)} \cos(G_D |x|) \left(\frac{L_a}{|x|} \right)^{2g-1}, \quad (2.39)$$

see App. 2.C. The result captures the large length scale behavior for $L \geq L_a$. Here v_1 denotes the effective defect strength on the scale L_a , cf. Eq. (2.28), and $|x|$ is the normal distance from the defect plane. There are additional contributions to Eq. (2.39) coming from the higher harmonics in \mathcal{H}_D . They are less important since they are proportional to v_k on the scale L_a and they decay as $|x|^{-2k^2g+1}$ with $k \geq 2$. Although the defect is irrelevant in renormalization group sense, it leads to Friedel-like oscillations in the density.

If the defect plane is not parallel to the applied magnetic field, Friedel oscillations occur as well. However, the amplitude is exponentially suppressed. The amplitude of density oscillations with reciprocal lattice vectors $\mathbf{G} = G(\cos \alpha, -\sin \alpha)$ (for a definition of the angles α and β see Fig. 2.2) decays beyond the distance $1/(G|\sin \beta|)$ from the defect plane. Similar physics occur in classical two-dimensional systems with a columnar defect [60, 61].

Relevant defect

The strength of a relevant defect grows under renormalization relative to the elastic and the impurity energy. On the scale

$$L_v \approx \max \left\{ L_a, L_a \left(\frac{ca^4}{vL_a} \right)^{1/(1-g)} \right\}, \quad (2.40)$$

the energies become of the same order and perturbation theory breaks down. On larger scales, the defect potential can be described effectively through the boundary condition $u_x(x=0, y, z) = 0$ for the displacement field at the defect plane. With this constraint the system gains maximal energy from the defect and the complete energy of the system is minimized. First, we calculate displacement correlations

$$\mathcal{G}_{\text{pin},ij}(x, x'; \mathbf{r}_{\parallel} - \mathbf{r}'_{\parallel}) = T^{-1} \overline{\langle u_i(\mathbf{r}) u_j(\mathbf{r}') \rangle} \quad (2.41)$$

with the above boundary condition at the defect and $\mathbf{r} = (x, \mathbf{r}_{\parallel})$. We find in momentum space (see App. 2.D)

$$\tilde{\mathcal{G}}_{\text{pin},ij}(x, x; \mathbf{q}) = \lim_{n \rightarrow 0} \left[\tilde{\mathcal{G}}_{ij}^{11}(0, \mathbf{q}) - \sum_{\alpha\gamma} \tilde{\mathcal{G}}_{ix}^{1\alpha}(|x|, \mathbf{q}) \tilde{\mathcal{Q}}_{\alpha,\gamma}^{-1}(\mathbf{q}) \tilde{\mathcal{G}}_{xj}^{1\gamma}(|x|, -\mathbf{q}) \right], \quad (2.42)$$

where \mathbf{q} is the in-plane momentum and $\tilde{\mathcal{G}}^{\alpha,\beta}$ is the inverse of $\tilde{\mathcal{G}}_{\alpha,\beta}^{-1}$ given by Eq. (2.18). i, j stand for x, y and \mathcal{Q} is given by Eq. (2.33). It can be shown that the displacement correlations on scales larger than L_v are given by

$$\overline{\langle u_i(\mathbf{r}) u_j(\mathbf{r}') \rangle} = \lim_{n \rightarrow 0} T \left[\mathcal{G}_{ij}^{11}(0, \mathbf{0}) - (\hat{\mathbf{x}} \cdot \hat{\mathbf{i}})(\hat{\mathbf{x}} \cdot \hat{\mathbf{j}}) \mathcal{G}_{xx}^{11}(2|x|, \mathbf{0}) \right]. \quad (2.43)$$

Using this result, we obtain for the average change in the FL density

$$\overline{\langle \delta\rho(\mathbf{r}, \mathbf{u}(\mathbf{r})) \rangle} = 2\rho_0 \sum_{m>0} \cos(mG_D x) \left(\frac{L_v}{|x|} \right)^{m^2 g}. \quad (2.44)$$

These oscillations resemble Friedel oscillations which can be also found in Luttinger liquids with an isolated impurity [62] or in classical two-dimensional systems with a columnar defect [60, 61].

The amplitude of the Friedel oscillations decays as a power law with an exponent g and $2g - 1$ for a relevant and an irrelevant defect, respectively. For an irrelevant defect the amplitude decays more rapidly than for a relevant defect. In the absence of point impurities the defect is always relevant in the renormalization group sense, and the amplitude of the Friedel oscillations remains finite for $|x| \rightarrow \infty$.

2.4 Finite density of weak defects

2.4.1 Model

In this section we consider a finite density of parallel planar defects with random position. We assume that defects extend along the entire sample and are aligned parallel to the applied magnetic field. There is a competition between the two random potentials from planar defects and point impurities. The defects tend to localize the FLs and hence favor order along the defect planes while point impurities promote FL wandering.

The Hamiltonian reads

$$\mathcal{H} = \mathcal{H}_0 + \int d^3r [V_P(\mathbf{r}) + V_D(\mathbf{r})] \rho(\mathbf{r}, \mathbf{u}), \quad (2.45)$$

where \mathcal{H}_0 is the elastic Hamiltonian of Eq. (2.2) and V_P is the pinning potential resulting from point impurities, see Eq. (2.5). The defect pinning potential is $V_D(\mathbf{r}) = -v \{ \sum_i \delta_\xi(x - x_i) - 1/\ell_D \}$ where we assumed that the defect planes are parallel to the yz -plane and ℓ_D is a mean defect spacing. The δ -function is assumed to have a finite width of the order of the superconductor coherence length ξ . The defect potential is uncorrelated along the x -axis,

$$\overline{V_D(\mathbf{r}_1) V_D(\mathbf{r}_2)} = \frac{v^2}{\ell_D} \delta_\xi(x_1 - x_2). \quad (2.46)$$

We discuss the case where the gap between two defect planes typically contains many FLs, i.e., $\xi \ll \ell \ll \ell_D$. Note that orientation of the defects (i.e. value of ℓ) is otherwise arbitrary.

After averaging over the defect positions, the replica Hamiltonian for the defects reads

$$\mathcal{H}_D^n = -\frac{(v\rho_0)^2}{2T\ell_D} \int d^3\mathbf{r}_1 d^3\mathbf{r}_2 \sum_{\alpha,\beta} \delta_\xi(x_1 - x_2) \left\{ -2\nabla_{\mathbf{x}}\mathbf{u}^\alpha(\mathbf{r}_1) \sum_{\mathbf{G}} e^{i\mathbf{G}[\mathbf{x}_2 - \mathbf{u}^\beta(\mathbf{r}_2)]} \right. \\ \left. + \nabla_{\mathbf{x}}\mathbf{u}^\alpha(\mathbf{r}_1) \nabla_{\mathbf{x}}\mathbf{u}^\beta(\mathbf{r}_2) + \sum_{\mathbf{G}_1, \mathbf{G}_2} e^{i\mathbf{G}_1[\mathbf{x}_1 - \mathbf{u}^\alpha(\mathbf{r}_1)]} e^{i\mathbf{G}_2[\mathbf{x}_2 - \mathbf{u}^\beta(\mathbf{r}_2)]} \right\}, \quad (2.47)$$

where $\mathbf{x} = (x, y)$. The defects are assumed to be sufficiently weak so that terms of the order v^3/ℓ_D and higher can be neglected. The first term does not contribute to \mathcal{H}_D^n due to the oscillatory factor $e^{i\mathbf{G}\mathbf{x}_2}$ and the third term contributes only for reciprocal vectors perpendicular to the defects satisfying $\mathbf{G}_1 = -\mathbf{G}_2 = n\mathbf{G}_D$ with integer n . Introducing the relative coordinate $x_r = x_1 - x_2$ and taking into account that $\delta_\xi(x_r)$ is finite for $|x_r| \leq \xi$, we approximate the displacement field as $u_x(x_2 + x_r, y_1, z_1) \approx u_x(x_2, y_1, z_1)$. This approximation is justified since the displacement field varies slowly over the FL spacing. Then Eq. (2.47) can be written as

$$\mathcal{H}_D^n = -\frac{1}{2T} \int_{x_1, y_1, z_1, y_2, z_2} \sum_{\alpha,\beta} \left\{ \sigma \nabla_{\mathbf{x}}\mathbf{u}^\alpha(x_1, y_1, z_1) \nabla_{\mathbf{x}}\mathbf{u}^\beta(x_1, y_2, z_2) \right. \\ \left. + R_D [u_x^\alpha(x_1, y_1, z_1) - u_x^\beta(x_1, y_2, z_2)] \right\}, \quad (2.48)$$

where

$$R_D(u_x) = \sigma \sum_{n \neq 0} \delta_{\xi^{-1}}(nG_D) e^{inG_D u_x} \quad (2.49)$$

and we defined $\int_x = \int dx$ and $\sigma = (v\rho_0)^2/\ell_D$. After averaging over point impurities, the complete replica Hamiltonian is $\mathcal{H}^n = \mathcal{H}_P^n + \mathcal{H}_D^n$, where \mathcal{H}_P^n is given by Eq. (2.14).

The first term in Eq. (2.48) comes from the coupling of the defect potential to the slowly varying part of the FL density $\sim \nabla_{\mathbf{x}}\mathbf{u}$. This term does not contribute to the glassy properties of the system, since it can be eliminated by a simple transformation [59]¹. We will discuss this term in more detail

¹Since the defects are weak, the effects we are interested in become visible on large length scales. Hence, we can introduce a coarse grained version of the defect potential $\tilde{V}(x) = \int dx' V_D(x')/L_w$, where the integration is over a segment of length $L_w \gg \ell_D$.

later. The remaining part of the replica pinning energy \mathcal{H}^n is invariant under the transformations

$$u_x^\alpha(\mathbf{r}) \rightarrow u_x^\alpha(\mathbf{r}) + f_x(x), \quad (2.50)$$

$$u_y^\alpha(\mathbf{r}) \rightarrow u_y^\alpha(\mathbf{r}) + f_y(\mathbf{r}), \quad (2.51)$$

where $f_x(x)$ and $f_y(\mathbf{r})$ are arbitrary functions. Eq. (2.50) represents an approximate symmetry if the defect potential has a finite width. However, with increasing length scale, deviations from the symmetry become less important. These symmetries show that the elastic coefficient c_{11} is not renormalized. Not renormalized are also the elastic moduli which determine the energy cost for tilting the FLs only in the y direction (i.e. the term $c_{44}(\partial_z u_y)^2$) and for changing only the displacement u_y along the x -axis (i.e. the term $c_{66}(\partial_x u_y)^2$). These symmetries are commonly denoted as statistical tilt symmetry [63]. However, the defects are an important source of anisotropy and other elastic properties of the FLL will be affected. For example, the energy cost for FL tilting as well as FLL shearing parallel and perpendicular to the planes will differ considerably. Also, due to the defect planes the system is not invariant under arbitrary rigid rotations of the FLL around z axis and rotational modes will appear in the elastic Hamiltonian under renormalization [64]. Note that for the FLL with point disorder only, none of the elastic constants will be renormalized since the disorder correlation function $R_P(\mathbf{u})$ is invariant under the more general transformation $\mathbf{u}^\alpha(\mathbf{r}) \rightarrow \mathbf{u}^\alpha(\mathbf{r}) + \mathbf{f}(\mathbf{r})$.

Planar defects in the form of twin boundaries that are perpendicular to the copper oxide planes very often appear in $\text{YBa}_2\text{Cu}_3\text{O}_{7-x}$ (YBCO) [39, 40, 42]. YBCO is a high temperature superconductor and within high accuracy it is uniaxially anisotropic [2]. YBCO can be reasonably well described within a continuum anisotropic model, while for more strongly layered superconductors a different description is needed. The elastic description for anisotropic superconductors can be found in the review article by Blatter et al. [2]. The number of independent elastic moduli increases with respect to the isotropic case that we discussed in Sec. 2.2. However, if the magnetic

In that case the central limit theorem shows that $\tilde{V}(x)$ is Gaussian distributed with $\overline{\tilde{V}(x)\tilde{V}(x')} = v^2/\ell_D\delta(x-x')$. In the planar defect Hamiltonian, the slowly varying part of the FL density couples only to $\mu(x) = \int_{|q_x|\sim 0} \tilde{V}(q_x) \exp[iq_x x]/(2\pi)$ while to the periodic part of the FL density couples $W(x) = \sum_n \int_{|q_x|\sim 0} \tilde{V}(nG_D + q_x) \exp[i(q_x + nG_D)x]/(2\pi)$, where $n \neq 0$ is an integer number. Since the Gaussian distributed potential satisfies $\overline{\tilde{V}(q)\tilde{V}(q')} = 2\pi v^2/\ell_D\delta(q+q')$, the potentials $\mu(x)$ and $W(x)$ are not correlated, $\overline{W(x)\mu(x)} = 0$. By applying the transformation $u'(\mathbf{r}) = u(\mathbf{r}) - \int_0^x dx_1 \mu(x_1)/c_{11}$ and averaging over $W(x)$, we get only the second term of the replica Hamiltonian of Eq. (2.48) and the first term has been eliminated.

field is applied perpendicular to the copper oxide planes, the model given by Eq. (2.2) as well as the considerations in the following sections is directly applicable also for YBCO.

2.4.2 Functional renormalization group approach

In the previous section we treated a single defect plane as a perturbation to the Bragg glass fixed point. Now, we consider both the planar defects and the point impurities as a perturbation to the ideal Shubnikov phase. Notice that Eq. (2.49) depends only the displacement field u_x . Since we focus below on the effect of the defect planes, it seems to be justified to start from a simplified model in which only the displacement $u_x \equiv u$ of the FLs perpendicular to the defect planes is considered. This model describes also a wide class of other systems which exhibit regular lattices of domain walls like magnets, charge density waves [18] and incommensurate systems [19].

In the absence of the defect planes, point impurities are relevant below four dimensions. We employ here an Imry–Ma–type argument [65] in combination with perturbation theory to see the effect of randomly distributed point impurities on the FLL. When the initially ordered FLL is distorted in a volume L^d by $u \sim \ell$, the typical energy gain is of the order $\sim (-R_p''(0)L^d)^{1/2}$ compared to the elastic energy loss $\sim L^{d-2}$. For $d < d_P = 4$ and sufficiently large $L \gg L_\xi \sim (-R_p''(0))^{1/(d-4)} \gg \ell$ the point disorder wins and the FLL becomes distorted. A more detailed study shows that in this case the FLL exhibits a phase with quasi-long-range order which is the previously discussed the Bragg glass phase (see Sec. 2.2). In this phase the positional correlation function S_G [see Eq. (2.9)] shows a power law decay.

Next we consider the Imry–Ma argument for planar defects in a volume $L_x^{d-2}L_zL_y$ without point impurities. The energy gain is of the order $(-R_D''(0)\ell^2L_x^{d-2})^{1/2}L_zL_y$. The elastic energy loss is $c_{11}L_zL_yL_x^{d-4}\ell^2$ since distortions are aligned parallel to the defects. The pinning energy gain wins and the FLL becomes disordered in the direction perpendicular to the defects for $L_x \gg L_D \sim (-c_{11}^2\ell^2/R_D''(0))^{1/(6-d)}$. L_D is the so-called Larkin length for the defects. The critical dimension above which weak planar defects are irrelevant is $d_D = 6$.

For an renormalization group approach is convenient to consider a generalization of our model to d dimensions. The defects remain two-dimensional with $d - 2$ transverse directions, while the displacement field remains uniaxial. In the following, we use a functional renormalization group approach [66, 67] in $d = 6 - \epsilon$ dimensions. We follow closely a related approach for columnar disorder [68] but do not rescale the renormalized quantities so that they correspond to the effective parameters measured on the scale L_x . Af-

ter having done calculation we became aware of work by Fedorenko [69]. Thermal fluctuations and point disorder are irrelevant for $\epsilon < 4$ and $\epsilon < 2$, respectively. Hence we can assume directly $T = 0$ and $R_P = 0$. To lowest order in ϵ the renormalization group flow equations read

$$\frac{d \ln c_{ii}}{d \ln L_x} = \frac{K_d R_D''''(0) L_x^\epsilon}{c_{11}^2}, \quad i = 4, 6, \quad (2.52)$$

$$\frac{d R_D(u)}{d \ln L_x} = \frac{K_d R_D''(u) L_x^\epsilon}{2c_{11}^2} [R_D''(u) - 2R_D''(0)], \quad (2.53)$$

where $K_d = S_{d-2}/(2\pi)^{d-2}$ and S_d denotes the surface of the d -dimensional unit sphere.

In a static situation the displacement field is independent on y and z since defects distort FLL planes that are parallel to the yz -plane on the whole. Since, by assumption, other sources of fluctuations are not present we can perform the integration over y and z in the Hamiltonian of Eq. (2.48) and obtain an effective $d - 2$ -dimensional Hamiltonian that describes the interaction of FLL planes with defect planes with $d - 2$ -dimensional random positions. This explains why the flow equation for R_D has the form as the one for the point disorder correlator R_P in $d - 2$ dimensions [9]. However, an important difference between the d -dimensional FLL with defects and the FLL planes with point impurities in $d - 2$ dimensions is the renormalization of elastic constants c_{44} and c_{66} in the former model.

For $L_x \rightarrow L_D$, $R_D''''(0)$ increases and at $L_x \approx L_D$ $R_D''(u)$ develops a cusp at $u = 0$. The cusp signals the appearance of metastable states the energy of which is very close to the ground state energy but which may be far apart in configuration space. The cusp results in diverging elastic constants c_{44} and c_{66} and in a change of the sign of $R_D''''(0^+)$ from positive to negative. If there is a small but finite tilt or shear of FLLs, $R_D''''(0)$ has to be replaced by $R_D''''(0^+)$ in Eq. (2.52), and on length scales $L_x > L_D$ the elastic constants decrease since $R_D''''(0^+)$ is then negative. Importantly, a new term of the form

$$\frac{1}{\ell} \int d^{d-2} x dy dz |\Sigma_y(\partial_y u) \hat{y} + \Sigma_z(\partial_z u) \hat{z}| \quad (2.54)$$

is generated in the Hamiltonian. $\Sigma_{z(y)}$ has the meaning of an interface tension of a domain wall perpendicular to z (y) axis, across which the displacement field changes by ℓ . They dominate the elastic energy for small u and are renormalized according to

$$c_{66}^{-1/2} \frac{d \Sigma_y}{d \ln L_x} = c_{44}^{-1/2} \frac{d \Sigma_y}{d \ln L_x} = R_D''''(0^+) L_x^{5-d} \frac{K_d \ell}{2c_{11}^{3/2}}. \quad (2.55)$$

Σ_z and Σ_y satisfy the relation $\Sigma_z/\Sigma_y = \sqrt{c_{44}}/\sqrt{c_{66}}$. Notice that c_{44} and c_{66} are renormalized in the same way such that their ratio remains constant under the renormalization group flow.

Next we estimate the Larkin length L_D from the flow equations. The function $R_D(u)$ is even and as long as it is analytic, all odd derivatives at $u = 0$ vanish. Assuming analyticity, the flow equation for $R_D''''(0)$ reads

$$\frac{dR_D''''(0)}{d \ln L_x} = \frac{4}{c_{11}^2} K_d L_x^\epsilon [R_D''''(0)]^2. \quad (2.56)$$

The solution on the length scale L_x is given by

$$R_D''''(0, L_x) = R_D''''(0, \lambda) \left[1 - R_D''''(0, \lambda) 4K_d (L_x^\epsilon - \lambda^\epsilon) / c_{11}^2 \epsilon \right]^{-1}, \quad (2.57)$$

where λ is the penetration depth and has a role of the small length scale cutoff. This shows that $R_D(0)$ diverges at

$$L_D \approx \left[\frac{\epsilon c_{11}^2}{4K_d R_D''''(0, \lambda)} \right]^{1/\epsilon}. \quad (2.58)$$

This result is in qualitative agreement with the estimate we obtained from scaling arguments since $R_D''''(0, \lambda) \ell^2 \sim R_D''(0, \lambda)$.

The fixed point function has for $0 \leq u < \ell$ the form [9]

$$R_D''(u, L_x) = -\frac{\epsilon c_{11}^2 L_x^{-\epsilon}}{6K_d} \left[\left(u - \frac{\ell}{2} \right)^2 - \frac{\ell^2}{12} \right] \quad (2.59)$$

and it has to be periodically continued in u with period ℓ . Note that if we would consider rescaled quantities, then in Eq. (2.59) $L_x^{-\epsilon}$ would be replaced by Λ^ϵ . In the case of a finite tilt (shear) for $L_x > L_D$ the elastic constant c_{44} (c_{66}) decreases as $c_{ii}(L_x) \sim (L_x/L_D)^{-\epsilon/3}$. A rough estimate for the saturation value for the interface tension is $\Sigma_z \sim \epsilon \ell^2 \sqrt{c_{11} c_{44}(\lambda)} / L_D$.

As has been pointed out by Fedorenko [69], the renormalization group equations for the elastic constants c_{44} , c_{66} and the interface tensions resemble those of the friction and driving force for the depinning transition of the FLL in the presence of point impurities [70]. The role of velocity is here played by tilt or shear and the elastic constants diverge at zero tilt and zero shear as the friction diverges in the static case. Also, as a threshold force exists for the depinning transition, the interface tension $\Sigma_{z(y)}$ determines the threshold force for tilting (shearing) the FLL, as we will see in the next subsection.

2.4.3 Properties of the planar glass

In this subsection we summarize the properties of the new phase that is described by the fixed point of the functional renormalization group analysis of the previous section and in the following is called "planar glass". We examine the response of the system to FL tilting, to a change in the longitudinal magnetic field and discuss the order of the FLL. We show that the new phase and its properties are robust against weak point impurities in $d = 3$ and $d = 4$.

When one changes the direction of the applied magnetic field by $H_x \hat{\mathbf{x}}$, the Hamiltonian changes by

$$\delta\mathcal{H} = -\frac{\phi_0\rho_0}{4\pi} \int d^3r H_x \partial_z u. \quad (2.60)$$

To tilt the FLs with respect to the z -axis, H_x has to overcome the interface energy $\sim \Sigma_z$ which results in a threshold field

$$H_{x,c} = 2\pi\sqrt{3} \frac{\Sigma_z a^2}{\phi_0 \ell}, \quad (2.61)$$

below which the FLs remain locked parallel to the planes. This is the transverse Meissner effect: a weak transverse magnetic field H_x is screened from the sample and c_{44} is infinite. Only for $H_x > H_{x,c}$ the average tilt of the FLs becomes nonzero and c_{44} is finite. In this way, by measuring the threshold field, Σ_z can be measured.

Moreover, there is a resistance against shear of the FLL. The shear deformation $\partial_y u_x$ is nonzero (and c_{66} is finite) only if the shear stress σ_{xy} is larger than a critical value $\sigma_{xy,c} = \Sigma_y/\ell$. Otherwise c_{66} is infinite. The divergence of c_{66} is a new property that does not appear in the Bose glass which, however, does also show a transverse Meissner effect.

An infinitesimal change in the longitudinal magnetic field $\delta H_z \hat{\mathbf{z}}$ changes the Hamiltonian by

$$\delta\mathcal{H} = -\frac{\phi_0\rho_0}{4\pi} \int d^3r \delta H_z \partial_x u \quad (2.62)$$

and allows to measure the longitudinal magnetic susceptibility given by $\chi = \phi_0\rho_0 \partial \langle \partial_x u \rangle / \partial \delta H_z$. The disorder averaged susceptibility is

$$\bar{\chi} = \frac{(\phi_0\rho_0)^2}{4\pi c_{11}}, \quad (2.63)$$

as shown in App. 2.E. It is independent of disorder as a result of the statistical tilt symmetry [63]. The glassy properties of the system can most easily be

seen by the sample to sample fluctuations of the magnetic susceptibility. Perturbation theory yields (see App. 2.E)

$$\frac{\overline{\chi^2} - \bar{\chi}^2}{\bar{\chi}^2} = \frac{R_D''''(0)L_x^\epsilon}{5c_{11}^2} \sim \left(\frac{L_x}{L_D}\right)^\epsilon, \quad (2.64)$$

i.e. the sample to sample fluctuations of the susceptibility grow with the scale $L_x \lesssim L_D$, $d < 6$. We cannot expect that this result is quantitatively correct for large L_x , but qualitatively it demonstrates the relevance of defects and it provides a signature of a glassy phase [59]. Although we were not able to prove it, $\overline{\chi^2}/\bar{\chi}^2 - 1$ will most likely approach a finite universal value for $L_x \gg L_D$ in $d < 6$.

The positional correlation function is obtained to first order in perturbation theory, combined with a functional renormalization group analysis for $6 > d > 4$. It reads

$$S_{\mathbf{G}_D}(\mathbf{x}, y, z) \sim |\mathbf{x}|^{-\eta_D}, \quad (2.65)$$

where $\eta_D = (\pi/3)^2(6-d)$. A detailed derivation of this result is presented in App. 2.F. In order to study the behavior in $d \leq 4$, we have to reconsider the first term of Eq. (2.48). It results from the coupling of the defect potential to the slowly varying part of the FL density ($\sim \partial_x u$). By taking into account that at a scale L_x the displacement field behaves as $u \sim L_x^\zeta$, we find that the σ -term scales as $\sim L_y^2 L_z^2 L_x^{d-4+2\zeta}$. When we compare the latter term to the squared elastic Hamiltonian $\sim L_y^2 L_z^2 L_x^{2(d-4+2\zeta)}$ that describes the cost of deviations of u in the \mathbf{x} directions only (since the FLs are completely ordered parallel to the defects on sufficiently large scales in the absence of point impurities), we find that the σ -term becomes relevant if $d-4+2\zeta \leq 0$. For logarithmic roughness ($\zeta = 0$) it is relevant for $d \leq 4$. Since the other part of the defect pinning energy $\sim R_D(u)$ scales in the same way as the elastic energy, the σ -term is the dominant part of the pinning energy and determines the FL roughness.

First, we consider the case without point impurities and then treat them perturbatively. Applying a Flory-type argument [3], i.e., assuming that the elastic energy and the dominant part of the defect energy scale in the same way, we find, following the discussion above, that in $d = 3$ the roughness exponent is $\zeta = 1/2$. More detailed calculations [71, 72] confirm our result, leading to

$$S_{\mathbf{G}_D}(x, y, z) \sim e^{-|x|/\xi_c}, \quad (2.66)$$

where $\xi_c \approx L_D$. Note that there is a shift of dimension $d \rightarrow d+2$ between the model studied in Refs. [71, 72] to our model since the FLs are ordered in the

yz -plane. In Refs. [71, 72] a related one-dimensional system with point impurities at zero temperature is studied. There is a nontrivial renormalization of σ coming from the defect potential that couples to the periodic part of the FL density [71]. The σ -term does not contribute to the renormalization of R_D , since the σ -term can be eliminated in every step of the renormalization group procedure by applying the transformation that does not affect the correlator R_D , as discussed at the beginning of this section. That is why Σ_z and Σ_y will be generated also for $d \leq 4$. Villain and Fernandez [71] found from a non-perturbative renormalization group approach that for $d \leq 4$ the defect-induced disorder flows to strong coupling. However, our study of the strong coupling limit in Sec. 2.5 shows that this limit gives qualitatively the same result as the case investigated in this section.

To summarize, the planar glass phase is characterized by (i) diverging shear and tilt moduli but a finite compressibility, (ii) a transverse Meissner effect as well as a resistance against shear deformation, (iii) sample to sample fluctuations of the longitudinal magnetic susceptibility and (iv) an exponential decay of positional correlations in the direction perpendicular to the defects in $d = 3$.

Since point disorder may formally become relevant below $d = 4$, we consider the stability of the planar glass with respect to weak point impurities. We find that the pinning energy due to point impurities in $d = 3$ behaves as

$$\begin{aligned} \overline{\langle \mathcal{H}_P \rangle} &= \rho_0 \sum_{n \neq 0} \int d\mathbf{r} V_P(\mathbf{r}) e^{inG_D x} e^{-(nG_D)^2 \langle u^2 \rangle / 2} \\ &\sim \rho_0 \sqrt{n_{\text{imp}} v_p^2 L_y L_z L_x} e^{-L_x / (2\xi_c)} \end{aligned} \quad (2.67)$$

and from this we conclude that weak point impurities are an irrelevant perturbation. Similarly, it can be shown that pinning energy of randomly distributed columnar defects decays exponentially with L_x and hence does not destroy the planar glass.

2.4.4 Stability of the Bragg glass and the weakly pinned Bose glass

In this subsection we continue discussion of the competition between pinning effects due to point impurities, columnar and planar defects. We shall show that the weakly pinned Bose glass is stable with respect to weak point impurities but unstable with respect to weak planar defects. Moreover, we shall demonstrate that the Bragg glass phase is unstable with respect to both weak planar and weak columnar defects. The resulting phase diagram is shown schematically in Fig. 2.1.

First we discuss the stability of the Bragg glass phase in analogy to the test for stability of the planar glass in the previous subsection. We note that the correlation functions in the Bragg glass phase can also be obtained from a model with a uniaxial displacement field of FLs [10]. A uniaxial displacement field describes also properly charge density waves, a stack of membranes under tension and domain walls in magnets. Justified by these observations, we first consider a uniaxial displacement field in the direction perpendicular to the defect planes. At the Bragg glass fixed point in $d = 3$ the pinning energy of the planar defects behaves as

$$\begin{aligned} \overline{\langle \mathcal{H}_D \rangle} &= \rho_0 \sum_{n \neq 0} \int d\mathbf{r} V_D(\mathbf{r}) e^{inG_D x} e^{-(nG_D)^2 \langle u^2 \rangle / 2} \\ &\sim \rho_0 \sqrt{v^2 L^5 / \ell_D} L^{-\pi^2 / 18}. \end{aligned} \quad (2.68)$$

When we compare this energy to the pinning energy of point impurities,

$$\overline{\langle \mathcal{H}_P \rangle} \sim \sqrt{L^3 R_p^*(0)} \sim L, \quad (2.69)$$

we find that planar defects are a relevant perturbation. Note that at the Bragg glass fixed point the system is isotropic, i.e., $L_x = L_y = L_z = L$. In Eq. (2.69) we used the fact that the fixed point correlator on the length scale L behaves as $R_p^*(0) \sim L^{-1}$ [cf. Eq. (2.19)]. Next, we consider perturbatively weak randomly distributed columnar defects aligned with the magnetic field. The potential created by columnar defects $V_C(\mathbf{r}) = v_c [\sum_i \delta_\xi(x - x_i) \delta_\xi(y - y_i) - n_{cd}]$ couples to the FL density. n_{cd} is the concentration of the columnar defects. The pinning energy of columnar defects at the Bragg glass fixed point scales as

$$\begin{aligned} \overline{\langle \mathcal{H}_C \rangle} &= \rho_0 \sum_{n \neq 0} \int d\mathbf{r} V_C(\mathbf{r}) e^{inG_D x} e^{-(nG_D)^2 \langle u^2 \rangle / 2} \\ &\sim \rho_0 \sqrt{v_c^2 n_{cd} L^4} L^{-\pi^2 / 18}, \end{aligned} \quad (2.70)$$

and drives the system away from the Bragg glass fixed point.

A functional renormalization group analysis of weak columnar defects in $d = 5 - \epsilon$ yields a stable phase with a zero temperature fixed point that is characterized by a power law decay of the positional correlation function with an exponent $\eta_C = (\pi/3)^2(5 - d)$ and a transverse Meissner effect [68]. One can expect that this phase, found for a uniaxial displacement field, applies to the case where the FL density is larger than the columnar defect density, corresponding to the so called weakly pinned Bose glass. In order to study

the stability of this phase in $d = 3$ with respect to planar defects and point impurities, we compare the scaling

$$\overline{\langle \mathcal{H}_D \rangle} \sim \rho_0 \sqrt{v^2 L^3 L_z^2 / \ell_D} L^{-(\pi/3)^2}, \quad (2.71)$$

$$\overline{\langle \mathcal{H}_C \rangle} \sim \sqrt{R_C^*(0) L^2 L_z^2} \sim L_z, \quad (2.72)$$

$$\overline{\langle \mathcal{H}_P \rangle} \sim \rho_0 \sqrt{v_p^2 n_{\text{imp}} L^2 L_z} L^{-(\pi/3)^2} \quad (2.73)$$

of the different pinning energies, where we used $L_x = L_y = L$ and columnar disorder fixed point correlator $R_C^*(0) \sim L^{-2}$. We conclude that weak point impurities are irrelevant but weak planar defects are relevant in the weakly pinned Bose glass.

Next we examine the stability of the Bragg glass phase by considering a vector displacement field. This displacement field reveals the triangular lattice structure of the FLL. By changing the orientation of the defect planes, the number of FLs that are pinned by the defects changes. In $d = 3$ we have

$$\overline{\langle \mathcal{H}_D \rangle} \sim \rho_0 \sqrt{v^2 L^5 / \ell_D} e^{-G_D^2 \overline{\langle u_x^2 \rangle} / 2} \sim L^{\frac{5}{2}-g}, \quad (2.74)$$

$$\overline{\langle \mathcal{H}_C \rangle} \sim \rho_0 \sqrt{v_c^2 n_{\text{cd}} L^4} e^{-\langle (\mathbf{G}_0 \mathbf{u})^2 \rangle / 2} \sim L^{2-\eta/2}, \quad (2.75)$$

$$\overline{\langle \mathcal{H}_P \rangle} \sim \sqrt{L^3 R_P^*(0)} \sim L, \quad (2.76)$$

where g is given by Eq. (2.27), $|\mathbf{G}_0| = 4\pi/(\sqrt{3}a)$ is the shortest vector of the reciprocal lattice and η is the exponent of the positional correlation function in the Bragg glass phase. Weak columnar defects are always a relevant perturbation, while weak planar defects are relevant only if they satisfy $g < g_c = 3/2$, i.e., only if they are parallel to the main crystallographic planes of the FLL. Here we neglected the influence of weak planar defects on the elasticity of the FLL. In fact, the defects lead to an additional anisotropy in the elastic energy which is associated with a larger energy for deformations with nonzero $\partial_y u_x$ and $\partial_z u_x$. Through a renormalization of the elastic constants g is renormalized downwards. Therefore, stronger planar defects lead to an increased $g_c > 3/2$, rendering additional orientations of defects relevant. However, it is likely that in the case of a finite density of parallel defect planes, the FLL will rotate to a position in which it reaches maximum overlap with the defects. Then the planar defects will be parallel to the main lattice planes and the Bragg glass is unstable.

2.5 Finite density of strong defects

In this section we consider the FLL with a finite density of parallel, randomly distributed defect planes that are aligned to the magnetic field. The defects

are assumed to be sufficiently strong so that the Larkin length [see Eq. (2.58)] is of the order of the mean defect spacing or smaller, $L_D \lesssim \ell_D$. In this case the defect potential can not be treated perturbatively with respect to the elastic energy, and a new approach is required. Here we derive an effective Hamiltonian that is defined only at the defect planes. We determine the ground state configuration of the FLL and calculate the positional correlation function. We show that a transverse Meissner effect as well as a resistance against shear deformations appears also in this case.

The Hamiltonian in $d = 3$ dimensions reads

$$\mathcal{H} = \mathcal{H}_0 + \sum_i^{N_D} \mathcal{H}_{D,i}, \quad (2.77)$$

where \mathcal{H}_0 is the elastic Hamiltonian given by Eq. (2.2) and $\mathcal{H}_{D,i}$ is the pinning energy of the defect plane at the position $x = x_i$, see Eq. (2.23). N_D denotes the number of defects. In this section we consider a simplified model involving only uniaxial displacements perpendicular to the defects $\mathbf{u} = u\hat{\mathbf{x}}$. In Sec. 2.7 we shall discuss the implications of the generalization to a two-dimensional vector displacement. The part of \mathcal{H}_D that describes the coupling of the pinning potential to the slowly varying part of the FL density ($\sim \partial_x u$) leads only to an increase in the FL density at the defects and can be eliminated by applying the transformation

$$u(\mathbf{r}) \rightarrow u(\mathbf{r}) - \frac{v\rho_0}{c_{11}} \sum_{i=1}^{N_D} \text{sgn}(x - x_i). \quad (2.78)$$

The Hamiltonian then becomes

$$\mathcal{H} = \mathcal{H}_0 - 2v\rho_0 \sum_{i=1}^{N_D} \int_{y,z} \sum_{k>0}^{[\ell/\xi]_G} \cos \{kG_D [u(x, y, z) - \alpha_i]\}, \quad (2.79)$$

where $\alpha_i = x_i + v\rho_0(i - 1)/c_{11}$. For simplicity we assume that all defects have the same strength.

In order to obtain a Hamiltonian that is isotropic in the yz -plane, we introduce the rescaled coordinate $z' = z\sqrt{c_{66}/c_{44}}$ and define $u'(y, z') = u(y, z)$. We shall omit the primes below. We proceed by studying the ground state of the displacement field for a given distribution of planar defects, assuming that a strong defect potential suppresses thermal fluctuations. First we solve the saddle point equation in the gap between the defects with prescribed, but arbitrary, boundary conditions at the defects $u_i(y, z) = u(x_i, y, z)$ with Fourier transform $\tilde{u}_i(\mathbf{q}) = \tilde{u}(x_i, \mathbf{q})$, $\mathbf{q} = (q_y, q_z)$. In the ground state configuration the FLs are completely aligned to the defect planes and $u(x_i, y, z)$ is

independent of y, z . However, we derive the saddle point solution and the effective Hamiltonian for a more general displacement field configuration at the defect planes since this will be necessary for a discussion of the transverse Meissner effect below as well as the FL dynamics in Sec. 2.6. In the following we use the notation $\Delta A_i = A_{i+1} - A_i$ for any quantity A . The solution of the saddle point equation between two defect planes reads, with $x \in [x_i, x_{i+1}]$,

$$\begin{aligned} \tilde{u}(x, \mathbf{q}) = & \frac{\tilde{u}_i(\mathbf{q})}{\sinh(q'\Delta x_i)} \sinh[q'(x_{i+1} - x)] \\ & + \frac{\tilde{u}_{i+1}(\mathbf{q})}{\sinh(q'\Delta x_i)} \sinh[q'(x - x_i)], \end{aligned} \quad (2.80)$$

where $q' = \sqrt{c_{66}/c_{11}q}$. Note that we have solved the saddle point equation between the defects within a continuum model and not on the lattice. This amounts to setting the momentum cutoff $\Lambda \rightarrow \infty$. After substituting this solution into the Hamiltonian of Eq. (2.79) and integrating over x , the Hamiltonian reduces to

$$\begin{aligned} \mathcal{H} = & \frac{\sqrt{c_{11}c_{44}}}{2} \int \frac{d^2q}{(2\pi)^2} q \sum_{i=1}^{N_D-1} \left\{ \frac{|\tilde{u}_{i+1}(\mathbf{q}) - \tilde{u}_i(\mathbf{q})|^2}{\sinh\left(q\Delta x_i \sqrt{\frac{c_{66}}{c_{11}}}\right)} \right. \\ & \left. + (|\tilde{u}_i(\mathbf{q})|^2 + |\tilde{u}_{i+1}(\mathbf{q})|^2) \tanh\left(\frac{q\Delta x_i}{2} \sqrt{\frac{c_{66}}{c_{11}}}\right) \right\} \\ & - 2v\rho_0 \sqrt{\frac{c_{44}}{c_{66}}} \sum_{i=1}^{N_D} \int_{y,z} \sum_{k>0}^{[\ell/\xi]_G} \cos\{kG_D [u_i(y, z) - \alpha_i]\}. \end{aligned} \quad (2.81)$$

A similar Hamiltonian has been obtained for a Luttinger liquid with point impurities [73].

Next we study the ground state of the FLL. In the limit $v \rightarrow \infty$ the FLs are completely aligned to the defects and $u_i(y, z) = u_i$. Then the Hamiltonian of Eq. (2.81) becomes

$$\frac{\mathcal{H}}{L^2} \sqrt{\frac{c_{66}}{c_{44}}} = \frac{c_{11}}{2} \sum_{i=1}^{N_D-1} \frac{(u_{i+1} - u_i)^2}{\Delta x_i} - 2v\rho_0 \sum_{i=1}^{N_D} \sum_{k>0}^{[\ell/\xi]_G} \cos\left[k \frac{2\pi}{\ell} (u_i - \alpha_i)\right], \quad (2.82)$$

where L is the system size. For $u_i = \ell n_i + \alpha_i$, where n_i is an integer number, the energy gain of the FLs from the defect potential is maximal. We determine n_i such that the elastic energy is minimal and find the ground state

configuration to be degenerate and given by [74]

$$u_i^{(n)} = \ell \left(\frac{\alpha_i}{\ell} - \sum_{j < i} \left[\frac{\Delta\alpha_j}{\ell} \right]_G + n \right), \quad (2.83)$$

where n is an integer number. Note that this is the ground state configuration for an arbitrary defect strength in the special case when $\Delta\alpha_i/\ell - [\Delta\alpha_i/\ell]_G = 0$ for all i . Then the FLs are just shifted in order to gain energy from the defects without any elastic energy loss. However, for randomly distributed defect planes that satisfy $\ell_D \gg \ell$, $\Delta\alpha_i/\ell - [\Delta\alpha_i/\ell]_G$ is uniformly distributed in the interval $[-1/2, 1/2]$. Using the central limit theorem, we find that the positional correlation function decays exponentially fast in the x direction,

$$S_{\mathbf{G}_D}(\mathbf{r}) \sim e^{-|x|/\xi_c}, \quad x \gg \ell_D \quad (2.84)$$

with $\xi_c \approx 6\ell_D/\pi^2$. This shows that the limits of weak and strong planar defects lead to the same behavior of the positional correlations in $d = 3$. The correlation length in both cases is determined by the Larkin length of the defects.

From the shifted boundary conditions $u_i(y, z \rightarrow \infty) = u_i^0 + \ell$ and $u_i(y, 0) = u_i^0$ one can obtain also the interface tension Σ_z and it turns out to be finite. We do not quote the result here since it is cutoff dependent and hence non-universal. Also, a general expression that is valid for all ratios of the elastic constants is not available. A similar analysis shows that the surface tension Σ_y is finite. Hence, strong defects lead to a transverse Meissner effect as well as a resistance against shear deformations. The finite values of Σ_z and Σ_y might be interesting to probe experimentally.

2.6 Flux line creep

Pinning centers play an important role in preventing FL motion in type-II superconductors and may lead to a nonlinear resistivity $\ln \rho \sim -J^{-\mu}$ for $J \rightarrow 0$ which depends on the so-called creep exponent μ [2, 3]. In this section we study the effect of planar defects on the FL dynamics in the direction perpendicular to the defect planes. The defects are assumed to be parallel to the applied magnetic field. For a single defect plane we show that the creep exponent is $\mu = 1$, apart from logarithmic corrections. We find that many planar defects act as a more effective source of pinning than point impurities [8] and columnar defects [2, 34, 35]. They considerably slow down the FLs in comparison to the Bragg glass and the Bose glass, leading to a creep exponent $\mu = 3/2$ for the planar glass.

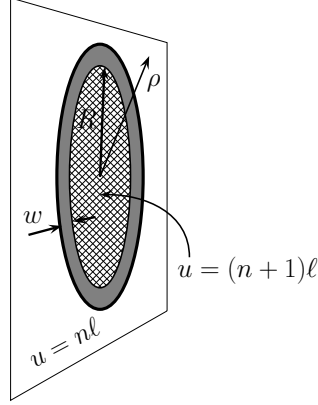


Figure 2.4: Schematic illustration of a droplet with radius R and width w at a defect plane.

2.6.1 Single defect

First we discuss the creep of FLs in the presence of a single planar defect, aligned to the applied magnetic field and without point impurities, for currents parallel to the defect and perpendicular to the magnetic field. The Hamiltonian is given by

$$\mathcal{H} = \mathcal{H}_0 + \mathcal{H}_D + \mathcal{H}_{\text{force}}, \quad (2.85)$$

where the part describing elastic deformations, \mathcal{H}_0 , is given by Eq. (2.2), the defect pinning energy \mathcal{H}_D by Eq. (2.23) and the Lorentz force contribution reads

$$\mathcal{H}_{\text{force}} = - \int d^3\mathbf{r} \{ \mathbf{J}(\mathbf{r}) \times \mathbf{B}(\mathbf{r}) \} \cdot \mathbf{u}(\mathbf{r}). \quad (2.86)$$

$\mathbf{J}(\mathbf{r})$ is the current density, $\mathbf{B}(\mathbf{r})$ is the magnetic induction and the speed of light is set to unity. Since we will consider only FL dynamics normal to the defect and since the defect potential depends only on the perpendicular displacement field, it appears plausible to simplify our model and to consider a uniaxial displacement field in the direction perpendicular to the defect plane.

The defect plane is a relevant perturbation in the Shubnikov (mixed) phase for all orientations of the plane (in contrast to the case when point impurities are present) since thermal fluctuations do not roughen the FLL in $d = 3$ at low temperatures. This can be easily seen from the renormalization group equation (2.30) by setting $g = 0$. Under renormalization the weak defect potential that couples to the periodic part of the FL density grows and

flows to strong coupling. Since we are interested in the small current densities $J \rightarrow 0$ which probe large length scales, we shall study only the strong defect plane below. Our results apply also to weak defects at sufficiently large length scales or small currents.

In the absence of a current, the FLs are aligned to the defect plane and the ground state is highly degenerate. Different ground states differ by a shift of the displacement field by ℓ because the energy does not depend on which FLL plane is pinned by the defect. This degeneracy is broken when a current is turned on and the original ground state becomes unstable. The system now evolves into a new metastable state that is lower in energy and in which the FLs are shifted by ℓ . This process is enabled via the formation of droplets which are nuclei of new metastable states. The competition between bulk energy gain and elastic energy loss determines the energy (and size) of the critical droplet. The energy of the critical droplet corresponds to the energy barrier that the FLs have to overcome when evolving to a new state. Thermally activated FL hopping over barriers with energy $E_{\text{drop}}^*(J)$ determines the resistivity through the Arrhenius law [75, 76]

$$\rho(J) \sim e^{-E_{\text{drop}}^*(J)/T}. \quad (2.87)$$

Therefore, we need to estimate $E_{\text{drop}}^*(J)$.

We proceed by deriving an effective Hamiltonian that is defined on the defect plane ($x = 0$). By integrating out the displacement field off the defect we get (see App. 2.B)

$$\begin{aligned} \mathcal{H}_{\text{eff}} = & \frac{1}{2} \int \frac{d^2 \mathbf{q}}{(2\pi)^2} |\tilde{u}(0, q_y, q_z)|^2 [\tilde{\mathcal{G}}(0, \mathbf{q})]^{-1} \\ & - 2v\rho_0 \int dydz \sum_{k>0}^{[\ell/\xi]_G} \cos [kG_D u(0, y, z)] \\ & - \tilde{u}(0, \mathbf{q} = 0) \int dx J(x) B(x). \end{aligned} \quad (2.88)$$

Here $\mathbf{q} = (q_y, q_z)$ is the in-plane momentum, $\tilde{u}(0, q_y, q_z) = \tilde{u}(x = 0, q_y, q_z)$ and

$$\tilde{\mathcal{G}}(0, \mathbf{q}') = \frac{\arctan \left[\frac{\Lambda}{|\mathbf{q}'|} \sqrt{\frac{c_{11}}{c_{66}}} \right]}{\pi |\mathbf{q}'| \sqrt{c_{11} c_{66}}}, \quad (2.89)$$

where $\mathbf{q}' = (q_y, \sqrt{c_{44}/c_{66}} q_z)$ and $\Lambda = 2\pi/\lambda$. Since the system is translationally invariant in the yz -plane, the current density and magnetic induction depend only on x . In order to simplify the computations, we make the system

isotropic in the yz -plane by the rescaling $z' = z(c_{66}/c_{44})^{1/2}$ and $u'(\mathbf{r}') = u(\mathbf{r})$. In the following we will omit the primes.

The critical droplet is a solution of the saddle point equation for the Hamiltonian of Eq. (2.88) with fixed boundary conditions $u(0, \rho \rightarrow 0) = (n+1)\ell$ and $u(0, \rho \rightarrow \infty) = n\ell$ with $\rho = (y^2 + z^2)^{1/2}$ and n integer. For the precise solution see, e.g., a related discussion for a single strong impurity in a Luttinger liquid by Giamarchi [21]. The shape of the droplet is characterized by its radius R and the width w of the droplet wall (see Fig. 2.4) so that the displacement field obeys approximately

$$u(0, \rho) \approx \begin{cases} (n+1)\ell, & \rho \in [0, R] \\ n\ell, & \rho \in [R+w, \infty]. \end{cases} \quad (2.90)$$

The exact shape of the droplet wall is not essential for the discussion that follows. We assume that it smoothly interpolates between $(n+1)\ell$ and $n\ell$. The width w of the droplet wall does not depend on the radius for small currents $J \rightarrow 0$. In this limit the critical droplet radius is much larger than the width $R \gg w$ so that the energy loss is balanced by the energy gain from the Lorentz force (see e.g. [77] and references therein). The critical droplet radius and energy is determined by maximizing the droplet energy $E_{\text{drop}}(R)$.

Since across the droplet wall the FLs are not aligned to the defect plane, a strong defect tends to reduce the width of the wall. Then, the large \mathbf{q} behavior of the propagator of Eq. (2.89), $[\tilde{\mathcal{G}}(0, \mathbf{q})]^{-1} \approx (\pi c_{66} q^2)/\Lambda$, becomes important at the wall since it describes elastic deformations on small length scales. For sufficiently strong defects ($w \simeq \Lambda^{-1}$) the precise form of the droplet wall is determined by the interplay between the elastic energy $\sim q^2$ and the defect pinning energy. The energy loss for FLs at the defect plane is [21] $E_{\text{core}} \sim Rv^{1/2}$, as known from droplets in the sine-Gordon model.

The elastic energy loss outside the plane, due to the deformation of the FLs at the defect plane is determined by the low \mathbf{q} behavior of the propagator of Eq. (2.89), $[\tilde{\mathcal{G}}(0, \mathbf{q})]^{-1} \approx 2\sqrt{c_{11}c_{66}}|\mathbf{q}|$, since the deformation occurs across the large scale R . It captures the three-dimensional nature of the FLL by its non-local form $\sim |\mathbf{q}|$. This is obvious when the elastic energy is written as

$$\mathcal{H}_{\text{el}} = \frac{\sqrt{c_{11}c_{44}}}{4\pi} \int d^2\mathbf{r}_1 \int d^2\mathbf{r}_2 \frac{[u(\mathbf{r}_1) - u(\mathbf{r}_2)]^2}{(\mathbf{r}_1 - \mathbf{r}_2)^3}. \quad (2.91)$$

Here \mathbf{r}_1 and \mathbf{r}_2 lay in the defect plane and satisfy $|\mathbf{r}_1 - \mathbf{r}_2| > \lambda$. The long-ranged elasticity in the effective two-dimensional elastic Hamiltonian of Eq. (2.91) results from fluctuations outside the defect plane that have been integrated out. Since $R \gg w$, the precise form of the droplet wall is not important for estimating \mathcal{H}_{el} and we can assume $w = 0$ (corresponding

to $v \rightarrow \infty$). Then we obtain for the elastic energy

$$E_{\text{el}} \approx 2\sqrt{c_{11}c_{44}}\ell^2 R \log(R/\lambda). \quad (2.92)$$

This result can be interpreted as the energy of charges of equal sign (corresponding to kinks in the displacement field) which are placed along a circle of radius R and interact via the three-dimensional Coulomb potential.

The energy losses mentioned above are balanced by an energy gain due to the Lorentz force that is described by the last term of Eq. (2.88),

$$E_{\text{force}} \approx \ell R^2 \pi \sqrt{\frac{c_{44}}{c_{66}}} \int dx J(x) B(x). \quad (2.93)$$

When we estimate E_{force} , a finite width of the droplet wall can be neglected since $R \gg w$. The total droplet energy then reads

$$\begin{aligned} E_{\text{drop}} &\approx E_{\text{el}} + E_{\text{core}} - E_{\text{force}} \\ &\approx \alpha R \log\left(\frac{R}{\lambda}\right) + R\beta - \gamma R^2, \end{aligned} \quad (2.94)$$

where $\alpha = 2(c_{11}c_{44})^{1/2}\ell^2$, $\beta \sim v^{1/2}$ and $\gamma = \pi(c_{44}/c_{66})^{1/2}\ell \int dx J(x)B(x)$. The creep rate is determined by the droplet with the largest total energy E_{drop} which is called the critical droplet. Solving the equations $\partial_R E_{\text{drop}} = 0$ and $\partial_R^2 E_{\text{drop}} < 0$ we find the size R^* and the energy E_{drop}^* of the critical droplet. Increasing of the droplet radius beyond R^* does not cost any energy and droplet freely expands. For $R \rightarrow \infty$ the system reaches a new metastable state in which all FLs are shifted by ℓ perpendicular to the defect. The nonlinear resistivity is given by the Arrhenius law. In the limit of a vanishing current density, i.e., for large β/γ , we get

$$\begin{aligned} \rho &\sim e^{-E_{\text{drop}}^*/T} \\ &\sim \exp\left\{-\frac{1}{4\gamma T} \left[\left(\beta + \alpha \log \frac{\beta + \alpha}{2\lambda\gamma} \right)^2 - \alpha^2 \right] \right\}. \end{aligned} \quad (2.95)$$

Prefactors are not determined here since in the limit of a vanishing current density the current-voltage characteristic is dominated by the exponential factor of Eq. (2.95). The result for ρ yields the creep exponent $\mu = 1$ plus logarithmic corrections. To estimate the coefficient γ we need to know how the current density and the magnetic induction vary in space. This is a tedious analysis which goes beyond the scope of the present study and is left for further investigation.

Next we examine how randomly distributed weak point impurities around the defect plane affect the FL creep for $J \rightarrow 0$. A weak defect is relevant in the renormalization group sense only for $g < 1$ and it then flows to the strong coupling limit. Criteria for the relevance of a strong defect with an arbitrary orientation are not available. Therefore we study below only the strong coupling limit for a defect that is oriented parallel to the main FLL planes. We expect that the liberation from the defect plane is the limiting factor for the FL motion so that the creep exponent is reduced compared to its value in the Bragg glass phase.

The shape of the droplet is again given by Eq. (2.90) but now the impurities control the fluctuations of the FLs outside the defect. Without point impurities, the displacement field decays outside the defect plane as $u(x, \rho = 0) \approx (\ell/2)(R/x)^2$ for $x \gg R$. Point-like impurities induce additional displacement fluctuations and the droplet-induced deformations are no longer long-ranged. This can be seen from the correlation function in the presence of a relevant defect that follows from Eq. (2.43),

$$\langle [u(x, \rho) - u(0, \rho)]^2 \rangle = \frac{1}{2} \langle [u(x, \rho) - u(-x, \rho)]^2 \rangle_{BG}. \quad (2.96)$$

The subscript BG means that the correlation function is computed at the Bragg glass fixed point. Since the right hand side of Eq. (2.96) is of the order a^2 for $x \approx L_a$ we conclude that the droplet extends up to L_a from the defect. This yields for the energy gain from the Lorentz force the rough estimate $E_{\text{force}} \approx JBL_aR^2\ell$ where J is the mean current density inside the droplet. Hence, in the limit $J \rightarrow 0$ resistivity is

$$\rho(J) \sim \exp \left[-\frac{C_1}{J} \left(\log \frac{C_2}{J} \right)^2 \right], \quad (2.97)$$

where C_1 and C_2 depend on T , B , on the strength and concentration of the impurities, and on the defect strength. This result shows that a single relevant defect plane indeed slows down the FL creep in comparison to the Bragg glass phase.

2.6.2 Finite density of weak defects

Here we consider FL creep perpendicular to many weak defects with random positions but in the absence of point impurities, cf. Sec. 2.4. The motion of FL bundles under the influence of the Lorentz force is again driven by the nucleation of critical droplets [2]. A typical droplet is schematically shown in Fig. 2.5. For small currents, the droplet extends over many defect planes

in order to balance elastic and pinning energy loss with bulk energy gain from the Lorentz force. For small current densities, the FLL is properly described in terms of the interface tensions Σ_y and Σ_z , see Eq. (2.54), which are appropriate on sufficiently large length scales. The energy of the droplet is then of the form

$$E_{\text{drop}} \approx \sqrt{\frac{c_{44}}{c_{66}}} L_x^{d-2} R^2 \left(\frac{c_{11} \ell^2}{L_x^2} + \frac{\Sigma_y}{R} - JB\ell \right). \quad (2.98)$$

The elastic energy cost for the formation of the droplet consists of two terms. The first term of Eq. (2.98) is the energy of a wide domain wall of width $\sim L_x$ parallel to yz -plane. The second term of Eq. (2.98) describes the energy of a narrow cylindrically shaped domain wall perpendicular to yz -plane. In the estimate of E_{drop} we have taken into account that the elastic energy and the energy from planar disorder scale in the same way. The last term of Eq. (2.98) is the energy gain from the Lorentz force. J (B) is to be understood as the mean current density (magnetic induction) averaged over the defect spacing. Note that we have used again the rescaling $z' = (c_{66}/c_{44})^{1/2} z$.

In Eq. (2.98) we have taken into account the logarithmic roughness of the displacement field, corresponding to the roughness exponent $\zeta = 0$. We have ignored logarithmic corrections. The σ -term of Eq. (2.48), that is responsible for the roughness exponent $\zeta = 1/2$, can be eliminated by the simple transformation that was discussed in Sec. 2.4 and hence it does not affect the FL dynamics. In case of a potential breakdown of the ϵ expansion (cf. Sec. 2.4.2) in $d = 3$ and the existence of a strong coupling fixed point [71] see Sec. 2.6.3.

To determine the critical droplet we solve $\partial_{L_x} E_{\text{drop}} = 0$ and $\partial_R E_{\text{drop}} = 0$. We find for the critical radius R^* and the critical length L_x^* of the droplet

$$\frac{R^*}{\Sigma_y} \sim \frac{L_x^{*2}}{c_{11} \ell^2} \sim \frac{1}{JB\ell}. \quad (2.99)$$

This yields for $d = 3$ the nonlinear resistivity in the limit $J \ll J_D$,

$$\rho(J) \sim e^{-(J_D/J)^{3/2}}, \quad J_D = \mathcal{C} \frac{(\Sigma_y \Sigma_z)^{2/3} (c_{11}/\ell)^{1/3}}{BT^{2/3}}. \quad (2.100)$$

Here \mathcal{C} is positive numerical constant of order unity. Thus the nonlinear resistivity is considerably reduced compared to the Bragg glass phase and to a single defect plane in the presence of impurities.

In the similar way one can consider the creep in the presence of randomly distributed columnar defects that are aligned to the applied magnetic field and have a mean spacing that is larger than FL spacing. Based on a functional renormalization group analysis in $d = 5 - \epsilon$ dimensions [68], we obtain

the creep exponent $\mu = 1$. This result is in agreement with the one derived in Blatter et al. [2] by other means. The result is expected to apply to the weakly pinned Bose glass phase.

2.6.3 Finite density of strong defects

Here we discuss the analog of the previous subsection in the limit of strong defects, see Sec. 2.5. The ground state degeneracy given by Eq. (2.83) is broken when a current is applied. The system evolves between different ground states via the formation of critical droplets. For small currents $J \ll c_{11}\ell/(B\ell_D^2)$ the critical droplet extends over many defect planes and we obtain the creep exponent $\mu = 3/2$. For moderate currents with $c_{11}\ell/(B\ell_D^2) \ll J \ll v/(\phi_0\xi\ell_D)$ the droplet forms only at a single defect plane and we recover Eq. (2.95) with $\gamma \approx (c_{44}/c_{66})^{1/2}\ell\ell_D JB$, i.e., a creep exponent $\mu = 1$.

We assume that the saddle point solution for u_i with fixed boundary conditions $u_i(\rho \rightarrow 0) = u_i^{(n+1)}$ and $u_i(\rho \rightarrow \infty) = u_i^{(n)}$ obeys Eq. (2.90). At each defect plane, the radius R_i and the center of the droplet can be different. However, it is plausible to assume that in the saddle point configuration the droplet is centered at the same lateral position in each plane and all droplets have the same radius R since the droplet tends to maximize its volume while keeping the surface minimal. Specifically, we assume that the droplet is located between the s th and the $(s+m)$ th defect plane.

The width of the droplet wall for a sufficiently strong defect potential satisfies $w \ll \ell_D$ and $w \ll R$. The precise form of the wall is not important in finding the energy of a domain wall parallel to the defects as well as the bulk energy gain. Hence, we set the width of the droplet to zero which yields for the Fourier transform of the displacement at the i th defect plane

$$\tilde{u}_i(\mathbf{q}) = 2\pi R\ell \frac{J_1(qR)}{q} + u_i^{(n)}(2\pi)^2\delta(\mathbf{q}), \quad (2.101)$$

where J_1 is the Bessel function of the first kind. Due to the transport current we have to add to the Hamiltonian of Eq. (2.81) the additional energy

$$H_{\text{force}} = - \sum_{i=1}^{N_D-1} \int_{x_i}^{x_{i+1}} dx f(x) \left\{ \frac{\tilde{u}_i(\mathbf{0})}{\Delta x_i} (x_{i+1} - x) + \frac{\tilde{u}_{i+1}(\mathbf{0})}{\Delta x_i} (x - x_i) \right\}, \quad (2.102)$$

where $f(x) = (c_{44}/c_{66})^{1/2}J(x)B(x)$. By substituting the Eq. (2.101) into Eq. (2.81), we find that the droplet energy has a different form for $R \gg \ell_D\sqrt{c_{66}/c_{11}}$ and $R \ll \ell_D\sqrt{c_{66}/c_{11}}$.

First we discuss the case $R \gg \ell_D \sqrt{c_{66}/c_{11}}$. The droplet energy reads then

$$E_{\text{drop}} = \Sigma_x R^2 \pi + \Sigma_y 2R\pi m \ell_D - JB\ell R^2 \pi m \ell_D \sqrt{\frac{c_{44}}{c_{66}}}. \quad (2.103)$$

In order to explain and interpret the first term of Eq. (2.103), we consider an excited state with

$$u_i^\pm = \begin{cases} u_i^{(n)} & \text{for } i \leq k \\ u_i^{(n\pm 1)} & \text{for } i > k. \end{cases} \quad (2.104)$$

This state describes a domain wall parallel to the defects. Using Eq. (2.82), it can be shown that for a given disorder realization the energy cost of such wall per unit surface area is

$$\Sigma_x^\pm(k) = c_{11} \sqrt{\frac{c_{44}}{c_{66}}} \frac{\ell^2}{2\Delta x_k} \left[1 \pm 2 \left(\frac{\Delta\alpha_k}{\ell} - \left[\frac{\Delta\alpha_k}{\ell} \right]_G \right) \right]. \quad (2.105)$$

Since the droplet consists of two such walls (see Fig. 2.5), the surface tension in the first term of Eq. (2.103) is given by

$$\Sigma_x = \Sigma_x^+(s-1) + \Sigma_x^-(s+m). \quad (2.106)$$

The droplet takes advantage of fluctuations in the surface tension Σ_x and the lowest value of Σ_x for a droplet of length $L_x = m\ell_D$ is typically of the order $c_{11} \sqrt{c_{44}/c_{66}} \ell^2 / L_x$ when $\ell_D \gg \ell$. We point out that this result is in agreement with the statistical tilt symmetry.

The second term of Eq. (2.103) is the energy cost for the domain wall perpendicular to the defects with surface tension Σ_y . We do not provide here an explicit expression for Σ_y , for the reasons discussed in Sec. 2.5. Note that Σ_y carries information about the strength and density of defect planes. By ignoring the spatial variations of J and B , we get the average bulk energy gain to be given by the last term in Eq. (2.103).

By solving $\partial_m E_{\text{drop}} = 0$ and $\partial_R E_{\text{drop}} = 0$ we determine the radius R^* and length $L_x^* = m^* \ell_D$ of the critical droplet. With this parameters, Eq. (2.103) yields the energy of the critical droplet. We find that this energy leads, up to unimportant prefactors, to the same nonlinear resistivity as in the weak pinning case of Eq. (2.100). This result is valid for sufficiently small currents such that $R^* \gg \ell_D \sqrt{c_{66}/c_{11}}$ and $m^* \gg 1$. The latter condition results from treating m as a continuous variable which is a reasonable approximation for critical droplet that extends across a large number of defect planes. These

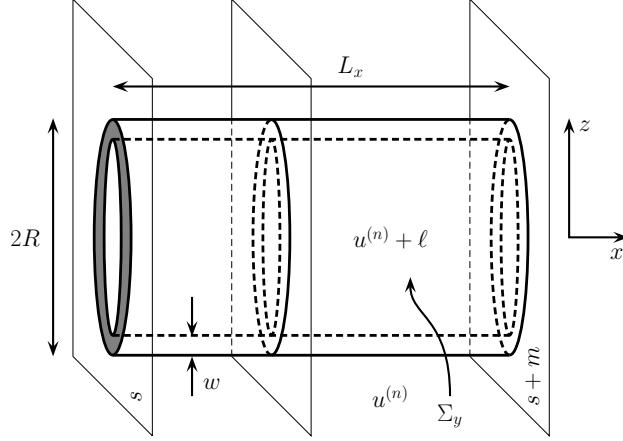


Figure 2.5: Schematic representation of a cylindrically shaped droplet of radius R and length L_x that extends across more than one defect plane. It drives the system into the new metastable state $u^{(n)} + \ell$. Note that domain walls parallel to the defects are wide (not shown here), while the cylindrically shaped domain wall is narrow (of width w).

conditions translate to the requirement $J \ll c_{11}\ell/(B\ell_D^2)$ for the current density.

Next, we shortly discuss the droplet expansion when it reaches the radius R^* and the length L_x^* . By analyzing the Hessian matrix of E_{drop} we find that the eigenvector that points into the direction of the free droplet expansion has a x -component that is much smaller than its ρ -component, i.e., an expansion of the cross-section of the cylinder is favorable over an expansion of its length. In order to describe a potential growth in the x -direction, one has to know the set of numbers $\Sigma_x(i)^\pm$ that depends on the disorder realization. However, the droplet will get stuck between planes with low Σ_x and a further expansion along the x -axis costs energy.

Droplets occur and expand independently across the entire sample. After the FLs have moved in some regions, the boundaries of these regions will be favorable sites for emergence of new droplets [77]. Indeed, after the formation and expansion of a droplet up to the $(i-1)$ th defect plane such that $u_k = u_k^{(n+1)}$ for $k \leq i-1$ and $u_k = u_k^{(n)}$ for $k \geq i$, the new surface tension reads

$$\Sigma_x^+(i-1) = -\Sigma_x^-(i-1) < 0. \quad (2.107)$$

The reason for this result is that after the droplet expansion an additional FLL plane appears with respect to the initial ground state between i th and $(i-1)$ th planes and the FLs are compressed. The formation of a new droplet at the i th plane is favorable because it allows the system to relax into the new ground state configuration between $(i-1)$ th and i th plane. Since the droplet described by Eq. (2.103) has the longest life time, the resistivity is

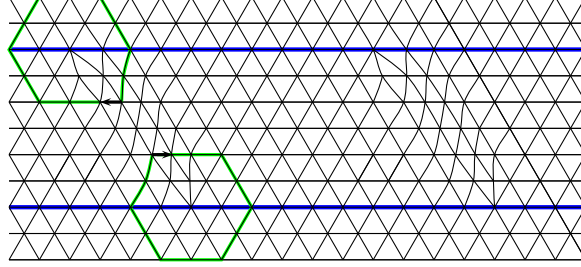


Figure 2.6: (Color online) Array of edge dislocations that is located at the defects (thick blue lines) in order to relax shear strain. The Burgers vector is parallel to the defects.

determined by $\rho \sim \exp(-E_{\text{drop}}^*/T)$, where the critical energy E_{drop}^* is given by Eq. (2.103) evaluated at R^* , L_x^* .

When comparing Eq. (2.100) with the creep exponent $\mu = 1/2$ of the defect free Bragg glass phase, we see that defect planes act as a more efficient source of pinning in stabilizing superconductivity than point impurities. However, we have considered only typical droplets in estimating Σ_x . For system sizes $L \gg \ell_D$ it is likely that rare regions with untypically large Σ_x will appear and in turn determine the resistivity. We leave this problem for further investigations.

Next, we consider the case $R \ll \ell_D \sqrt{c_{66}/c_{11}}$. From the second term of Eq. (2.81) we find that for m defect planes the energy loss given by Eq. (2.92). The first term in Eq. (2.81), that describes the coupling between neighboring defects, provides a much smaller contribution than the second term and can be neglected. Then the defects are effectively decoupled, and the nucleus energy is

$$E_{\text{drop}} = mE_{\text{single}}. \quad (2.108)$$

Here E_{single} is the energy of the droplet that appears in the case of a single defect plane. It is given by Eq. (2.94) with the system size replaced by the mean defect distance ℓ_D . The nucleus energy grows with increasing m so that it is minimal for $m = 1$ and the critical droplet is located at one defect plane only. Nonlinear resistivity is then again given by Eq. (2.95), but with $\gamma \approx (c_{44}/c_{66})^{1/2} \ell \ell_D J B$. This result is valid for intermediate currents $c_{11} \ell / (B \ell_D^2) \ll J \ll v / (\phi_0 \xi \ell_D)$.

2.7 Dislocations

For a finite density of randomly distributed parallel planar defects with the magnetic field aligned to them, and with a mean defect spacing that is larger

than FL spacing, we find a new phase of FLs at low temperatures, the planar glass. We considered mainly a simplified model with a uniaxial displacement field (which is also applicable to a wide class of other systems). Here we comment on possible consequences of this simplification by taking into account also the displacement field u_y parallel to the defects. The part of the defect Hamiltonian that describes the coupling of the defect potential to the slowly varying part of FL density can be eliminated by transforming u_x as described by Eq. (2.78). For strong planar defects each defect plane is occupied by a single FL layer and hence $u_x^{(ni)}(x_i, y, z) = \ell n_i + \alpha_i$ for all y, z in order to maximize the pinning energy gain. Even in the absence of point disorder the displacement u_y does not vanish. This can be seen most easily in the case of isotropic elasticity where the following relations hold

$$\sigma \partial_x u_x = -\partial_y u_y, \quad \sigma = \frac{c_{11} - c_{66}}{c_{11} + c_{66}}. \quad (2.109)$$

Here σ is the Poisson number with $-1 < \sigma < 1$ [52]. The strain $\partial_x u_x$ in the gap between the defects at x_{i+1} and x_i is

$$\partial_x u_x \approx 1 + \frac{v\rho_0}{c_{11}\Delta x_i} + \ell \frac{\Delta n_i}{\Delta x_i}, \quad (2.110)$$

where we used the notation $\Delta A_i = A_{i+1} - A_i$ for a variable A . The difference of the strain $\partial_y u_y$ in neighboring gaps is then

$$\Delta \partial_y u_y \approx -\sigma \ell \left[\frac{\Delta n_{i+1}}{\Delta x_{i+1}} - \frac{\Delta n_i}{\Delta x_i} + \frac{v\rho_0}{c_{11}\ell} \left(\frac{1}{\Delta x_{i+1}} - \frac{1}{\Delta x_i} \right) \right], \quad (2.111)$$

which is of the order $\pm\sigma\ell/\ell_D$. On the scale L_y this implies $\Delta u_y \sim \pm\sigma\ell L_y/\ell_D$. To avoid a diverging shear energy, dislocations with a Burgers vector parallel to the y -direction occur at the defect planes (see Fig. 2.6). Their distance along the y -direction is of the order ℓ_D/σ . The energy of a pair of edge dislocations with anti-parallel Burgers vectors at a distance ℓ_D is [78]

$$E_{\text{edge}} \approx \frac{c_{66}}{2\pi} a^2 L_z \ln \left(\frac{\ell_D}{a} \right). \quad (2.112)$$

This energy has to be compared with the energy gain from the defects which is of the order

$$E_D \approx -\frac{\ell}{\sigma\xi} L_z v \ell_D \rho_0. \quad (2.113)$$

Hence for $\sigma c_{66} a^3 \xi \ll \ell_D v$ the energy of the dislocations is overcompensated by the defect planes and dislocations will be present.

In general, the network of additional FLL sheets spanned by the dislocations will be complicated. The network follows from the solution of the equations of two-dimensional elasticity with the boundary condition $u_x(x_i, y, z) \equiv u_x^{(n_i)}(x_i, y, z)$ and the dislocation density $b_y(x_i, y)$ at each defect. The energy has to be minimized first with respect to $b_y(x_i, y)$ and then with respect to n_i [79]. The resulting state is completely ordered along the z -direction. It is also ordered in the sense that the interface tensions Σ_z and Σ_y are nonzero. A change in the boundary conditions with $u_x(x, y, z \rightarrow \infty) = u_x(x, y, z \rightarrow 0) + \ell$ increases again the energy. Hence the transverse Meissner effect as well as the resistance against FLL shearing perpendicular to the defects is still present. Bond-orientational order [80] persists since disclination pairs remain bound in the cores of the edge dislocations.

Since the Burgers vectors of the dislocations are always parallel to the defect planes, creep along the x -direction is not facilitated. Under the assumption that the distribution of Σ_x is uniform even in the presence of dislocations we recover the creep law of Eq. (2.100). To describe creep parallel to the defects one has to take into account the interaction between dislocation, a problem not considered so far [16, 81]. We leave this for further studies. For weak pinning qualitatively the same behavior can be expected on scales $L_x \gg L_D$, in particular if the defect potential flows under the renormalization group to strong coupling. If the sample exhibits two orthogonal families of (non-intersecting) defects, long-range order in the x and y direction is destroyed even without point impurities on scales larger than L_D . The creep is then limited by the slowest mechanism and hence Eq. (2.100) is likely to be valid for all current directions in the xy -plane.

2.8 Conclusions

In this chapter of the thesis we have studied the influence of a single planar defect on the stability of the Bragg glass phase and the effect of many defect planes on the FLL. To conclude, we have found that the necessary condition for a weak planar defect to become a relevant perturbation in the Bragg glass phase is that it is oriented parallel to the magnetic field. In this case, its influence on the Bragg glass phase can be characterized by the value of a single parameter $g \equiv \frac{3}{8}\eta(a/\ell)^2$ which depends both on the exponent η describing the decay of the positional correlations in the Bragg glass phase and on the orientation of the defect with respect to the FLL. a and ℓ are the mean spacing of the FLs in absence of the defect plane and the distance between the lattice planes of the Abrikosov lattice, parallel to the defect, respectively. A weak defect turned out to be relevant if $g < 1$, i.e., if it is

parallel to one of the main crystallographic planes of the FLL.

Studying the order of the FLs around a defect we have found that the FL density averaged over point impurities shows periodic order with an amplitude decaying as a power law with the normal distance to the defect plane. For a relevant defect on scales larger than L_v , the exponent controlling the power law is g . For the definition of L_v , see Eq. (2.40). For $g > 1$ a weak defect is irrelevant (in the sense of the renormalization group approach) and the density profile decays faster, with a larger exponent $2g - 1 > 1$, on scales larger than the positional correlation length L_a . For a weak defect tilted against the applied magnetic field we have found that FL density oscillations decay exponentially fast. We have investigated also the dynamics of FL bundles perpendicular to the relevant defect for small current densities $J \rightarrow 0$. The nonlinear resistivity is $\rho(J) \sim \exp\left[-\frac{C_1}{J} \left(\log \frac{C_2}{J}\right)^2\right]$ where C_1 and C_2 depend on various parameters such as temperature, magnetic induction, density and strength of point impurities as well as the strength of the defect plane. We concluded that a single relevant defect plane slows down the FL creep in comparison to the Bragg glass phase.

There are interesting connections of some of the aspects of our results to related two-dimensional classical or one-dimensional quantum models. A single planar defect in the Bragg glass phase resembles the presence of a single columnar defect in a FLL confined to a plane [60, 61, 82] or a frozen impurity in a Luttinger liquid [62, 83]. In all three cases the bulk phases on both sides of the defect are characterized by logarithmically diverging displacement correlations. The parameter g plays the role of a temperature in the two-dimensional classical case and of the Luttinger liquid parameter in the one-dimensional quantum case. The periodic order seen around the defect plane has its counterpart in Friedel oscillations around an impurity in Luttinger liquids. Whereas in the one- (two-) dimensional case the relevance of an impurity is controlled by tuning the interaction strength (temperature), in the present case a change in g can be accomplished by changing the orientation of the defect with respect to the FLL. Transport properties of our system are, however, different from the ones in the related systems.

In this chapter we have also examined the effect of a finite density of randomly distributed parallel planar defects on the FLL at low temperatures with the magnetic field aligned parallel to the defects. We have considered the case when the mean defect spacing is much greater than FL spacing. Our results may be directly applicable to a wide class of other systems with planar defects, like a stack of membranes under tension, charge density waves [18], domain walls in magnets and incommensurate systems [19], since we consider a simplified model with a uniaxial displacement field perpendicu-

lar to the defects. We have found a new phase, the planar glass, that is characterized by (i) diverging shear (tilt) modulus that determines the energy cost for a shearing (tilting) of the FLL in the direction perpendicular to the planes; (ii) finite compressibility; (iii) sample to sample fluctuations of the longitudinal magnetic susceptibility; (iv) an exponential decay of the positional correlations in the direction perpendicular to the defects and (v) a creep exponent $\mu = 3/2$ for creep in the direction perpendicular to the defects for small currents $J \rightarrow 0$. The planar glass is different from the Bragg glass and the Bose glass phase and from the phase found for equally spaced defects [84]. The planar glass is stable over a finite range of tipping angles of the applied magnetic field away from the direction parallel to the planar defects, i.e., it is characterized by a transverse Meissner effect. Similarly, the planar glass is characterized by a resistance against shear deformations that are perpendicular to the defects. Naturally, realistic samples contain both point and correlated disorder (like columnar and/or planar defects). We have found that the planar glass is stable against both weak point and weak columnar disorder. The schematic phase diagram is shown in Fig. 2.1. When we considered a vector displacement field, we have additionally found that strong disorder enforces arrays of dislocations in order to relax shear strain. They are located at the defects with a Burgers vector parallel to the defects. We have argued that the main properties of the planar glass remain unchanged by dislocations.

2.A Replica Hamiltonian for the defect free system

In this appendix the Hamiltonian for defect-free system is derived, using the replica approach for averaging over point impurities. The pinning energy of randomly distributed impurities reads (see Sec. 2.2)

$$\mathcal{H}_P = \int d^3\mathbf{r} V_P(\mathbf{r})\rho_0 \left\{ -\nabla_{\mathbf{x}}\mathbf{u}(\mathbf{r}) + \sum_{\mathbf{G}\neq 0} e^{i\mathbf{G}[\mathbf{x}-\mathbf{u}(\mathbf{r})]} \right\}, \quad (2.114)$$

where $\mathbf{x} = (x, y)$. If the system is characterized by a roughness exponent ζ , displacements vary with the scale L as $u \sim L^\zeta$, $\zeta < 1$. The elastic energy scales as $L^{d-2+2\zeta}$, and the first and second terms of Eq. (2.114) scale as $L^{(d-2+2\zeta)/2}$ and $L^{d/2}$, respectively. These simple scaling arguments show that the coupling of the divergence of the displacement field to the disorder potential is irrelevant with respect to the elastic energy in $d > 2$ and the second term of Eq. (2.114) is relevant for $d < 4$. Since we are interested

in the behavior on large length scales in $d = 3$ dimensions, we can neglect the first term of Eq. (2.114). After performing the disorder average, the replicated pinning energy reads

$$\begin{aligned}
\mathcal{H}_P^n &\approx -\frac{v_p^2 n_{\text{imp}} \rho_0^2}{2T} \sum_{\alpha, \beta=1}^n \int_{\mathbf{r}, \mathbf{r}'} \delta_\xi(\mathbf{x} - \mathbf{x}') \delta(z - z') \\
&\quad \sum_{\mathbf{G}, \mathbf{G}' \neq 0} e^{i\mathbf{G}[\mathbf{x} - \mathbf{u}^\alpha(\mathbf{r})] + i\mathbf{G}'[\mathbf{x}' - \mathbf{u}^\beta(\mathbf{r}')] } \\
&= -\frac{v_p^2 n_{\text{imp}} \rho_0^2}{2T} \sum_{\alpha, \beta=1}^n \int_{z, \mathbf{x}} \sum_{\mathbf{G} \neq 0} e^{i\mathbf{G}[\mathbf{x} - \mathbf{u}^\alpha(\mathbf{x}, z)]} \\
&\quad \sum_{\mathbf{G}' \neq 0} \int_{\mathbf{x}_r} \delta_\xi(\mathbf{x}_r) e^{i\mathbf{G}'[\mathbf{x} + \mathbf{x}_r - \mathbf{u}^\beta(\mathbf{x} + \mathbf{x}_r, z)]} \\
&\approx -\frac{v_p^2 n_{\text{imp}} \rho_0^2}{2T} \sum_{\alpha, \beta=1}^n \int_{z, \mathbf{x}} \sum_{\mathbf{G}, \mathbf{G}' \neq 0} e^{i\mathbf{x}(\mathbf{G} + \mathbf{G}')} \\
&\quad e^{-i[\mathbf{G}\mathbf{u}^\alpha(\mathbf{x}, z) + \mathbf{G}'\mathbf{u}^\beta(\mathbf{x}, z)]} \delta_{\xi-1}(\mathbf{G}'). \tag{2.115}
\end{aligned}$$

Using the relative coordinate $\mathbf{x}_r = \mathbf{x}' - \mathbf{x}$ and the fact that $\delta_\xi(\mathbf{x}_r)$ is nonzero only for $|\mathbf{x}_r| \leq \xi$, we approximate the slowly varying displacement field as $\mathbf{u}^\beta(\mathbf{x} + \mathbf{x}_r, z) \approx \mathbf{u}^\beta(\mathbf{x}, z)$, where $\delta_{\xi-1}(\mathbf{G})$ is the Fourier transform of $\delta_\xi(\mathbf{x})$. Since the displacement field varies slowly on the scale of the FLL constant, the integral over \mathbf{x} vanishes for all combinations of \mathbf{G} and \mathbf{G}' except for $\mathbf{G} = -\mathbf{G}'$ when the oscillatory factor $e^{i\mathbf{x}(\mathbf{G} + \mathbf{G}')}$ becomes one. The replicated pinning Hamiltonian can now be written as

$$\begin{aligned}
\mathcal{H}_P^n &= -\frac{v_p^2 n_{\text{imp}} \rho_0^2}{2T} \sum_{\alpha, \beta=1}^n \int_{\mathbf{r}} \sum_{\mathbf{G} \neq 0} e^{i\mathbf{G}[\mathbf{u}^\alpha(\mathbf{r}) - \mathbf{u}^\beta(\mathbf{r})]} \delta_{\xi-1}(\mathbf{G}) \\
&= -\frac{1}{2T} \sum_{\alpha, \beta=1}^n \int_{\mathbf{r}} R_P[\mathbf{u}^\alpha(\mathbf{r}) - \mathbf{u}^\beta(\mathbf{r})]. \tag{2.116}
\end{aligned}$$

2.B Effective Hamiltonian on the defect plane

In this appendix we present a functional integral approach for the derivation of the effective Hamiltonian on the defect plane for the case of a FLL with point impurities and a single defect plane. Since the pinning energy of the planar defect involves only the displacement perpendicular to the defect, u_x , we integrate out u_x outside the defect and u_y across the entire sample. The

partition function can be written as

$$Z = \int \mathcal{D}\varphi(\mathbf{r}_D) \int \mathcal{D}\mathbf{u}(\mathbf{r}) e^{-\frac{\mathcal{H}}{T}} \prod_{\mathbf{r}_D} \delta[u_x(\mathbf{r}_D) - \varphi(\mathbf{r}_D)], \quad (2.117)$$

where $\mathcal{H} = \mathcal{H}_0 + \mathcal{H}_P + \mathcal{H}_D$. The displacement at the defect is constrained to be $u_x(\mathbf{r}_D) = \varphi(\mathbf{r}_D)$ and this constraint is implemented by δ -functions in the functional integral. The defect is aligned to the magnetic field and \mathbf{r}_D is given by Eq. (2.21). After averaging over point impurities we get

$$\begin{aligned} \overline{Z}^n &= \int \mathcal{D}[\varphi^\alpha(\mathbf{r}_D)] e^{-\sum_\alpha \frac{\mathcal{H}_D(\varphi^\alpha)}{T}} \int \mathcal{D}[\mathbf{u}^\alpha(\mathbf{r})] e^{-\frac{\mathcal{H}_0^n}{T}} \prod_{\alpha, \mathbf{r}_D} \delta[u_x^\alpha(\mathbf{r}_D) - \varphi^\alpha(\mathbf{r}_D)] \\ &= \int \mathcal{D}[\varphi^\alpha(\mathbf{r}_D)] e^{-\frac{\mathcal{H}_{\text{eff}}^n(\varphi^\alpha)}{T}}, \end{aligned} \quad (2.118)$$

where \mathcal{H}_0^n is given by Eq. (2.17) and $\int \mathcal{D}[\varphi^\alpha(\mathbf{r}_D)] = \prod_{\alpha=1}^n \int \mathcal{D}\varphi^\alpha(\mathbf{r}_D)$. Using the function integral representation

$$\prod_{\alpha, \mathbf{r}_D} \delta[u_x^\alpha(\mathbf{r}_D) - \varphi^\alpha(\mathbf{r}_D)] = \int \mathcal{D}[\Lambda^\alpha(\mathbf{r}_D)] e^{i \sum_\alpha \int_{\mathbf{r}_D} \Lambda^\alpha(\mathbf{r}_D) [u_x^\alpha(\mathbf{r}_D) - \varphi^\alpha(\mathbf{r}_D)]} \quad (2.119)$$

of the δ -function, we obtain for the effective replica Hamiltonian $\mathcal{H}_{\text{eff}}^n$ the equation

$$e^{-\frac{\mathcal{H}_{\text{eff}}^n}{T}} = e^{-\sum_\alpha \frac{\mathcal{H}_D(\varphi^\alpha)}{T}} \int \mathcal{D}[\Lambda^\alpha(\mathbf{r}_D)] \left\langle e^{i \sum_\alpha \int_{\mathbf{r}_D} \Lambda^\alpha(\mathbf{r}_D) [u_x^\alpha(\mathbf{r}_D) - \varphi^\alpha(\mathbf{r}_D)]} \right\rangle_{\mathcal{H}_0^n} \quad (2.120)$$

up to a constant. Here $\langle \dots \rangle_{\mathcal{H}}$ denotes the thermal average with respect to \mathcal{H} . For this average we obtain

$$\begin{aligned} \left\langle e^{i \sum_\alpha \int_{\mathbf{r}_D} \Lambda^\alpha(\mathbf{r}_D) [u_x^\alpha(\mathbf{r}_D) - \varphi^\alpha(\mathbf{r}_D)]} \right\rangle_{\mathcal{H}_0^n} &= \\ e^{-i \sum_\alpha \int_{\mathbf{r}_D} \Lambda^\alpha(\mathbf{r}_D) \varphi^\alpha(\mathbf{r}_D)} e^{-\sum_{\alpha, \beta} \frac{1}{2} \int_{\mathbf{r}_{D1}, \mathbf{r}_{D2}} \Lambda^\alpha(\mathbf{r}_{D1}) \Lambda^\beta(\mathbf{r}_{D2}) T \mathcal{G}_{xx}^{\alpha, \beta}(\mathbf{r}_{D1} - \mathbf{r}_{D2})}, \end{aligned} \quad (2.121)$$

where $\langle \tilde{u}_x^\alpha(\mathbf{q}) \tilde{u}_x^\beta(\mathbf{q}') \rangle_{\mathcal{H}_0^n} = T(2\pi)^d \tilde{\mathcal{G}}_{xx}^{\alpha, \beta}(\mathbf{q}) \delta(\mathbf{q} + \mathbf{q}')$. The effective Hamiltonian reads

$$\begin{aligned} \mathcal{H}_{\text{eff}}^n &= - \sum_\alpha \sum_{k>0} 2v_k \rho_0 \int d\mathbf{r}_D \cos \{k G_D [\delta - \varphi^\alpha(\mathbf{r}_D)]\} \\ &\quad + \frac{1}{2} \sum_{\alpha, \beta} \frac{1}{(2\pi)^{d-1}} \int d^{d-1} \mathbf{q} \varphi^\alpha(\mathbf{q}) \tilde{\mathcal{Q}}_{\alpha, \beta}^{-1}(\mathbf{q}) \varphi^\beta(-\mathbf{q}), \end{aligned} \quad (2.122)$$

where $\tilde{\mathcal{Q}}(\mathbf{q}) = \tilde{\mathcal{G}}_{xx}(x=0, \mathbf{q})$ and here \mathbf{q} is the in-plane momentum.

2.C Density oscillations for an irrelevant defect plane

In this appendix we analyze the thermal and disorder average of the FL density around an irrelevant defect plane in the presence of point impurities by perturbation theory in v . For the local density variations we have

$$\overline{\langle \delta\rho[\mathbf{r}, \mathbf{u}(\mathbf{r})] \rangle} = \lim_{n \rightarrow 0} \int \mathcal{D}[\mathbf{u}^\alpha] \delta\rho[\mathbf{r}, \mathbf{u}_1(\mathbf{r})] e^{-\beta[\mathcal{H}_0^n + \sum_\alpha \mathcal{H}_D(u_x^\alpha)]}, \quad (2.123)$$

where $\delta\rho[\mathbf{r}, \mathbf{u}(\mathbf{r})] = \rho[\mathbf{r}, \mathbf{u}(\mathbf{r})] - \rho_0$ and $u_1(\mathbf{r})$ is the displacement field with replica index $\alpha = 1$. To the zeroth order we get

$$\overline{\langle \delta\rho[\mathbf{r}, \mathbf{u}(\mathbf{r})] \rangle} = \lim_{n \rightarrow 0} \langle \delta\rho[\mathbf{r}, \mathbf{u}_1(\mathbf{r})] \rangle_{\mathcal{H}_0^n} = 0, \quad (2.124)$$

since $\langle u^2(\mathbf{r}) \rangle_{\mathcal{H}_0^n} = \infty$. To capture the physics correctly, we have to calculate mean FL density at least to first order in v (see the discussion in Sec. 2.3.4),

$$\begin{aligned} \langle \delta\rho[\mathbf{r}, \mathbf{u}(\mathbf{r})] \rangle &= -\beta \lim_{n \rightarrow 0} \sum_{\alpha=1}^n \langle \delta\rho[\mathbf{r}, \mathbf{u}_1(\mathbf{r})] \mathcal{H}_D(\mathbf{u}^\alpha) \rangle_{\mathcal{H}_0^n} \\ &= \beta \lim_{n \rightarrow 0} \left\{ \langle \delta\rho[\mathbf{r}, \mathbf{u}_1(\mathbf{r})] \mathcal{H}_D(\mathbf{u}_2) \rangle_{\mathcal{H}_0^n} - \langle \delta\rho[\mathbf{r}, \mathbf{u}_1(\mathbf{r})] \mathcal{H}_D(\mathbf{u}_1) \rangle_{\mathcal{H}_0^n} \right\}. \end{aligned} \quad (2.125)$$

$u_2(\mathbf{r})$ is the displacement field with replica index $\alpha = 2$. First, we obtain the average of the long wavelength part of the FL density. It can be shown that

$$\begin{aligned} &\langle \nabla_{\mathbf{x}} \mathbf{u}^\beta(\mathbf{r}) \cos[G_D \delta - \mathbf{G}_D \mathbf{u}^\alpha(\mathbf{r}_D)] \rangle_{\mathcal{H}_0^n} = \\ &\nabla_{\mathbf{x}} \left\{ T \sin(G_D \delta) \langle \cos[\mathbf{G}_D \mathbf{u}^\alpha(\mathbf{r}_D)] \rangle_{\mathcal{H}_0^n} \mathcal{G}^{\alpha, \beta}(\mathbf{r}_D - \mathbf{r}) | \mathbf{G}_D \right\} \\ &\quad - T \cos(G_D \delta) \langle \sin[\mathbf{G}_D \mathbf{u}^\alpha(\mathbf{r}_D)] \rangle_{\mathcal{H}_0^n} \mathcal{G}^{\alpha, \beta}(\mathbf{r}_D - \mathbf{r}) | \mathbf{G}_D \left. \right\}, \end{aligned} \quad (2.126)$$

where $\mathbf{r} = (\mathbf{x}, z)$ and $\mathcal{G}^{\alpha, \beta}(\mathbf{r})$ is the propagator given by Eq. (2.18). Since $\langle \sin[\mathbf{G}_D \mathbf{u}^\alpha(\mathbf{r}_D)] \rangle_{\mathcal{H}_0^n} = \langle \cos[\mathbf{G}_D \mathbf{u}^\alpha(\mathbf{r}_D)] \rangle_{\mathcal{H}_0^n} = 0$ this contribution vanishes.

A finite difference between the expression $\langle \delta\rho(\mathbf{u}_1) \mathcal{H}_D(\mathbf{u}_2) \rangle_{\mathcal{H}_0^n}$ and the expression $\langle \delta\rho(\mathbf{u}_1) \mathcal{H}_D(\mathbf{u}_1) \rangle_{\mathcal{H}_0^n}$ appearing in Eq. (2.125) can result from the thermal part of the propagator that is diagonal in replica indices,

$$\begin{aligned} &\lim_{n \rightarrow 0} \langle \delta\rho[\mathbf{u}^\alpha(\mathbf{r})] \mathcal{H}_D(\mathbf{u}^\beta) \rangle_{\mathcal{H}_0^n} = \\ &\lim_{n \rightarrow 0} \left\{ \frac{2v_1 \rho_0^2}{T} \int_{\mathbf{r}_D} \sum_{\mathbf{G} \neq \mathbf{0}} e^{i\mathbf{G} \cdot \mathbf{x}} \left\langle e^{-i\mathbf{G} \cdot \mathbf{u}^\alpha(\mathbf{r})} \cos\{G_D[\delta - u_x^\beta(\mathbf{r}_D)]\} \right\rangle_{\mathcal{H}_0^n} \right\} = \\ &\lim_{n \rightarrow 0} \left\{ \frac{v_1 \rho_0^2}{T} \int_{\mathbf{r}_D} \sum_{\mathbf{G} \neq \mathbf{0}} e^{i\mathbf{G} \cdot \mathbf{x}} (e^{iG_D \delta} I_+ + e^{-iG_D \delta} I_-) \right\}, \end{aligned} \quad (2.127)$$

where $I_{\pm} = e^{-\frac{1}{2}\langle[\mathbf{G}\cdot\mathbf{u}^{\alpha}(\mathbf{r})\pm\mathbf{G}_D\cdot\mathbf{u}^{\beta}(\mathbf{r}_D)]^2\rangle_{\mathcal{H}_0^n}}$ and $\int_{\mathbf{r}_D}$ denotes the integration along the defect plane. Analyzing I_+ (I_-), we conclude that it is nonzero only for $\mathbf{G} = -\mathbf{G}_D$ ($\mathbf{G} = \mathbf{G}_D$) and

$$I_{\pm} \approx e^{\frac{G_D^2 T}{4\pi c} \frac{\delta_{\alpha,\beta}}{|\mathbf{r}-\mathbf{r}_D|}} \left(\frac{L_a}{|\mathbf{r}-\mathbf{r}_D|} \right)^{2g}. \quad (2.128)$$

This yields

$$\begin{aligned} \overline{\langle\delta\rho(\mathbf{r})\rangle} &\approx \frac{v_1\rho_0^2}{T} (e^{-iG_D(x-\delta)} + e^{iG_D(x-\delta)}) \int_{\mathbf{r}_D} \left(\frac{L_a}{|\mathbf{r}-\mathbf{r}_D|} \right)^{2g} \left(e^{\frac{G_D^2 T}{4\pi c} \frac{1}{|\mathbf{r}-\mathbf{r}_D|}} - 1 \right) \\ &\approx \frac{4\pi v_1\rho_0^2 L_a^2}{T} \cos[G_D(x-\delta)] \left(\frac{G_D^2 T}{2\pi c} \right)^{2-2g} F\left(\frac{G_D^2 T}{4\pi c|x-\delta|} \right), \end{aligned} \quad (2.129)$$

where $F(x) = \sum_{n=1}^{\infty} \frac{1}{n!} \frac{x^{2g+n-2}}{2g+n-2}$. For very small temperatures the main contribution is

$$\overline{\langle\delta\rho(\mathbf{r})\rangle} \approx \frac{v_1\rho_0^2 G_D^2 L_a}{c(2g-1)} \cos[G_D(x-\delta)] \left(\frac{L_a}{|x-\delta|} \right)^{2g-1} + \mathcal{O}(T). \quad (2.130)$$

The result captures the large scale behavior since it is valid on scales larger than $L \geq L_a$. Here v_1 denotes the effective defect strength measured on the scale L_a , and $|x-\delta|$ is the distance to the defect plane. Additional contributions to Eq. (2.130), coming from the higher harmonics in \mathcal{H}_D , are less important since they are proportional to the coefficients v_k at scale $L = L_a$ and their amplitudes decay as $|x-\delta|^{-2k^2g+1}$ with integer $k \geq 2$.

2.D Density oscillations for a relevant defect plane

In this appendix we study the displacement correlation functions and average FL density profile for a relevant defect plane in the presence of point impurities. As shown in the main text above, on sufficiently large length scales pinning effects can be taken into account through the boundary condition $u_x(\mathbf{r}_D) = 0$ at the defect plane. For simplicity we take the defect to be at the coordinate origin, i.e., we set $\delta = 0$. First we calculate the generating function

$$\overline{Z^n[\mathbf{j}^{\alpha}(\mathbf{r})]} = \int \mathcal{D}[\mathbf{u}^{\alpha}] e^{-\frac{\mathcal{H}_0^n[\mathbf{u}^{\alpha}]}{T}} e^{\sum_{\alpha} \int_{\mathbf{r}} \mathbf{j}^{\alpha}(\mathbf{r}) \mathbf{u}^{\alpha}(\mathbf{r})} \prod_{\alpha, \mathbf{r}_D} \delta[u_x^{\alpha}(\mathbf{r}_D)]. \quad (2.131)$$

Using the representation of the delta-function of Eq. (2.119) we get

$$\overline{Z^n[\mathbf{j}^\alpha(\mathbf{r})]} = e^{\frac{T}{2} \sum_{\alpha,\beta} \int_{\mathbf{r}_1, \mathbf{r}_2} \mathbf{j}^\alpha(\mathbf{r}_1) \Gamma^{\alpha,\beta}(\mathbf{r}_1, \mathbf{r}_2) \mathbf{j}^\beta(\mathbf{r}_2)}, \quad (2.132)$$

where

$$\begin{aligned} \Gamma^{\alpha\beta}(\mathbf{r}_1, \mathbf{r}_2) &= \mathcal{G}^{\alpha\beta}(\mathbf{r}_1 - \mathbf{r}_2) \\ &- \sum_{\gamma\kappa} \int_{\mathbf{r}_{D1}\mathbf{r}_{D2}} \mathcal{G}^{\alpha\gamma}(\mathbf{r}_1 - \mathbf{r}_{D1}) | \hat{\mathbf{x}} \rangle \tilde{\mathcal{Q}}_{\gamma\kappa}^{-1}(\mathbf{r}_{D1} - \mathbf{r}_{D2}) \langle \hat{\mathbf{x}} | \mathcal{G}^{\kappa\beta}(\mathbf{r}_2 - \mathbf{r}_{D2}) \end{aligned} \quad (2.133)$$

and $\tilde{\mathcal{Q}}$ is given by Eq. (2.33) and $\mathcal{G}^{\alpha,\beta}$ is the inverse of $\mathcal{G}_{\alpha,\beta}^{-1}$ given by Eq. (2.18). The displacement correlation function is given by the relation $\overline{\langle \mathbf{u}(\mathbf{r}) \mathbf{u}(\mathbf{r}') \rangle} = \lim_{n \rightarrow 0} \frac{\delta^2 \overline{Z^n}}{\delta \mathbf{j}^1(\mathbf{r}) \delta \mathbf{j}^1(\mathbf{r}')}\Big|_{\mathbf{j}^\alpha=0}$. Denoting by \mathbf{q} the in-plane momentum, we get in momentum space

$$\tilde{\mathcal{G}}_{\text{pin},ij}(x, x; \mathbf{q}) = \lim_{n \rightarrow 0} \left[\tilde{\mathcal{G}}_{ij}^{11}(0, \mathbf{q}) - \sum_{\alpha\gamma} \tilde{\mathcal{G}}_{ix}^{1\alpha}(|x|, \mathbf{q}) \tilde{\mathcal{Q}}_{\alpha\gamma}^{-1}(\mathbf{q}) \tilde{\mathcal{G}}_{xj}^{1\gamma}(|x|, -\mathbf{q}) \right], \quad (2.134)$$

where $\mathcal{G}_{\text{pin},ij}(x, x'; \mathbf{r}_\parallel - \mathbf{r}'_\parallel) = T^{-1} \overline{\langle u_i(\mathbf{r}) u_j(\mathbf{r}') \rangle}$ with $\mathbf{r} = (x, \mathbf{r}_\parallel)$. The indices i, j take the values x, y . All propagators and their inverse that appear in the previous equations have the form $\mathbf{X}_{\alpha,\beta} = \delta_{\alpha,\beta} \mathbf{X}_d + \mathbf{X}_n$, where α, β are replica indices. The only nonzero contribution to the second term of Eq. (2.134) comes from the product of all "diagonal" parts (\mathbf{X}_d) of the propagators or only one "nondiagonal" (\mathbf{X}_n) and two diagonal (in replica indices) in the limit $n \rightarrow 0$. Denoting by $X_{ij,a} = \lim_{n \rightarrow 0} \langle \hat{i} | \mathbf{X}_a | \hat{j} \rangle$, where $a = d, n$, one has

$$\begin{aligned} \tilde{\mathcal{G}}_{\text{pin},ij}(x, x; \mathbf{q}) &= \tilde{\mathcal{G}}_{ij,d}(0, \mathbf{q}) - \tilde{\mathcal{G}}_{ix,d}(|x|, \mathbf{q}) \tilde{\mathcal{G}}_{jx,d}(|x|, \mathbf{q}) \tilde{\mathcal{Q}}_d^{-1}(\mathbf{q}) \\ &+ \tilde{\mathcal{G}}_{ij,n}(0, \mathbf{q}) - \tilde{\mathcal{G}}_{ix,d}(|x|, \mathbf{q}) \tilde{\mathcal{G}}_{jx,d}(|x|, \mathbf{q}) \tilde{\mathcal{Q}}_n^{-1}(\mathbf{q}) \\ &+ \tilde{\mathcal{Q}}_d^{-1}(\mathbf{q}) \tilde{\mathcal{G}}_{jx,n}(|x|, \mathbf{q}) \tilde{\mathcal{G}}_{ix,d}(|x|, \mathbf{q}) \\ &+ \tilde{\mathcal{Q}}_d^{-1}(\mathbf{q}) \tilde{\mathcal{G}}_{ix,n}(|x|, \mathbf{q}) \tilde{\mathcal{G}}_{jx,d}(|x|, \mathbf{q}). \end{aligned} \quad (2.135)$$

For isotropic elasticity the relation

$$\tilde{\mathcal{G}}_{ix,d}(|x|, \mathbf{q}) \tilde{\mathcal{G}}_{jx,d}(|x|, \mathbf{q}) \tilde{\mathcal{Q}}_d^{-1}(\mathbf{q}) = (\hat{\mathbf{x}} \cdot \hat{\mathbf{i}})(\hat{\mathbf{x}} \cdot \hat{\mathbf{j}}) \tilde{\mathcal{G}}_{ij,d}(2|x|, \mathbf{q}) \quad (2.136)$$

holds. After integrating the terms of the second and the third line of Eq. (2.135) over \mathbf{q} we find that the displacement correlations on scales larger than L_v (2.40) read

$$\overline{\langle u_i(\mathbf{r}) u_j(\mathbf{r}') \rangle} = \lim_{n \rightarrow 0} \left\{ T \mathcal{G}_{ij}^{11}(0, \mathbf{0}) - T (\hat{\mathbf{x}} \cdot \hat{\mathbf{i}})(\hat{\mathbf{x}} \cdot \hat{\mathbf{j}}) \mathcal{G}_{xx}^{11}(2|x|, \mathbf{0}) \right\}. \quad (2.137)$$

Next, we shall calculate the disorder and thermal average of the FL density

$$\overline{\langle \delta \rho(\mathbf{r}) \rangle} = \rho_0 \sum_{\mathbf{G} \neq 0} e^{i\mathbf{G}\mathbf{x}} \overline{\langle e^{-i\mathbf{G}\mathbf{u}} \rangle}, \quad (2.138)$$

using

$$\overline{\langle e^{-i\mathbf{G}\mathbf{u}} \rangle} = \lim_{n \rightarrow 0} \langle e^{-i\mathbf{G}\mathbf{u}_1} \rangle = \lim_{n \rightarrow 0} e^{-\frac{1}{2} \langle (\mathbf{G}\mathbf{u}_1(\mathbf{r}))^2 \rangle} \quad (2.139)$$

and

$$\lim_{n \rightarrow 0} \langle [\mathbf{G}\mathbf{u}_1(\mathbf{r})]^2 \rangle = \lim_{n \rightarrow 0} T [G^2 \mathcal{G}_{xx}^{11}(\mathbf{0}) - (\mathbf{G} \cdot \hat{\mathbf{x}})^2 \mathcal{G}_{xx}^{11}(2|x|, \mathbf{0})]. \quad (2.140)$$

Since $\lim_{n \rightarrow 0} \mathcal{G}_{xx}^{11}(\mathbf{0})$ is divergent we conclude that only terms with a reciprocal vector \mathbf{G} perpendicular to the defect plane contribute in Eq. (2.138) and

$$\overline{\langle \delta \rho(\mathbf{r}) \rangle} = 2\rho_0 \sum_{m>0} \cos(mG_D x) \left(\frac{L_v}{|x|} \right)^{m^2 g}, \quad (2.141)$$

where m is an integer number.

2.E Sample-to-sample fluctuations of the magnetic susceptibility

In this appendix we examine the influence of planar defects on the longitudinal magnetic susceptibility. An infinitesimal change in the longitudinal magnetic field $\delta H_z \hat{\mathbf{z}}$ changes the Hamiltonian of Eq. (2.45) in the case of a uniaxial displacement field perpendicular to the defects by

$$\delta \mathcal{H} = -\frac{\phi_0 \rho_0}{4\pi} \int d^3 r \delta H_z \partial_x u. \quad (2.142)$$

Since the change of the magnetic induction is $B = \rho_0 \phi_0 \partial_x u$, the longitudinal magnetic susceptibility reads

$$\chi = \rho_0 \phi_0 \frac{\partial \langle \partial_x u \rangle}{\partial \delta H_z} = -\frac{4\pi}{V} \frac{\partial^2 F}{\partial \delta H_z^2}, \quad (2.143)$$

where F is the free energy. It is convenient to consider a generalization of this model to d dimensions where \mathbf{x} is a $d - 2$ -dimensional vector and x_1 is

the component of \mathbf{x} in the direction of the displacement u . Applying the transformation $u \rightarrow u + hx_1/c_{11}$, the additional term given by Eq. (2.142) can be shifted away yielding

$$\mathcal{H}(h, u) = \mathcal{H}_0(u) - \frac{h^2}{2c_{11}}V + \mathcal{H}_D(u + hx_1/c_{11}), \quad (2.144)$$

where $V = L_x^{d-2}L_zL_y$ and $h = \delta H_z \rho_0 \phi_0 / (4\pi)$. The pinning energy of planar defects \mathcal{H}_D can be written as

$$\begin{aligned} \mathcal{H}_D(u) &= \int d\mathbf{r} V_D(\mathbf{x}) \rho_s(u, \mathbf{r}) + \int d\mathbf{r} V_D(\mathbf{x}) \rho_p(u, \mathbf{r}) \\ &= \mathcal{H}_D^s + \mathcal{H}_D^p, \end{aligned} \quad (2.145)$$

where ρ_s and ρ_p are the slowly varying and periodic part of the FL density, respectively. Next, we would like to compute the average $\bar{\chi}$. The free energy is given by

$$\begin{aligned} F(h) &= -T \log \left(\int \mathcal{D}u e^{-\mathcal{H}(h, u)/T} \right) \\ &= -\frac{h^2}{2c_{11}}V - \rho_0 \frac{h}{c_{11}} \int d\mathbf{r} V_D(\mathbf{x}) - T \log Z_1, \end{aligned} \quad (2.146)$$

where Z_1 is the partition function for

$$\mathcal{H}_1(h, u) = \mathcal{H}_0(u) + \mathcal{H}_D^s(u) + \mathcal{H}_D^p(u + hx_1/c_{11}). \quad (2.147)$$

Using replicas, the disorder averaged free energy can be written as

$$\bar{F} = -\frac{h^2}{2c_{11}}V - T \lim_{n \rightarrow 0} \frac{\overline{Z_1^n} - 1}{n}. \quad (2.148)$$

Here $\overline{Z_1^n} = \int \mathcal{D}[u^\alpha] \exp[-\mathcal{H}_1^n/T]$ where \mathcal{H}_1^n is the replica Hamiltonian that follows from $\mathcal{H}_1(h, u)$. Since $\mathcal{H}_1(h, u)$ has the same statistical properties as $\mathcal{H}(0, u)$, i.e., it yields the same replica Hamiltonian, the only dependence on h in \bar{F} comes from the first quadratic term in Eq. (2.148). Due to this so-called statistical tilt symmetry [63], the disorder averaged susceptibility

$$\bar{\chi} = -\frac{4\pi}{V} \frac{\partial^2 \bar{F}}{\partial \delta H_z^2} = \frac{(\rho_0 \phi_0)^2}{4\pi c_{11}} \quad (2.149)$$

is disorder independent. The important quantity is the sample-to-sample variations of the susceptibility. The free energy can be written as

$$F(h) = -\frac{h^2}{2c_{11}}V + F_0 - T \log \langle e^{-\mathcal{H}_D(u + hx_1/c_{11})/T} \rangle_{\mathcal{H}_0}, \quad (2.150)$$

where F_0 is the free energy of the system that is described by the elastic Hamiltonian only. To first order in perturbation theory with respect to $\sim v$ we get

$$\Delta F(h) = F(h) - \overline{F(h)} = \langle \mathcal{H}_D (u + hx_1/c_{11}) \rangle_{\mathcal{H}_0}. \quad (2.151)$$

For a system of linear size L_x in the x direction we find

$$\begin{aligned} \overline{\Delta F(h_1)\Delta F(h_2)} &= 2(v\rho_0)^2 n_{\text{pd}} (L_y L_z)^2 \\ &\times \int d\mathbf{x} \sum_{n>0}^{[\ell/\xi]_G} e^{-(nG_D)^2 \langle u^2 \rangle_{\mathcal{H}_0}} \cos \left[nG_D \frac{(h_1 - h_2) x_1}{c_{11}} \right], \end{aligned} \quad (2.152)$$

where n_{pd} denotes the density of defects. Differentiation with respect to h_1 and h_2 leads to

$$\frac{\overline{\Delta \chi^2}}{\overline{\chi}^2} = \frac{R_D''''(0)L_x^\epsilon}{5c_{11}^2} \sim \left(\frac{L_x}{L_D} \right)^\epsilon, \quad (2.153)$$

where we have taken into account the irrelevance of thermal fluctuation. Since $\epsilon > 0$ for $d < 6$, the sample-to-sample fluctuations grow with the scale L_x . One cannot expect that this result is quantitatively correct for large L_x . However, qualitatively it demonstrates the relevance of defects and it is a signature of a glassy phase. For $L_x > L_D$ we expect that $\overline{(\Delta \chi)^2}/\overline{\chi}^2$ approaches a finite universal value for $d < 6$.

2.F Positional correlation function

In this appendix the positional correlation function of the FLL with planar defects will be calculated, using perturbation theory and results from the functional renormalization group analysis presented in Sec. 2.4. The positional correlation functions have been calculated before for the FLL with point impurities for a uniaxial displacement field [9, 10] and for a vector displacement field [11, 12]. We perform the computations along the lines of these references.

In a functional renormalization group procedure, after integrating out fast modes in an infinitesimal shell with $\Lambda/b \leq q \leq \Lambda$, one can choose to keep the cutoff in momentum space fixed using the rescaling

$$\mathbf{x}' = \frac{\mathbf{x}}{b} \quad \mathbf{z}' = \frac{\mathbf{z}}{b^x} \quad \mathbf{q}'_x = b\mathbf{q}_x \quad \mathbf{q}'_z = b^x \mathbf{q}_z, \quad (2.154)$$

where $\mathbf{z} = (y, z)$. The displacement field is not rescaled due to the periodicity of R_D . This implies $u(\mathbf{q}) = b^{d-2+2\chi}u'(\mathbf{q}')$. We need to obtain the renormalization group flow of the correlation function

$$\begin{aligned}
\langle u(\mathbf{q}_1)u(\mathbf{q}_2) \rangle &= Z^{-1} \int \mathcal{D}u(\mathbf{q}) e^{-\beta\mathcal{H}} u(\mathbf{q}_1)u(\mathbf{q}_2) \\
&= Z^{-1} \int \mathcal{D}u^{<}(\mathbf{q}) u(\mathbf{q}_1)u(\mathbf{q}_2) \int \mathcal{D}u^{>}(\mathbf{q}) e^{-\beta\mathcal{H}} \\
&= Z^{-1} \int \mathcal{D}u^{<}(\mathbf{q}) u(\mathbf{q}_1)u(\mathbf{q}_2) e^{-\beta\mathcal{H}_l(u^{<}(\mathbf{q}))} \\
&= b^{2(d-2+2\chi)} \langle u'(\mathbf{q}'_1)u'(\mathbf{q}'_2) \rangle, \tag{2.155}
\end{aligned}$$

where $\mathcal{H} = \mathcal{H}_0 + \int V_D(x)\rho(u, \mathbf{r})$. Here $u^{<}(\mathbf{q})$ are modes that satisfy $q < \Lambda/b$ and \mathcal{H}_l is the Hamiltonian that applies to the scale $l = \log b$ with b very close to unity. Using Eq. (2.155), we obtain a differential equation for $\langle u(\mathbf{q}_1)u(\mathbf{q}_2) \rangle$. We get

$$\langle u(\mathbf{q}_1)u(\mathbf{q}_2) \rangle = b^{2(d-2+2\chi)} \langle u'(\mathbf{q}'_1)u'(\mathbf{q}'_2) \rangle, \tag{2.156}$$

where the only restriction on b is $q_i < \Lambda/b$, $i = 1, 2$.

First, we calculate $\langle u(\mathbf{q}_1)u(\mathbf{q}_2) \rangle$ to lowest order in v ,

$$\begin{aligned}
\langle u(\mathbf{q}_1)u(\mathbf{q}_2) \rangle &= \langle u(\mathbf{q}_1)u(\mathbf{q}_2) \rangle_{\mathcal{H}_0} \\
&+ \frac{1}{2T^2} \lim_{n \rightarrow 0} \sum_{\beta, \gamma} \int_{\mathbf{x}, \mathbf{z}_1, \mathbf{z}_2} \langle u_1(\mathbf{q}_1)u_1(\mathbf{q}_2) R_D[u^\beta(\mathbf{x}, \mathbf{z}_1) - u^\gamma(\mathbf{x}, \mathbf{z}_2)] \rangle_{\sum_\alpha \mathcal{H}_0(u^\alpha)}, \tag{2.157}
\end{aligned}$$

where u_1 is the displacement field with replica index $\alpha = 1$. We use the periodicity of R_D by writing $R_D(u) = \sum_n R_n \cos(nG_D u)$. From this we find that at the planar glass fixed point

$$\langle u(\mathbf{q}_1)u(\mathbf{q}_2) \rangle = \frac{-(2\pi)^{d+2}}{(c_{11}q_{1x}^2)^2} R_D^{*''}(0) \delta(\mathbf{q}_{1x} + \mathbf{q}_{2x}) \delta(\mathbf{q}_{1z}) \delta(\mathbf{q}_{2z}), \tag{2.158}$$

where the rescaled fixed point correlator is

$$R_D^{*''}(u) = -\frac{\epsilon c_{11}^2 \Lambda^\epsilon}{6K_d} [(u - \ell/2)^2 - \ell^2/12] \tag{2.159}$$

for $0 \leq u < \ell$. Choosing $b = \Lambda/\max\{q_{1x}, q_{2x}\}$ in Eq. (2.156) so that it is justified to calculate the correlation function appearing on the right hand

side of Eq. (2.156) at the fixed point, and using the result of Eq. (2.158), we get

$$\langle u(\mathbf{q}_1)u(\mathbf{q}_2) \rangle = \frac{(2\pi)^{2d}}{36S_{d-2}} \frac{\Lambda^{2(6-d)}}{q_{1x}^{d-2}} \epsilon \ell^2 \delta(\mathbf{q}_{1x} + \mathbf{q}_{2x}) \delta(\mathbf{q}_{1z}) \delta(\mathbf{q}_{2z}). \quad (2.160)$$

Note that in Eq. (2.160) only displacements with $\mathbf{q}_{1x} = -\mathbf{q}_{2x}$ are coupled as it would be the case for a quadratic Hamiltonian. Therefore one can write down an effective quadratic Hamiltonian in the \mathbf{q}_x -momentum space that reproduces the correlations to first order in ϵ . The positional correlation function shows the power law behavior

$$S_{GD} \approx |\mathbf{x}|^{-\epsilon(\pi/3)^2}. \quad (2.161)$$

We point out that this result is valid only for $d > 4$. In $d \leq 4$ dimensions the part of the pinning potential related to the slowly varying part of the FL density also becomes relevant and further analysis is needed, see Sec. 2.4.

2.G List of recurrent symbols

Symbol	Quantity	Definition
a	flux line lattice constant	
\mathbf{B}	magnetic induction	
$c_{ii} \quad i = 1, 4, 6$	elastic constants	Eq. (2.2)
\mathbf{G}	reciprocal lattice vector	
$g = \frac{3}{8}\eta(\frac{a}{\ell})^2$	parameter controlling the relevance of the single defect plane	Eq. (2.27)
$G_D = \frac{2\pi}{\ell}$	shortest reciprocal lattice vector perpendicular to the defect(s)	Sec. 2.3
\mathcal{H}_0	elastic energy of distortions of the flux line lattice	Eq. (2.2)
\mathcal{H}_P	pinning energy of point impurities	Eq. (2.5)
\mathcal{H}_0^n	effective quadratic replica Hamiltonian for Bragg glass	Eq. (2.17)
\mathcal{H}_D	pinning energy of a planar defect	Eq. (2.23)
J	current density	
L_ξ	Larkin length	Eq. (2.11)
L_a	positional correlation length	Sec. 2.2
ℓ_D	mean distance between defects	Sec. 2.4
L_D	Larkin length for planar defects	Sec. 2.4
n_{imp}	density of point impurities	

Symbol	Quantity	Definition
n_D	unit vector perpendicular to the defect plane	
\mathbf{r}_D	position vector of the defect plane	Eq. (2.21)
R_P	point disorder correlation function	Eq. (2.15)
R_D	planar disorder correlation function	Eq. (2.49)
R_D^*	fixed point value of R_D	
$S_{\mathbf{G}}(\mathbf{r})$	positional correlation function	Sec. 2.2
S_d	surface of d -dimensional unit sphere	
T	temperature	
$u_i(y, z)$	displacement field at a planar defect with $x = x_i$	
u_x	displacement field perpendicular to the defects	
v_p	strength of point impurities	Sec. (2.2)
V_P	pinning potential resulting from point impurities	Eq. (2.2)
v	defect strength	Sec. 2.3
V_D	pinning potential resulting from planar defects	Sec. 2.4
$[x]_G$	the closest integer to x	
δ	defect distance to the origin	
ζ	roughness coefficient	Sec. 2.2
η	power law exponent of positional correlation function in the Bragg glass regime	Sec. 2.2
Λ	momentum cutoff	Sec. 2.2
λ	penetration depth	Sec. 2.2
ξ_{RF}	roughness exponent in random force regime	Sec. 2.2
ξ_{RM}	roughness exponent in random manifold regime	Sec. 2.2
ξ_{BG}	roughness exponent in the Bragg glass regime	Sec. 2.2
ξ	superconductor coherence length	
ξ_c	correlation length	
$\rho(\mathbf{u}, \mathbf{r})$	flux line density	Eq. (2.6)
ρ_0	background FL density	Eq. (2.6)

Symbol	Quantity	Definition
$\bar{\Sigma}_{y(z)}$	interface tension of a domain wall perpendicular to z (y) axis	Eq. (2.54)
ϕ_0	flux quantum	Sec. 2.2

Voltage-current characteristics in thin superconducting films

3.1 Introduction

In two-dimensional systems with a continuous symmetry the effects of thermal fluctuations are much more pronounced than in their three-dimensional counterparts. The long-wavelength excitations lead to a divergence in the fluctuations of the phase of the order parameter. As a result of this divergence the mean value of the order parameter vanishes and two-dimensional systems can not be characterized by a true long-range order [85, 86], while analogous three-dimensional systems can exhibit true long-range order at low temperatures. However, in two-dimensional crystals, superfluids, XY magnets and thin superconducting films there is still quasi-long-range order at low temperatures, meaning that the order parameter correlation function decays as a power law with distance. This quasi-long-range order is destroyed through the unbinding of vortex-antivortex pairs which takes place at the Berezinskii-Kosterlitz-Thouless (BKT) transition temperature [87, 88, 89]. Above the transition the system is characterized by an exponential decay of the order parameter correlation function and therefore exhibits short-range order.

Resistive properties of three-dimensional superconductors are associated with the motion of vortex (flux) lines which are present in equilibrium due to an external magnetic field penetration, see Chapter 2. In bulk superconductors, vortices are not present in zero magnetic field due to the high energy cost of an individual vortex line. As a result a sample is superconducting in the absence of an external magnetic field. In thin superconducting films this is not the case since the vortex free energy can be of the order $k_B T$ due to a small film thickness. Hence, vortices can appear even in the absence of an external field, crucially influencing transport properties of a film. The benchmark of the BKT transition in thin superconducting films is the abrupt change of the voltage-current characteristic at the transition. Below the transition vortices and antivortices are bound into pairs. In the presence

of a transport current, that tends to separate a pair, there is a finite energy barrier that has to be overcome in order to break a vortex pair and produce free vortices. Therefore, thermally activated pairs can dissociate, resulting in a nonlinear voltage-current relation $V \propto j^{\delta(T)}$, where $\delta(T) > 1$ [90, 91] and j is the current density. At the BKT transition $\delta(T_{\text{BKT}}) = 3$ [90, 91], while right above the transition free vortices induce Ohmic behavior $V \sim j$ [4]. This universal jump in the coefficient δ has been observed in experiments, see e.g. Refs. [92, 93]. In this chapter we consider transport properties of a thin superconducting film taking into account the influence of quantum fluctuations on the unbinding of vortex pairs. At sufficiently low temperatures the quantum tunneling of vortices through the barrier turns out to be more probable than the thermal activation over the barrier. As a result the system is characterized by a different voltage-current relation than the above mentioned one.

This chapter is organized as follows. In Sec. 3.2, we introduce a model for a thin superconducting film. In Sec. 3.3, we briefly summarize the main properties of the low and high temperature phases and the BKT transition between them. In Sec. 3.4, we study transport characteristics of the system at different temperatures. In Sec. 3.5, we summarize the results and discuss the influence of dissipation arising from the coupling of the system to its environment.

3.2 Model

We consider a thin superconducting film in zero magnetic field characterized by the penetration depth λ , the superconductor coherence length ξ and a film thickness $d \ll \lambda$. The z axis is chosen to be perpendicular to the film. It is convenient to decompose the phase of the order parameter into a slowly varying regular spin wave part φ_{sw} and a singular vortex part φ_v . Then the Hamiltonian can be written as $\mathcal{H} = \mathcal{H}_{sw} + \mathcal{H}_v$, where the spin wave part is given by [91]

$$\mathcal{H}_{sw} = \frac{J}{2} \int d\mathbf{r}^2 (\nabla \varphi_{sw})^2, \quad (3.1)$$

and the vortex part is

$$\mathcal{H}_v = \sum_i n_i^2 (E_c + E_v) + \frac{1}{2} \sum_{i \neq j} n_i n_j V_{\text{int}}(|\mathbf{r}_i - \mathbf{r}_j|), \quad (3.2)$$

where the sums run over all vortices. We assume that the amplitude of the order parameter is constant outside the vortex cores. The vorticity

and the position vector of i th vortex are denoted by n_i and \mathbf{r}_i , respectively. $J = \phi_0^2 d / (16\pi^3 \lambda^2)$ and ϕ_0 is the flux quantum. E_c is the vortex core energy, E_v denotes the vortex energy (outside the core) and $V_{\text{int}}(r)$ is the interaction energy of two vortices separated by a distance r . While in three-dimensional superconductors vortex lines interact logarithmically for distances smaller than λ and for larger separations the interaction between them exponentially decreases with distance, in two-dimensional superconducting systems the vortex interaction is [94, 95]

$$V_{\text{int}}(r) \approx 2\pi J \begin{cases} \ln \frac{4\lambda_{\text{eff}}}{r} - \gamma, & r \ll \lambda_{\text{eff}} \\ \frac{2\lambda_{\text{eff}}}{r}, & \lambda_{\text{eff}} \ll r, \end{cases} \quad (3.3)$$

where $\lambda_{\text{eff}} = \lambda^2/d$ plays the role of the effective penetration depth and γ is the Euler constant. In thin superconducting films the effective penetration depth is much larger than the bulk penetration depth, $\lambda_{\text{eff}} \gg \lambda$. The screening is weaker than in three-dimensional systems because the screening currents are confined to a thin film only, while vortices in a film interact primarily through the free space adjacent to the film. The single vortex energy reads [94]

$$E_v \approx \pi J \left(\ln \frac{4\lambda_{\text{eff}}}{\xi} - \gamma \right). \quad (3.4)$$

Since λ_{eff} is of the order of fractions of a centimeter for film thicknesses $d = 1-10$ nm, it is usually larger than the sample size L [96]. Then, effectively there is no screening and Eqs. (3.3,3.4) are not valid any more, but the following holds

$$V_{\text{int}}(r) \approx 2\pi J \ln \frac{L}{r}, \quad (3.5)$$

$$E_v \approx \pi J \ln \frac{L}{a}, \quad (3.6)$$

where a is the small scale cutoff. In the following, we will consider the case where $\lambda_{\text{eff}} > L$. Then, the Hamiltonian of Eq. (3.2) can be rewritten as

$$\mathcal{H}_v \approx \sum_i n_i^2 E_c - \pi J \sum_{i \neq j} n_i n_j \ln \frac{|\mathbf{r}_i - \mathbf{r}_j|}{a} + \left(\sum_i n_i \right)^2 E_v. \quad (3.7)$$

This Hamiltonian also describes vortices in superfluid films, two-dimensional XY magnets and a Coulomb gas in two dimensions where the vorticity of vortices determines the electric charge of particles. The influence of a transport current on vortices is described by

$$\mathcal{H}_{\text{force}} = - \sum_i n_i \mathbf{f} \cdot \mathbf{r}_i, \quad (3.8)$$

where $\mathbf{f} = (\mathbf{j} \times \hat{\mathbf{z}})\phi_0 d/c$ is the Lorentz force acting on vortices. The unit vector perpendicular to the film is denoted by $\hat{\mathbf{z}}$, \mathbf{j} is the current density and c is the speed of light.

3.3 BKT transition

In this section we briefly review the main characteristics of the BKT transition in thin films. We start with a simple heuristic argument and then discuss results of more elaborate calculations involving the renormalization group method.

Some understanding of the BKT transition can be obtained by examining the free energy of an individual vortex [88]

$$\begin{aligned} F &= E_c + E_v - TS \\ &\approx \pi J \ln \frac{L}{a} - T \ln \left(\frac{L}{a} \right)^2 \\ &= 2 \left(\frac{\pi J}{2} - T \right) \ln \frac{L}{a}. \end{aligned} \quad (3.9)$$

In the following, we set the Boltzmann constant equal to one. The entropy is $S \approx \ln (L/a)^2$ since the vortex core can be placed anywhere in the sample. From Eq. (3.9) one obtains that vortices are favorable above the transition temperature $T_{\text{BKT}} = \pi J/2$. This simple argument correctly determines the transition temperature provided that the coupling constant J is replaced by the renormalized coupling $\tilde{J} = \nu_s(T)J$, where $0 \leq \nu_s(T) \leq 1$ is a function of temperature. Note that if $\lambda_{\text{eff}} < L$ the vortex energy is given by Eq. (3.4) and from the above argument one concludes that free vortices are present at any finite temperature in a superconducting film.

Going beyond the simple argument presented above requires a more detailed theory, which allows for a finite density of vortices near T_{BKT} . Different authors contributed to the detailed understanding of the BKT transition and the following picture arose during the time [87, 88, 89, 97, 98, 99]: At low temperatures vortices are bound into vortex–antivortex pairs. The interaction between a vortex and an antivortex that make a pair is screened by smaller vortex pairs, leading to a downward renormalization of the coupling constant $J \rightarrow \tilde{J}$. The system can be effectively described by Eq. (3.1) with the replacement $J \rightarrow \tilde{J}$ and the correlation function of the order parameter $\Psi(\mathbf{r})$ behaves as

$$\langle \Psi(\mathbf{r})\Psi(\mathbf{0}) \rangle \sim \left(\frac{a}{r} \right)^\eta, \quad \eta = \frac{T}{2\pi\tilde{J}}, \quad (3.10)$$

for temperatures $T < T_{\text{BKT}}$. At T_{BKT} the vortex pairs dissociate and as a result the coupling constant \tilde{J} vanishes at higher temperatures. At the transition there is a universal jump of the coupling constant $\tilde{J}(T_{\text{BKT}})/T_{\text{BKT}} = 2/\pi$, which implies that the superfluid (areal) density $\rho_s = \nu_s(T)d|\Psi|^2 = \tilde{J}(2m_e/\hbar)^2$ has a universal jump [98]

$$\frac{\rho_s}{T} = \begin{cases} 8m_e^2/(\hbar^2\pi), & T \rightarrow T_{\text{BKT}}^-, \\ 0, & T \rightarrow T_{\text{BKT}}^+, \end{cases} \quad (3.11)$$

where m_e denotes the electron mass. Note that the jump depends only on fundamental constants. Also the exponent η takes the universal value $\eta = 1/4$ at the transition. All derivatives of the free energy remain continuous at the transition which is a rather peculiar property of this transition. The presence of free vortices in the high temperature phase ($T > T_{\text{BKT}}$) leads to an exponential decay of the correlation function

$$\langle \Psi(\mathbf{r})\Psi(\mathbf{0}) \rangle \sim \exp \left[-\frac{r}{\xi_{\text{BKT}}(T)} \right]. \quad (3.12)$$

The correlation length behaves as [91]

$$\xi_{\text{BKT}}(T) \approx \xi(T) \exp \left[\sqrt{b \frac{T_c - T}{T - T_{\text{BKT}}}} \right], \quad (3.13)$$

where T_c is the mean-field transition temperature above which $\langle |\Psi|^2 \rangle = 0$. The parameter b is nonuniversal and for superconducting thin films typically ranges from 2 up to 16 [2]. The correlation length can be interpreted as the length above which the vortices become free and therefore the density of free vortices is $n_v \sim \xi_{\text{BKT}}^{-2}$.

3.4 Transport

In this section we investigate voltage-current characteristics of a thin superconducting film focusing on the influence of quantum fluctuations on vortex-antivortex unbinding. At high temperatures resistive properties of a superconducting film are determined by thermal activation processes, leading to vortex-antivortex unbinding. When the temperature decreases the probability of activation processes becomes smaller, and therefore, at sufficiently low temperatures thermal activation is replaced by a quantum tunneling of vortices which determines a voltage-current relation.

In order to include effects of quantum fluctuations on vortex-antivortex nucleation we have to add to the Hamiltonian of Eq. (3.7) the kinetic energy term. Then, the Euclidian action is given by

$$S = \int_{-\hbar/(2T)}^{\hbar/(2T)} d\tau \left(\frac{M}{2} \sum_i (\partial_\tau \mathbf{r}_i)^2 + \mathcal{H}_v + \mathcal{H}_{\text{force}} \right), \quad (3.14)$$

where $\mathbf{r}_i(\tau)$ are the world lines of the vortices and M denotes the vortex mass. We neglect here a dissipation arising from the coupling of the system to its environment and discuss the influence of dissipation on transport properties in Sec. 3.5.

To determine the vortex production rate Γ for asymptotically small currents, we consider the appearance of a vortex-antivortex pair and its subsequent separation driven by the Lorentz force. Assuming a symmetric process, the coordinates of the vortex \mathbf{r}_1 and the antivortex \mathbf{r}_2 satisfy $\mathbf{r}_1 = -\mathbf{r}_2 = \mathbf{r}$ with $\mathbf{f}\mathbf{r} = fr$. The action of the vortex pair can be rewritten as

$$S = \int d\tau [M(\partial_\tau r)^2 + U(r)], \quad (3.15)$$

$$U(r) = 2\pi J \ln \left(\frac{2r}{\xi} \right) - 2fr + 2E_c. \quad (3.16)$$

We have chosen the small scale cutoff to be of the order of the superconductor coherence length, $a \approx \xi$. The unbinding of the pair in the presence of a transport current effectively reduces to a single particle motion in the potential $U(r)$. Note that the fact that the system is two-dimensional is important for pre-exponential factors in the vortex production rate Γ . However, in the following we will determine Γ with an exponential accuracy.

The vortex production rate Γ is given by [100]

$$\Gamma \sim \int_0^\infty dE \Gamma(E) e^{-E/T}, \quad (3.17)$$

where $\Gamma(E)$ denotes the zero temperature tunneling rate of a particle in the potential $U(r)$ having an energy E . In the WKB approximation $\Gamma(E)$ is given by [101]

$$\Gamma(E) = \begin{cases} e^{-4\sqrt{M} \int_{r_a(E)}^{r_b(E)} dr \sqrt{U(r)-E}/\hbar} & , \quad E < U_0 \\ (1 + e^{-2\pi(E-U_0)/(\hbar\omega)})^{-1} & , \quad E \gtrsim U_0. \end{cases} \quad (3.18)$$

The barrier height is $U_0 = U(r_c) = 2\pi J \left[\ln \left(\frac{2\pi J}{f\xi} \right) - 1 \right] + 2E_c$ and $r_{a/b}(E)$ satisfy $U(r_{a/b}) = E$, see Fig. 3.1. $\omega = \sqrt{-U''(r_c)/(2M)} = f\sqrt{1/(MJ\pi)}$

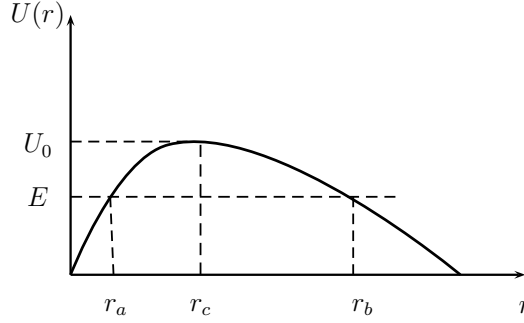


Figure 3.1: The potential barrier for the vortex-antivortex pair dissociation.

denotes the characteristic frequency at $r_c = \pi J/f$. The rate equation for the vortex density n_v is

$$\partial_t n_v = \Gamma - \frac{\xi^2}{\tau_{rec}} n_v^2, \quad (3.19)$$

where the first term describes the vortex production and the second term describes the annihilation of vortices and antivortices; ξ^2/τ_{rec} denotes the recombination parameter. In the steady state, the vortex density is $n_v = (\tau_{rec}\Gamma)^{1/2}/\xi$. Then, using the Bardeen-Stephen formula [4] one finds the voltage-current relation (V - I) to be

$$V = 2\pi\xi^2\rho_n n_v I = 2\pi\xi\rho_n I (\tau_{rec}\Gamma)^{1/2} \quad (3.20)$$

where ρ_n denotes the normal state resistivity of the film. In the following different regimes will be considered.

(i) At zero temperature the only nonvanishing contribution in Eq. (3.17) comes from $E = 0$. The generated voltage for asymptotically small currents ($f\xi/J \ll 1$) is

$$V \sim \Gamma^{1/2} \sim \exp\left(-\frac{S(0,0)}{2\hbar}\right), \quad (3.21)$$

$$\frac{S(0,0)}{c_1\hbar} \approx \frac{\sqrt{M}(2J\pi)^{3/2}}{\hbar f} \left(\ln \frac{2J\pi}{f\xi}\right)^{3/2}, \quad (3.22)$$

where c_1 is a positive numerical constant of order unity and

$$\frac{S(E,T)}{\hbar} = \frac{E}{T} + 4\sqrt{M} \int_{r_a}^{r_b} dr \frac{\sqrt{U(r) - E}}{\hbar} \quad (3.23)$$

is the action of the classical path of the particle in the potential $-U(r)$ with energy E . After having done the calculation we became aware of a work

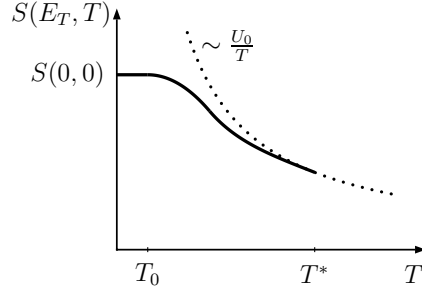


Figure 3.2: The crossover from the quantum regime ($T \leq T_0$) to the classical regime ($T > T^*$) is shown schematically. The vortex production rate is $\Gamma \sim \exp[-S(E_T, T)/\hbar]$.

done by Iengo and Jug [102] and by Ao [103] on the same problem. The result given by Eq. (3.21) is in agreement with the result of Ref. [102], while in Ref. [103] the same leading dependence on f is found, but a different logarithmic dependence on f . In Ref. [102] the result is obtained by different means, using a quantum electrodynamic formulation of the decay of the two-dimensional vacuum, since the instability of the supercurrent carrying state is the same as the instability of a vacuum in the presence of a constant electric field in which electron-positron pairs are created and driven by the electric field [102, 103].

We find that the result (3.21) is valid also at finite temperatures, as long as

$$T \leq T_0 \approx \frac{1}{c_2} \frac{\hbar f}{\sqrt{\pi 2 J M}} \frac{1}{\sqrt{\ln \frac{\pi 2 J}{f \xi}}} \quad (3.24)$$

where c_2 is a positive constant of order unity. By using the estimate for the vortex mass $M = 2m_e k_F d / \pi^3$ from Ref. [2], where m_e denotes the electron mass and k_F denotes the Fermi wave vector, Eqs. (3.22, 3.24) can be rewritten as

$$\frac{S(0, 0)}{\hbar} \approx 30 \frac{\nu j_0}{\kappa j} \left[\ln \left(\frac{j_0}{j} \right) \right]^{3/2}, \quad (3.25)$$

$$T_0 \approx \frac{0.1}{\nu_s(T_{\text{BKT}})} T_{\text{BKT}} \frac{\kappa j}{\nu j_0} \left[\ln \left(\frac{j_0}{j} \right) \right]^{-1/2}, \quad (3.26)$$

where we have used the bare value of the coupling constant J which is justified at low temperatures. Note that J is expected to be only slightly suppressed due to the renormalization, since typically $\nu_s(T_{\text{BKT}})$ is in the interval (0.5 – 0.9) [2]. The Ginzburg-Landau parameter is denoted by $\kappa = \lambda/\xi$, j_0 is the depairing current density and $\nu = d\sqrt{k_F/a_0}$ is proportional to the

number of atomic layers in the film, where a_0 is the Bohr radius. Note that Eqs. (3.25,3.26) are valid in the limit $j/j_0 \ll 1$.

In order to estimate the tunneling action we use the data for an indium oxide sample from Ref. [92]. We obtain $S(0,0)/\hbar \approx (1/j)10^{15}$ where the current density j is measured in units of A/m². Thus for small current densities $j \ll j_0 \approx 10^{13}$ A/m², the tunneling is exponentially suppressed.

(ii) At intermediate temperatures $T_0 < T < T^* = \hbar\omega/(2\pi)$, the main contribution in Eq. (3.17) comes from the stationary point E_T and the decay rate can be estimated as $\Gamma \sim \exp[-S(E_T, T)/\hbar]$. E_T obeys the equation $\partial_E S(E, T)|_{E_T} = 0$ that may be rewritten as

$$\frac{\hbar}{T} = 2\sqrt{M} \int_{r_a(E_T)}^{r_b(E_T)} dr \frac{1}{\sqrt{U(r) - E_T}} = \tau(E_T), \quad (3.27)$$

where $\tau(E)$ can be interpreted as the period of the classical motion of a particle with a mass $2M$ and energy E , in the potential $-U(r)$. Since $\tau(E)$ is the monotonically decreasing function of E for small currents, $\partial_E^2 S(E, T)|_{E_T} > 0$. Moreover, Eq. (3.27) has unique solution E_T for every T in a range $T_0 \leq T \leq T^*$. The solution satisfies $0 \leq E_T < U_0$, meaning that

$$\frac{\hbar}{T_0} = \tau(0) \geq \tau(E_T) \geq \frac{2\pi}{\omega}. \quad (3.28)$$

T^* is given by

$$T^* = \frac{\hbar f}{2\pi} \sqrt{\frac{1}{MJ\pi}} \approx T_{\text{BKT}} \frac{0.03}{\nu_s(T_{\text{BKT}})} \frac{\kappa j}{\nu j_0}, \quad (3.29)$$

where in the last estimate of Eq. (3.29) we have used the bare value of the coupling constant J .

(iii) At even higher temperatures $T^* < T \leq T_{\text{BKT}}$, the decay rate is dominated by $E > U_0$ [100, 104] and thermally activated breaking of vortex pairs dominates the dynamics. Then, from Eqs. (3.17,3.18) we obtain the decay rate to be given by the Arrhenius law $\Gamma \sim \exp[-S_{\text{class}}/\hbar]$ where $S_{\text{class}} = \hbar U_0/T$. The voltage-current relation reads [105, 106]

$$V \sim f e^{-U_0/(2T)} \sim j^{\delta(T)}, \quad (3.30)$$

$$\delta(T) = 1 + \pi J/T. \quad (3.31)$$

Taking into account the presence of other vortices through the replacement $J \rightarrow \tilde{J}$, the coefficient $\delta(T)$ can be rewritten as

$$\delta(T) = 1 + 2 \frac{\nu_s(T)}{\nu_s(T_{\text{BKT}})} \frac{T_{\text{BKT}}}{T}. \quad (3.32)$$

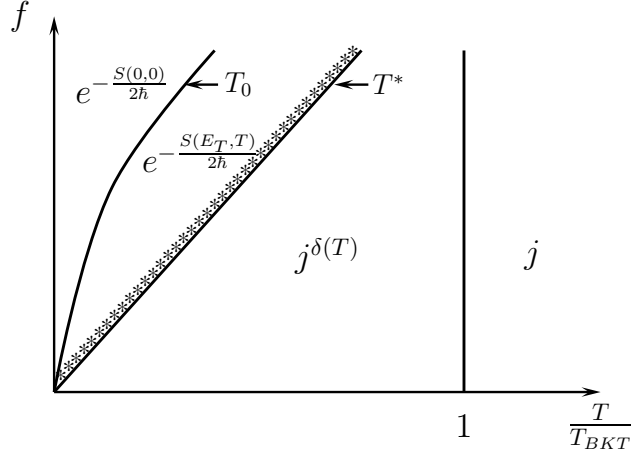


Figure 3.3: Voltage-current relations occurring at different temperatures are schematically shown. In the shaded region the quantum correction given by Eq. (3.38) applies.

At the BKT transition, we obtain the well known universal exponent $\delta(T_{\text{BKT}}) = 3$ that has been especially clearly measured in experiments by Fiory et al. [92] on In/In-O films and by Kadin et al. [93] on Hg-Xe alloy films.

(iv) At $T > T_{\text{BKT}}$ a finite density of free vortices $n_v \sim \xi_{\text{BKT}}^{-2}$ appears in equilibrium. As a result the system is characterized by a linear voltage-current relation [4]

$$V = 2\pi\rho_n \left(\frac{\xi}{\xi_{\text{BKT}}} \right)^2 I \quad (3.33)$$

for small enough currents (that probe length scales larger than ξ_{BKT}).

Next, we consider the crossover from the quantum regime ($T \leq T_0$) to the classical regime ($T > T^*$) in more detail. Within the semiclassical approximation the decay rate is with an exponential accuracy given by $\Gamma \sim \exp[-S_{\text{min}}/\hbar]$, where S_{min} is the action of the trajectory minimizing the Euclidian action of Eq. (3.15). For temperatures below T_0 the extremal action is $S_{\text{min}} = S(0, 0)$, in the intermediate region ($T_0 < T < T^*$) the minimal action is $S_{\text{min}} = S(E_T, T)$ and in the high temperature regime the trajectory extremizing the action is time independent, and therefore $S_{\text{min}} = \hbar U_0/T$. We find that S_{min} at T^* has a continuous first derivative with respect to temperature, while the second derivative has a jump:

$$\left. \frac{dS(E_T, T)}{dT} \right|_{T^*} = \left. \frac{dS_{\text{class}}}{dT} \right|_{T^*} \quad \text{and} \quad \left. \frac{d^2S(E_T, T)}{dT^2} \right|_{T^*} < \left. \frac{d^2S_{\text{class}}}{dT^2} \right|_{T^*}. \quad (3.34)$$

Following Ref. [107] we call this situation a second-order transition at the crossover point. The result of Eq. (3.34) is a general property of a massive

particle trapped in a metastable state formed by a potential $U(r)$, provided $\tau(E)$ is a monotonous function of energy [108]. The crossover from the classical to the quantum regime for our problem is schematically shown in Fig. 3.2.

Generally, in the case of a second-order transition the trajectory extremizing the action can be written in the form [107, 109]

$$r(\tau) = r_c + \sum_{n=0}^{\infty} a_n \cos\left(\frac{2\pi T}{\hbar} n\tau\right), \quad (3.35)$$

where the coefficients $|a_n| \ll |a_1|$ are small near the transition temperature T^* . Substituting $r(\tau)$ in Eq. (3.15), the action can be expanded in powers of a_n , yielding

$$S \approx \frac{U_0 \hbar}{T} + \alpha a_1^2 + \beta a_1^4, \quad (3.36)$$

where the coefficient α is negative below T^* and vanishes at the transition temperature T^* . Then the coefficient a_1 can be found from the minimization of the action S and the minimal action is

$$S_{\min} = U_0 \hbar / T - \alpha^2 / (4\beta). \quad (3.37)$$

Closely following Refs. [107, 109] we determine the coefficients α and β and find a quantum correction to the classical result:

$$V \sim \Gamma^{1/2} \sim \exp \left[-\frac{U_0}{2T} + \frac{(T^2 - T^{*2})^2 \sqrt{MJ^3}}{TT^{*3}} \frac{\pi^{5/2}}{\hbar f} \frac{1}{1 + 2(1 - 4(T/T^*)^2)^{-1}} \right]. \quad (3.38)$$

This result is valid near the transition, for temperatures approaching T^* from below. We conclude that the quantum effects significantly enhance the decay rate in comparison to the classical rate and it would be interesting to probe the result of Eq. (3.38) in experiments.

3.5 Discussions and conclusions

In this chapter we have studied voltage-current characteristics occurring in a thin superconducting film at different temperatures and in the absence of an external magnetic field, provided the film exhibits the BKT transition. We have derived the quantum creep law, see Eq. (3.21), and found the range of temperatures $0 \leq T \leq T_0$ where this law is applicable, see Eq. (3.24). We have determined the temperature T^* above which thermally activated

breaking of vortex pairs dominates the vortex nucleation, see Eq. (3.29). We have considered the region of intermediate temperatures $T_0 < T < T^*$ where a crossover from classical to quantum behavior occurs and have found the quantum correction to the classical result, see Eq. (3.38). The results are schematically summarized in Fig. 3.3.

Next, we briefly discuss the influence of dissipation on transport properties, since the coupling of the system to its environment makes the system dissipative. Dissipation can be included into our model through the formulation by Caldeira and Leggett [110] where a moving vortex interacts with a bath of quantum harmonic oscillators and the coupling between them is linear in the vortex position. In Ref. [102] the voltage-current relation at $T = 0$ for the dissipation-dominated case ($M \rightarrow 0$) is derived:

$$V \sim \exp \left[-2\pi^3 \frac{\eta}{\hbar} \frac{E_c(E_c + \frac{\eta\hbar}{M})}{f^2} \right], \quad (3.39)$$

where η measures the dissipation strength. At high enough temperatures the trajectory extremizing the action is time independent and the voltage-current dependence $V \sim I^{1+2T_{\text{BKT}}/T}$ remains valid, while the dissipation enters only through the prefactors [102]. A detailed analysis of transport properties for intermediate temperatures is missing. Following Refs. [107, 111] we find that in the dissipation-dominated case, i.e., $\eta/M \gg \omega$, the first derivative of the action S_{min} with respect to temperature has a jump at the crossover from the classical to the quantum regime. This situation corresponds to a so-called first-order transition [108]. Then, the approach developed in the seminal work by Larkin and Ovchinnikov [107, 109] on the classical-quantum crossover and applied above for the dissipation-free case, is no longer applicable. We leave this problem for a future study. However, in the case of intermediate friction, $\omega T/U_0 \ll \eta/M \ll \omega$, the result of Eq. (3.38) as well as the transition temperature T^* , given by Eq. (3.29), remain valid. At the end, we point out that it is of a great importance to include effects of disorder in the results presented in this chapter. Namely, even below T_{BKT} in the classical regime there is often an inconsistency between the nonlinear voltage-current relation given by Eq. (3.30) and measurements [91]. It is expected that disorder can resolve this puzzle [91].

The effect of randomness on the Mott state

4.1 Introduction

In 1958, Anderson pointed out that quantum-mechanical interference effects can lead to localization in fermionic disordered solids [112]. In three-dimensional noninteracting systems, disorder strength needs to overcome a certain threshold in order to localize all electron states, while in one and two space dimensions all states are localized for arbitrary small disorder [113]. Interaction between electrons reduces the effect of disorder and may lead to metallic behavior in two dimensions [114]. In this chapter we consider interacting one-dimensional systems. Interaction leads to a breakdown of the Fermi liquid theory and a Luttinger liquid is formed [20, 21]. As a result of the competition between collectively acting impurities and short-range interactions, for $K < 3/2$ at zero temperature electrons are localized and an insulating state, the Anderson insulator, is formed [32]. For weak external electric field E the electrical conductivity σ is nonlinear $\ln \sigma \sim -E^{-1/2}$ [77, 115]. Thermal fluctuations destroy the Anderson insulator and at finite temperatures the system is always in its delocalized phase, although disorder plays a significant role on length scales smaller than the thermal de Broglie wavelength of density excitations [74, 116]. Hence, at low but finite temperatures, the system exhibits variable range hopping and an exponentially small linear conductivity [77, 115]. These results are valid only if inelastic processes are allowed, i.e., a weak coupling to a dissipative bath is provided. The Anderson insulator is characterized by a finite ac linear conductivity at low frequencies [117, 118, 119] and a finite compressibility [32]. For a special case of noninteracting electrons $K = 1$ all mentioned characteristics of the Anderson insulator have been known for a long time [120, 121, 122].

In Mott insulators, on the other hand, an insulating behavior results from the blocking of sites by repulsive interaction between electrons [123]. Hence, the correlation effects become important. In one dimension it was early realized that interaction processes that do not conserve momentum,

the so-called umklapp processes, are responsible for the Mott insulating state appearing at half filling [124, 125]. Later, full description of Mott insulating states arising from any commensurate filling in one dimension was obtained [33]. The Mott insulator in one dimension is characterized by a gap Δ in the charge excitations and therefore by zero compressibility. At zero temperature the ac linear conductivity is zero for frequencies smaller than (twice) the energy gap. For simplicity we discuss spinless electrons in the following. At zero temperature and small electric field, the electrical conductivity is nonlinear $\ln \sigma \sim -E^{-1}$ [126]. At finite temperatures umklapp scattering processes become irrelevant in the thermodynamic limit [74], but at low temperatures linear dc conductivity is exponentially small $\ln \sigma \sim -\Delta/T$ [33].

A natural question is: What happens in systems when both disorder and an umklapp scattering processes are non-negligible? Is there, depending on the strength of the umklapp processes or disorder, a single transition between the Mott insulator and the Anderson insulator or is the scenario more complex? One-dimensional systems of this type have indeed been considered in a number of publications. Early work by Ma [127] using real-space renormalization group for the disordered Hubbard model suggests a direct transition from the Anderson to the Mott insulating phase. This result contrasts with more recent works [128, 129, 130] where a new type of order, different from the Mott insulator and Anderson insulator, was found. In particular in Refs. [129, 130] the existence of a new Mott glass phase was postulated which is supposed to be incompressible but has no gap in the ac conductivity. Analytical investigations are hampered by the strong coupling nature of the phases which does not allow a renormalization group study. Alternative approaches, like the variational method used in Refs. [129, 130], are difficult to control. In this chapter we reinvestigate this problem by different means. The results have been published in Ref. [131].

The present chapter is organized as follows. Sec. 4.2 describes a model. In Sec. 4.3, we discuss the generalized rigidities and relate both the compressibility and the ac conductivity to the kink energy of the bosonic displacement field describing electrons. In Sec. 4.4, renormalization group equations are presented, possible phases are discussed and the phase diagram is given. The chapter concludes with a summary of the results and with brief comments on the variational approach with replica symmetry breaking.

4.2 Model

We study the interplay between point impurities and a periodic commensurate potential in a one-dimensional interacting electron system. The Hamiltonian consists of three parts

$$\mathcal{H} = \mathcal{H}_0 + \mathcal{H}_{\text{dis}} + \mathcal{H}_w, \quad (4.1)$$

describing a pure Luttinger liquid (\mathcal{H}_0), the influence of disorder (\mathcal{H}_{dis}) and the periodic potential (\mathcal{H}_w). In terms of the bosonic displacement field $\varphi(x)$ and its canonically conjugated momentum $\Pi(x)$ that describe one-dimensional spinless electrons, the Hamiltonian of a pure Luttinger liquid is [21]

$$\mathcal{H}_0 = \int_0^L dx \frac{\hbar}{2\pi} v \left\{ \frac{K}{\hbar^2} (\pi\Pi)^2 + \frac{(\partial_x \varphi)^2}{K} \right\}. \quad (4.2)$$

L denotes the system length and v is the plasmon velocity. The electron density can be written as [132]

$$\rho(x) = \frac{k_F}{\pi} - \frac{1}{\pi} \partial_x \varphi(x) + \frac{k_F}{\pi} \sum_n e^{i2n[k_F x - \varphi(x)]}, \quad (4.3)$$

where k_F is the Fermi momentum. The influence of randomly distributed point impurities is modeled in the same manner as in Chapter 2, just the flux line density is now replaced by the electron density.

$$\mathcal{H}_{\text{dis}} = \int_0^L dx \rho(x) V_p(x), \quad (4.4)$$

where $V_P(x) = \sum_{i=1}^{N_{\text{imp}}} v_p \delta(x - x_i) - v_p n_{\text{imp}}$ and n_{imp} denotes the impurity density. For weak and dense enough impurities that act collectively, one can without loss of any important information to introduce a coarse grained disorder potential $\tilde{V}(y) = \int dx V_P(x)/L_p$, where the integration is over a segment of length L_p that contains y and satisfies $L \gg L_p \gg n_{\text{imp}}^{-1}$. The central limit theorem tells us that \tilde{V} is a Gaussian distributed disorder with a correlator

$$\overline{\tilde{V}(x)\tilde{V}(x')} = v_p^2 n_{\text{imp}} \delta(x - x'). \quad (4.5)$$

Then, the disorder Hamiltonian becomes

$$\mathcal{H}_{\text{dis}} = \int_0^L dx \left[-\frac{\partial_x \varphi(x)}{\pi} \mu(x) + \frac{k_F}{\pi} \left\{ \zeta^*(x) e^{i2\varphi(x)} + H.c. \right\} \right]. \quad (4.6)$$

To the slowly varying part of the electron density effectively couples only

$$\mu(x) = \frac{1}{L} \sum_{|q| \sim 2\pi/L} \tilde{V}_q e^{iqx} \quad (4.7)$$

which includes only momenta $|q| \sim 2\pi/L$. For the weak disorder, i.e., for $v_p^2 n_{\text{imp}}$ smaller than the Fermi energy, disorder produces effects only close to the two Fermi points. As a result, to the periodic part of the density couples only $\pm 2k_F$ components of the disorder potential

$$\zeta(x) = \frac{1}{L} \sum_{|q| \sim 2\pi/L} \tilde{V}_{q-2k_F} e^{iqx}. \quad (4.8)$$

$\mu(x)$ describes the forward scattering on the impurities, whereas $\zeta(x)$ ($\zeta(x)^*$) describes the so-called backward scattering process that changes the momentum of an electron for $2k_F$ ($-2k_F$). The complex conjugated number to x is denoted by x^* . Since for the Gaussian potential the following is satisfied $\overline{\tilde{V}_q \tilde{V}_{q'}} = v_p^2 n_{\text{imp}} L \delta_{q,-q'}$, potentials $\mu(x)$ and $\zeta(x)$ are not correlated. The correlation functions read

$$\overline{\mu(x)\zeta(x')} = 0 \quad (4.9)$$

$$\overline{\mu(x)\mu(x')} \approx v_p^2 n_{\text{imp}} \delta(x-x') \quad (4.10)$$

$$\overline{\zeta(x)\zeta(x')} = 0 \quad (4.11)$$

$$\overline{\zeta(x)\zeta^*(x')} \approx v_p^2 n_{\text{imp}} \delta(x-x'). \quad (4.12)$$

Strictly speaking, Eqs. (4.10,4.12) are not correct, but they do not influence accuracy of the following expressions and conclusions.

The Hamiltonian modeling the commensurate periodic potential is given by

$$\mathcal{H}_w = - \int_0^L dx W_0 \cos(2k_F x) \rho(x) = - \int_0^L dx W \cos(2\varphi(x)), \quad (4.13)$$

where $W = W_0 k_F / \pi$. We point out that the Hamiltonian of Eq. (4.1) describes also spinfull electrons at half filling in the disorder potential for very repulsive interactions ($K_\rho < 1/3$), where \mathcal{H}_w describes an umklapp process. Then $\varphi_\rho = \varphi / \sqrt{2}$, $\Pi_\rho = \sqrt{2}\Pi$ and $K_\rho = K/2$; for more details see Ref. [130]. Hence, we conclude that in one dimension there is no essential difference in the charge sector between a band insulator and the Mott insulator.

The Euclidean action reads

$$S = \int_0^{\hbar/T} d\tau \int_0^L dx \frac{\hbar}{2\pi K} \left\{ v (\partial_x \varphi)^2 + \frac{1}{v} (\partial_\tau \varphi)^2 \right\} + \int_0^{\beta\hbar} d\tau (\mathcal{H}_w + \mathcal{H}_{\text{dis}}) \quad (4.14)$$

where $\varphi = \varphi(x, \tau)$. We set the Boltzmann constant to one, $k_B = 1$. After averaging over the disorder we obtain the replica action

$$\begin{aligned} \frac{S^{(n)}}{\hbar} &= \frac{1}{2\pi K} \int_{\tau, x} \sum_{\alpha=1}^n \{(\partial_x \varphi^\alpha)^2 + (\partial_\tau \varphi^\alpha)^2 - W \cos(2\varphi^\alpha)\} \\ &\quad - \frac{\sigma}{(2\pi K)^2} \int_{\tau, \tau', x} \sum_{\alpha, \gamma=1}^n \partial_x \varphi^\alpha(x, \tau) \partial_x \varphi^\gamma(x, \tau') \\ &\quad - \frac{u^2}{(2\pi K)^2} \int_{\tau, \tau', x} \sum_{\alpha, \gamma=1}^n \cos\{2\varphi^\alpha(x, \tau) - 2\varphi^\gamma(x, \tau')\}, \end{aligned} \quad (4.15)$$

where $\int_\tau \equiv \int_0^{\lambda_T \Lambda} d\tau$ and $\int_x = \int_0^{\Lambda L} dx$. Here we introduced dimensionless space and imaginary time coordinates by the transformation $\Lambda x \rightarrow x$ and $\Lambda v \tau \rightarrow \tau$, where Λ is the large momentum cut-off. $\lambda_T = \hbar v / T$ denotes the thermal de Broglie wavelength of the plasmons. α, γ are replica indexes. We introduced dimensionless quantities

$$w = \frac{2\pi K W}{\hbar \Lambda^2 v}, \quad (4.16)$$

$$\sigma = \frac{2n_{\text{imp}}(v_p K)^2}{\Lambda v^2 \hbar^2} \quad (4.17)$$

$$u^2 = \frac{n_{\text{imp}}(2v_p K k_F)^2}{\Lambda^3 v^2 \hbar^2}, \quad (4.18)$$

which measure the strength of the periodic potential (w), of the forward scattering (σ) and of the backward scattering (u^2).

4.3 Rigidities and ac conductivity

4.3.1 Generalized rigidities

In this subsection we consider a connection between rigidities, which are related to the inverse compressibility and the conductivity of the system, and the so-called kink energies needed to produce a change $\delta\varphi(x, \tau) = \pm\pi$ in the displacement field. We show that if the rigidities diverge, the appropriate description is in terms of the kink energies ¹.

First, we consider the application of a fixed strain ϑ by imposing the boundary conditions $\varphi(0, \tau) = 0$ and $\varphi(L, \tau) = \pi\vartheta L\Lambda$. The boundary

¹We encountered a similar situation in Chapter 2, see Sec. 2.4.2. When elastic constants c_{44} and c_{66} become divergent, the description in terms of Σ_z and Σ_y takes place. Σ_z and Σ_y determine the kink energies in the displacement field $u(\mathbf{r})$.

condition in the τ -direction is assumed to be periodic. For $\vartheta \ll 1$ and $L \rightarrow \infty$ the corresponding increase of the ground state energy $\Delta E_0(\vartheta, 0) = E_0(\vartheta, 0) - E_0(0, 0)$ is clearly an even but not necessarily analytic function of ϑ . The ground state energy of the system can be calculated using $E_0 = -\lim_{T \rightarrow 0} [T \ln \{ \int D\varphi \exp(-S/\hbar) \}]$. Thus

$$\frac{\Delta E_0(\vartheta, 0)}{L} \Big|_{L \rightarrow \infty} \approx \begin{cases} (\Lambda\vartheta)^2/(2\kappa), & \Sigma_x = 0, \\ \Lambda\Sigma_x|\vartheta|, & \kappa = 0. \end{cases} \quad (4.19)$$

The right hand side of this relation has to be understood as follows: if $\Sigma_x = 0$, then the stiffness $1/\kappa$ describes the response to the twisted boundary conditions and the change of φ is spread over the whole sample. If, however, the system becomes incompressible ($\kappa = 0$), then the kink energy Σ_x is nonzero. In this case the change of φ from 0 to π occurs in a narrow kink region of width ξ much smaller than L . Note that the action of Eq. (4.14) is invariant under the transformation $\varphi \rightarrow \varphi + n\pi$ with n integer. The position of the kink is chosen such that the energy is minimal. The creation of a kink corresponds to adding (or removing) an electron at the kink position. A nonzero kink energy resembles the step free energy of a surface below the roughening transition [133]. If we apply instead of the fixed boundary conditions an external stress to the system, then Σ_x is of the order of the critical stress to generate the first kink ².

In a similar manner we can apply non-trivial boundary conditions in the τ -direction by choosing $\varphi(x, 0) = 0$ and $\varphi(x, \tau) = \pi j\tau/e$. This corresponds to imposing an external current $j = e\langle\partial_\tau\varphi\rangle/\pi$ at $x = 0$ and $x = L$:

$$\frac{\Delta E_0(0, j)}{L} \Big|_{L \rightarrow \infty} \approx \begin{cases} j^2/(2D), & \Sigma_\tau = 0, \\ \Sigma_\tau|j|/e, & D = 0. \end{cases} \quad (4.21)$$

$D = e^2\kappa v^2$ denotes the charge stiffness. D determines the Drude peak of the conductivity [21, 134]

$$\sigma(\omega) = D\pi\delta(\omega) + \sigma_{\text{reg}}(\omega). \quad (4.23)$$

In Lorentz invariant systems, as the Mott insulator, Σ_x and Σ_τ satisfy the relation $\Sigma_x = v\Sigma_\tau$, provided they are finite.

So far we assumed that Σ_x is self-averaging if $L \rightarrow \infty$. In the same way we may introduce a local kink energy by applying twisted boundary conditions over a large but finite interval $[x, x + L_x]$, $\Lambda^{-1} \ll L_x \ll L$. Then, Σ_x will depend on the size L_x of the chosen interval and in the previous equations has to be replaced by $\Sigma_x \rightarrow \Sigma_x(L_x)$.

² Similarly, in the Chapter 2, Σ_z determines the threshold magnetic field that has to be overcome in order to tilt the flux lines, and Σ_y determines the critical shear stress; see Eq. (2.61)

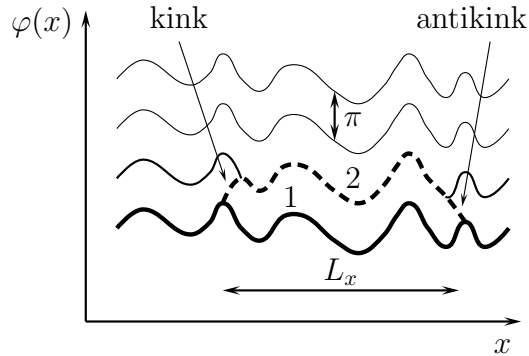


Figure 4.1: Kink and anti-kink in the displacement profile $\varphi(x)$. The thin lines represent the minima of the potential energy in the absence of the driving force, the bold line represent one metastable state and the dashed line represents the instanton configuration. Applying a fixed strain to the system only kinks (or anti-kinks) are enforced in the system.

4.3.2 Ac conductivity

In this subsection we show that the energy of the kink-antikink pair determines the gap in the ac conductivity. Then, by using the relation between the compressibility and the kink energy from the previous subsection, we conclude that incompressibility and the gap in the optical conductivity require each other.

In cases where D vanishes, the frequency dependent conductivity $\sigma(\omega)$ may still be nonzero, provided ω is finite. Spontaneous tunneling processes between metastable states and their instanton configurations will occur, see Fig. 4.1. Metastable states are here the classical ground states of Eq. (4.1). Different metastable states follow from each other by a shift of φ by a multiple of π . The instanton configuration connects two neighboring metastable states. Spontaneous tunneling leads to a level splitting of the two states of the order [135]

$$\delta E \approx \sqrt{4\Sigma_x^2(L_x) + C(\hbar v/\xi)^2 e^{-2L_x \Sigma_\tau/\hbar}}, \quad (4.24)$$

which has to match the energy $\hbar\omega$ of the external field. Here, \hbar/Σ_τ plays the role of the tunneling length and $C > 0$ is a numerical factor. This mechanism was first considered for noninteracting electrons by Mott [122] and later extended to the interacting case via instantons in Refs. [117, 118, 119]. Thus, to have a nonzero $\sigma(\omega)$ for arbitrary low frequency ω , it has to be satisfied $2\Sigma_x(L_x) < \omega\hbar \rightarrow 0$ that requires $2\Sigma_x(L_x) \rightarrow 0$ for a finite density of kink positions. This implies that the system is characterized by a finite compressibility.

4.4 Phase diagram

In this section we discuss the phase diagram of the model given by Eq. (4.1). We begin with a characterization of possible phases by attributing them to their renormalization group fixed points (denoted by superscript *). A subscript $_0$ stands for bare values. For small u , σ and w the lowest order renormalization group equations are:

$$\frac{dK}{dl} = -K(au^2 + bw^2) \quad (4.25)$$

$$\frac{d\sigma}{dl} = \sigma(1 - 2bw^2) \quad (4.26)$$

$$\frac{dw}{dl} = w(2 - K - \pi\sigma) \quad (4.27)$$

$$\frac{du^2}{dl} = u^2(3 - 2K) + \frac{\sigma w^2}{2\pi} \quad (4.28)$$

$$\frac{d\kappa}{dl} = -\kappa(z - 1 + bw^2) \quad (4.29)$$

As far as there is an overlap, the flow equations agree with those found in Refs. [136, 137]. The logarithm of the length scale is denoted by l , and a , b are positive non-universal constants. The dynamical critical exponent has been chosen to be $z = 1$, corresponding to the Luttinger liquid fixed point.

The Luttinger liquid phase is characterized by $u_L^* = w_L^* = 0$ and hence $\Sigma_x = \Sigma_\tau = 0$. $K_L^* > 0$ and $\kappa_L^* = K_L^*/(\hbar\pi v_L^*) > 0$. The fixed point is reached for sufficiently large values of K and σ . The long time and large scale behavior of the system is that of a clean Luttinger liquid characterized both by a finite compressibility κ_L^* and a finite charge stiffness $D_L = e^2\kappa_L^*v_L^{*2}$. The dynamical conductivity is given by $\sigma_{\text{reg}} = iD_L/\omega$. Note that the presence of the forward scattering term $\sim \mu(x)\partial_x\varphi$ does not change these results since it can be always removed by the transformation

$$\varphi(x) \rightarrow \varphi(x) + \frac{K}{\hbar v} \int_0^x dx' \mu(x'). \quad (4.30)$$

The Mott insulator is characterized by $K_M^* = \kappa_M^* = u_M^* = \sigma_M^* = 0$ but $w_M^* \gg 1$. Clearly the fixed point w_M^* is outside the applicability range of Eqs. (4.26-4.29) but nevertheless some general properties of this phase can be concluded. In the absence of disorder, the system is in the universality class of the two-dimensional classical sine-Gordon model which describes the Mott insulator to the Luttinger liquid transition and the roughening transition of a two-dimensional classical crystalline surface [133]. In the Mott insulating

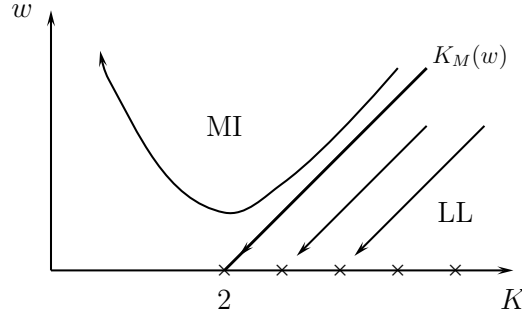


Figure 4.2: Schematic phase diagram shows the transition from the Mott insulator (MI) to the Luttinger liquid (LL) phase in the absence of disorder.

phase the compressibility and the Drude peak vanish. The system is characterized by a finite kink energy $\Sigma_x = v\Sigma_\tau \sim (\kappa_0\xi_M)^{-1}$, where ξ_M denotes the correlation length of the Mott insulating phase [133]. Σ_x vanishes at the Berezinskii-Kosterlitz-Thouless (BKT) transition to the Luttinger liquid phase as

$$\Sigma_x \sim \xi_M^{-1} \sim \exp \left[-\sqrt{\frac{b}{1 - K/K_M(w)}} \right], \quad (4.31)$$

where $b > 0$ is a non-universal number. $K_M(w) \geq 2$ and denotes the boundary between the Luttinger liquid and the Mott insulator, see Fig. 4.2. According to Eq. (4.24) the ac conductivity vanishes for $\omega \lesssim 2\Sigma_x/\hbar$.

The Anderson insulator is characterized by $w_A^* = K_A^* = 0$ and $u_A^* \gg 1$. $\kappa_A^* \approx \kappa_0$ is finite, which is the result of the statistical tilt symmetry [63]. In the absence of the commensurate potential the system is in the universality class of the two-dimensional sine-Gordon model with a random phase correlated in the τ -direction. The transition to the Luttinger liquid phase occurs at $K = K_A(u) \geq 3/2$ and is also of BKT type [32]. The Anderson insulator correlation length ξ_A satisfies the standard BKT form of Eq. (4.31), with the replacement $K_M(w) \rightarrow K_A(u)$.

Next, we consider $\Sigma_x(L_x)$ at a length scale $\xi_A \ll L_x \ll L$, such that the parameters are close to their fixed point values. The backward scattering term in the Hamiltonian of Eq. (4.6) can be effectively written as [77]

$$\mathcal{H}_{\text{back}} = \frac{2k_F}{\pi} \sqrt{\Lambda v_p^2 n_{\text{imp}}} \int dx \cos [2\varphi(x) + \alpha(x)], \quad (4.32)$$

where $\alpha(x)$ is a random phase uniformly distributed in the interval $[0, 2\pi]$ and satisfies $\overline{\exp [i\alpha(x) - i\alpha(x')]} = \Lambda^{-1}\delta(x - x')$. Then, in the same manner as in Secs. 2.5 and 2.6.3, one can determine the ground state configuration

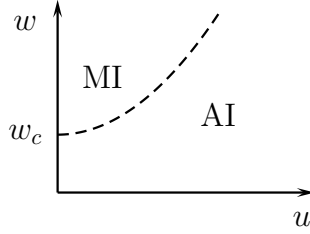


Figure 4.3: Schematic phase diagram for $K < 3/2$ with $w_c \sim \sigma^2$. MI (AI) denotes that the Mott (Anderson) insulating state is realized in indicated region of parameters.

and find the typical kink energy to be $\Sigma_x(L_x) \sim (\kappa_0 L_x)^{-1}$. Hence, the kink energy vanishes for $L_x \rightarrow \infty$ and the system is compressible. As already explained, a vanishing Σ_x is also crucial for the existence of the low frequency conductivity. The Anderson insulator is characterized by $\sigma(\omega) \sim \omega^2 \ln(\omega)^2$ as has been discussed in detail in Refs. [117, 118, 119]. This result can be understood in terms of tunneling processes between rare positions at which the kink energies $\Sigma_x(x)$ are much smaller than $1/(\kappa_0 L_x)$. Twisted boundary conditions in the τ -direction give a finite $\Sigma_\tau \sim \hbar(K_0 \xi_A)^{-1}$ [77].

Mott glass phase is new hypothetical phase that was proposed in Refs. [129, 130] to appear at $K \leq 1$ and to be characterized by a vanishing compressibility, $\kappa_G^* = 0$, but a nonzero optical conductivity at low frequencies. Since the phase is considered to be glassy, both fixed point values $w_G^*, u_G^* \gg 1$. By applying the transformation given by Eq. (4.30), one obtains two backward scattering terms in the Hamiltonian of Eq. (4.1). Then, similarly to the Anderson insulator, the ground state can be found by minimizing first the two backward scattering terms followed by minimization of the elastic energy. Although the ground state solution is now more involved than for the Mott insulator and the Anderson insulator, it is clearly periodic with period π . As before, kinks (or anti-kinks) with $\delta\varphi = \pm\pi$ allow the accommodation of twisted boundary conditions and the formation of instantons. A vanishing compressibility corresponds to a finite kink energy Σ_x which, according to (4.24), leads to a gap in the ac-conductivity. Here we make the reasonable assumption that it is the instanton mechanism which dominates the low frequency response [118]. Thus, in a system with a nonzero $\sigma(\omega)$ for small ω , also the compressibility has to be nonzero, contrary to the claims in Refs. [129, 130].

So far we assumed that the interactions are short-range. In the case of an Anderson insulator with additional long-range Coulomb interaction

$V(r) = e^2/(\epsilon_s r)$ the inverse compressibility is increased by [21]

$$\Delta\kappa^{-1} = \frac{2e^2}{\epsilon_s} \ln(Lk_F), \quad (4.33)$$

where ϵ_s is the dielectric constant. Thus, for $L \rightarrow \infty$ the system becomes incompressible. The effect of Coulomb interaction on the ac conductivity is known only for $K = 1$, where in the limit of small frequencies one obtains $\sigma(\omega) \sim \omega \ln \omega$ [138]. Therefore, the Anderson insulator is transformed into the Mott glass phase.

Having characterized possible phases, we now discuss the phase diagram of the model of Eq. (4.1). From Eq. (4.28) follows that the random backward scattering term is generated by forward scattering and the commensurate potential. Since $\sigma(l) \approx \sigma_0 e^l$, $\sigma(l)$ becomes large provided the initial value σ_0 is not too small. Then for $K < 3/2$, two Eigenvalues $\lambda_1 = 3 - 2K$ and $\lambda_2 = 4 - 2K - \sigma$ describing the renormalization group flow of u^2 and w^2 around the Luttinger liquid fixed point $u^* = w^* = 0$ have opposite sign: $u(l)$ increases whereas $w(l)$ decreases. Thus the hypothetical Mott glass phase, if it existed, could not reach up to the point $u = w = 0$, in contrast to the findings in Ref. [129]. From this, we conclude that for not too large values of w_0 the Anderson insulating phase is stable, as shown in Fig. 4.3.

To find the phase boundary to the Mott insulating phase, we consider the stability of the Mott insulator with respect to the formation of a kink by the disorder. To lowest order in the disorder, we obtain the kink energy in the Mott phase to be

$$\Sigma_x \sim \frac{\sqrt{w_0}}{\kappa_0} \left(1 - \frac{1}{\pi} \frac{\sigma_0^{1/2}}{w_0^{1/4}} - \frac{2}{\pi^2} \frac{u_0}{w_0^{3/4}} \right). \quad (4.34)$$

From the condition $\Sigma_x = 0$ one obtains the phase boundary between the Mott insulating phase and the Anderson insulating phase, as depicted in Fig. 4.3. A similar result follows from the self-consistent harmonic approximation. So far we considered only typical disorder fluctuations. If rare events are taken into account for Gaussian distributed $\zeta(x)$ and $\mu(x)$, then (4.34) remains valid with the replacements $\sigma_0 \rightarrow \sigma_0 \ln(L\Lambda)$ and $u_0^2 \rightarrow u_0^2 \ln(L\Lambda)$. Thus, the size of the Mott insulating phase is reduced, but finite, unless $L \rightarrow \infty$.

The phase diagram shown in Fig. 4.3 is also supported by the observation that the transformation (4.30) leaves only random backward scattering term of strength $u_0^2 + w_0^2 / (2\pi^4 \sigma_0)$ in the replicated action on sufficiently large length scales $L \gtrsim 1/(\sigma_0 \Lambda)$ [139]. This is only valid for weak bare disorder and commensurate potential. Therefore, the Anderson insulating phase occurs for sufficiently small quantum fluctuations, w and u . Thus, to conclude, we

only find three phases: the Luttinger liquid, Mott insulator and Anderson insulator.

4.5 Discussions and conclusions

We have shown in this chapter that an incompressible one-dimensional disordered Mott insulator has a vanishing optical conductivity in the limit of small frequencies. Our approach has some similarities with the treatment of the flat phase of a surface undergoing a roughening transition [133] and may be useful for other strong coupling problems as well. Adding (removing) a charge at a site x corresponds to the insertion of a $\delta\varphi(x) = \pm\pi$ kink in the bosonic field. The compressibility of the systems is determined by adding kinks (or antikinks) to the classical ground state of the system. If the kink energy is finite, the system is incompressible. Similarly, the optical conductivity follows from transitions between the ground state and the first excited state which involves kink-antikink pairs. We have shown that for vanishing kink energy, the level splitting between the ground and the excited state is exponentially small in the kink-antikink distance. A decreasing energy $\hbar\omega$ then drives transitions between levels of pairs of ever increasing distance, and hence the ac conductivity remains finite for small ω . This is no longer the case when the kink energy is finite: the energy of the kink-antikink pair is the lower bound for the level splitting, and hence the optical conductivity shows a gap of this size. Thus, as long as there is no true long-range interaction between charges, incompressibility and a gap in the optical conductivity require each other. Thus, there is no Mott glass phase for systems with short-range interaction only.

Finally, we briefly comment on the variational approach with replica symmetry breaking which has been used in Refs. [129, 130]. In the variational approach, the full Hamiltonian is replaced by a harmonic one which leads to the decoupling of Fourier components φ_q with different wavevector q . Without replica symmetry breaking, one obtains from this approach the results of perturbation theory which is valid only on scales smaller than the Larkin length. Replica symmetry breaking gives then the possibility of a further reduction of the free energy. The results obtained in this way are exact only in cases when the coupling between different Fourier components is irrelevant and the physics is dominated by the largest length scale. Thus, replica symmetry breaking is not an intrinsic property of the true solution of the problem, but a property of the variational approach. An illustrative example is the related problem of the interface roughening transition in a random potential [140]. The variational approach with replica symmetry breaking gives

three phases: a flat, a rough glassy, and an intermediate glassy flat phase [141]. The functional renormalization group method takes the coupling of different Fourier modes into account and gives only two phases: the flat and the rough phase, while the glassy flat phase is replaced by a crossover region with logarithmic roughness [140]. A similar situation may also exist in the present case.

Bibliography

- [1] M. Tinkham, *Introduction to Superconductivity* (McGraw–Hill, New York, 1996), 2nd ed.
 - [2] G. Blatter, M. V. Feigel'man, V. B. Geshkenbein, A. I. Larkin, and V. M. Vinokur, *Rev. Mod. Phys.* **66**, 1125 (1994).
 - [3] T. Nattermann and S. Scheidl, *Adv. Phys.* **49**, 607 (2000).
 - [4] J. Bardeen and M. J. Stephen, *Phys. Rev.* **140**, 1197A (1965).
 - [5] P. W. Anderson, *Phys. Rev. Lett.* **9**, 309 (1962).
 - [6] P. W. Anderson and Y. B. Kim, *Rev. Mod. Phys.* **36**, 39 (1964).
 - [7] A. I. Larkin, *Sov. Phys. JETP* **31**, 784 (1970).
 - [8] T. Nattermann, *Phys. Rev. Lett.* **64**, 2454 (1990).
 - [9] T. Giamarchi and P. Le Doussal, *Phys. Rev. Lett.* **72**, 1530 (1994).
 - [10] T. Giamarchi and P. Le Doussal, *Phys. Rev. B* **52**, 1242 (1995).
 - [11] T. Emig, S. Bogner, and T. Nattermann, *Phys. Rev. Lett.* **83**, 400 (1999).
 - [12] S. Bogner, T. Emig, and T. Nattermann, *Phys. Rev. B* **63**, 174501 (2001).
 - [13] T. Klein, I. Joumard, S. Blanchard, J. Marcus, R. Cubitt, T. Giamarchi, and P. Le Doussal, *Nature* **413**, 404 (2001).
 - [14] J. Kierfeld, T. Nattermann, and T. Hwa, *Phys. Rev. B* **55**, 626 (1997).
 - [15] D. S. Fisher, *Phys. Rev. Lett.* **78**, 1964 (1997).
 - [16] J. Kierfeld, H. Nordborg, and V. M. Vinokur, *Phys. Rev. Lett.* **85**, 4948 (2000).
 - [17] J. Kierfeld and V. Vinokur, *Phys. Rev. B* **69**, 024501 (2004).
-

-
- [18] G. Grüner, *Rev. Mod. Phys.* **60**, 1129 (1988).
- [19] A. D. Bruce and R. A. Cowley, *J. Phys. C* **11**, 3609 (1978).
- [20] F. D. M. Haldane, *J. Phys. C* **14**, 2585 (1981).
- [21] T. Giamarchi, *Quantum Physics in One Dimension* (Clarendon Press, 2003), 1st ed.
- [22] P. Nozieres and D. Pines, *Theory of Quantum Liquids* (Westview Press, Boulder, 1999).
- [23] M. Tzolov, B. Chang, D. S. A. Yin, J. M. Xu, and G. Brown, *Phys. Rev. Lett.* **92**, 075505 (2004).
- [24] J. Cummins and A. Zettl, *Phys. Rev. Lett.* **93**, 86801 (2004).
- [25] A. N. Aleshin, J. Y. Lee, S. W. Chu, S. W. Lee, B. Kim, S. J. Ahn, and Y. W. Park, *Phys. Rev. B* **69**, 214203 (2004).
- [26] W. Kang, H. L. Stormer, L. N. Pfeiffer, K. W. Baldwin, and K. W. West, *Nature* **59**, 403 (2000).
- [27] O. M. Auslaender, A. Yacoby, R. de Picciotto, K. W. Baldwin, L. N. Pfeiffer, and K. W. West, *Science* **295**, 825 (2002).
- [28] T. Stöferle, H. Moritz, C. Schori, M. Köhl, and T. Esslinger, *Phys. Rev. Lett.* **92**, 130403 (2004).
- [29] C. L. Kane and M. P. A. Fisher, *Phys. Rev. B* **46**, 15233 (1992).
- [30] C. L. Kane and M. P. A. Fisher, *Phys. Rev. Lett.* **68**, 1220 (1992).
- [31] A. Furusaki and N. Nagaosa, *Phys. Rev. B* **47**, 4631 (1993).
- [32] T. Giamarchi and H. J. Schulz, *Phys. Rev. B* **37**, 325 (1988).
- [33] T. Giamarchi, *Physica B* **230**, 975 (1997).
- [34] D. R. Nelson and V. M. Vinokur, *Phys. Rev. Lett.* **68**, 2398 (1992).
- [35] D. R. Nelson and V. M. Vinokur, *Phys. Rev. B* **48**, 13060 (1993).
- [36] I. F. Lyuksyutov, *Europhys. Lett.* **20**, 273 (1992).
- [37] L. Radzihovsky, *Phys. Rev. Lett.* **74**, 4923 (1995).
-

-
- [38] T. Roy and T. E. Mitchell, *Philos. Mag. A* **63**, 225 (1991).
- [39] G. W. Crabtree, W. K. Kwok, U. Welp, J. Downey, S. Flesher, K. G. Vandervoort, and J. Z. Liu, *Physica C* **185-189**, 282 (1991).
- [40] W. K. Kwok, S. Flesher, U. Welp, V. M. Vinokur, J. Downey, G. W. Crabtree, and M. M. Miller, *Phys. Rev. Lett.* **69**, 3370 (1992).
- [41] M. Oussena, P. A. J. de Groot, K. Deligiannis, A. V. Volkov, R. Gagnon, and L. Taillefer, *Phys. Rev. Lett.* **76**, 2559 (1996).
- [42] S. Sanfilippo, D. Bourgault, C. Villard, R. Tournier, P. G. Picard, E. Beaunon, A. Sulpice, Th. Fournier, and P. Germin, *Europhys. Lett.* **39**, 657 (1997).
- [43] M. C. Marchetti and V. M. Vinokur, *Phys. Rev. B* **51**, 16276 (1995).
- [44] G. J. Dolan, G. V. Chandrashekar, T. R. Dinger, C. Feild, and F. Holtzberg, *Phys. Rev. Lett.* **62**, 827 (1989).
- [45] L.-H. Tang and I. F. Lyuksyutov, *Phys. Rev. Lett.* **71**, 2745 (1993).
- [46] L. Balents and M. Kardar, *Europhys. Lett.* **23**, 503 (1993).
- [47] L. Balents and M. Kardar, *Phys. Rev. B* **49**, 13030 (1994).
- [48] T. Hwa and T. Nattermann, *Phys. Rev. B* **51**, 455 (1995).
- [49] T. Emig and T. Nattermann, *Phys. Rev. Lett.* **97**, 177002 (2006).
- [50] A. Petković, T. Emig, and T. Nattermann, *Phys. Rev. B* **79**, 224512 (2009).
- [51] A. Petković and T. Nattermann, *Phys. Rev. Lett.* **101**, 267005 (2008).
- [52] L. D. Landau and E. M. Lifshitz, *Elasticity theory* (Elsevier Butterworth Heinemann, 2004), 2nd ed.
- [53] M. V. Feigel'man, V. B. Geshkenbein, A. I. Larkin, and V. M. Vinokur, *Phys. Rev. Lett.* **63**, 2303 (1989).
- [54] S. E. Korshunov, *Phys. Rev. B* **48**, 3969 (1993).
- [55] M. Kardar, *J. Appl. Phys.* **61**, 3601 (1987).
- [56] T. Nattermann, *Europhys. Lett.* **4**, 1241 (1987).
-

-
- [57] M. Laver, E. M. Forgan, A. B. Abrahamsen, C. Bowell, Th. Geue, and R. Cubitt, *Phys. Rev. Lett.* **100**, 107001 (2008).
- [58] P. Le Doussal and K. J. Wiese, *Phys. Rev. E* **68**, 046118 (2003).
- [59] T. Hwa and D. S. Fisher, *Phys. Rev. Lett.* **72**, 2466 (1994).
- [60] W. Hofstetter, I. Affleck, D. R. Nelson, and U. Schollwöck, *Europhys. Lett.* **66**, 178 (2004).
- [61] I. Affleck, W. Hofstetter, D. R. Nelson, and U. Schollwöck, *J. Stat. Mech. Theor. Exp.* p. 10003 (2004).
- [62] R. Egger and H. Grabert, *Phys. Rev. Lett.* **75**, 3505 (1995).
- [63] U. Schulz, J. Villian, E. Brezin, and H. Orland, *J. Stat. Phys.* **51**, 1 (1988).
- [64] V. G. Kogan and L. J. Campbell, *Phys. Rev. Lett.* **62**, 1552 (1989).
- [65] J. Imry and S. K. Ma, *Phys. Rev. Lett.* **35**, 1399 (1975).
- [66] D. S. Fisher, *Phys. Rev. Lett.* **56**, 1964 (1986).
- [67] L. Balents and D. S. Fisher, *Phys. Rev. B* **48**, 5949 (1993).
- [68] L. Balents, *Europhys. Lett.* **24**, 489 (1993).
- [69] A. A. Fedorenko, *Phys. Rev. B* **77**, 094203 (2008).
- [70] T. Nattermann, S. Stepanow, L. H. Tang, and H. Leschhorn, *J. Phys. II France* **2**, 1483 (1992).
- [71] J. Villain and J. F. Fernandez, *Z. Phys. B* **54**, 139 (1984).
- [72] M. V. Feigelman, *Sov. Phys. JETP* **52**, 3 (1980).
- [73] S. V. Malinin and T. Nattermann, *Int. J. Mod. Phys. B* **21**, 4164 (2007).
- [74] A. Glatz and T. Nattermann, *Phys. Rev. B* **69**, 115118 (2004).
- [75] J. H. V. Hoff, *Etudes de Dynamiques Chimiques* (F. Muller and Co., Amsterdam, 1884).
- [76] S. Arrhenius, *Z. Phys. Chem.* **4**, 226 (1889).
- [77] S. V. Malinin, T. Nattermann, and B. Rosenow, *Phys. Rev. B* **70**, 235120 (2004).
-

-
- [78] E. H. Brandt, Phys. Rev. B. **34**, 6514 (1986).
- [79] P. F. Arndt and T. Nattermann, Phys. Rev. B. **63**, 134204 (2001).
- [80] B. I. Halperin and D. R. Nelson, Phys. Rev. Lett. **41**, 121 (1978).
- [81] P. Moretti, M.-C. Miguel, M. Zaiser, and S. Zapperi, Phys. Rev. B **69**, 214103 (2004).
- [82] L. Radzihovsky, Phys. Rev. B **73**, 104504 (2006).
- [83] C. L. Kane and M. P. A. Fisher, Phys. Rev. B **46**, 15233 (1992).
- [84] L. Balents and D. R. Nelson, Phys. Rev. Lett. **73**, 2618 (1994).
- [85] N. D. Mermin and H. Wagner, Phys. Rev. Lett. **17**, 1133 (1966).
- [86] P. C. Hohenberg, Phys. Rev B **158**, 383 (1967).
- [87] V. L. Berezinskii, Zh. Eksp. Teor. Fiz. **61**, 1144 (1971).
- [88] J. M. Kosterlitz and D. J. Thouless, J. Phys. C **6**, 1181 (1973).
- [89] J. M. Kosterlitz, J. Phys. C **7**, 1046 (1974).
- [90] B. I. Halperin and D. R. Nelson, J. Low Temp. Phys. **36**, 599 (1979).
- [91] P. Minnhagen, Rev. Mod. Phys. **59**, 1001 (1987).
- [92] A. T. Fiory, A. F. Hebard, and W. I. Glaberson, Phys. Rev. B **28**, 5075 (1983).
- [93] A. M. Kadin, K. Epstein, and A. M. Goldman, Phys. Rev. B **27**, 6691 (1983).
- [94] J. Pearl, Appl. Phys. Lett. **5**, 65 (1964).
- [95] J. Pearl, in Low Temperature Physics-LT9, edited by J. G. Daunt, D. O. Edwards, F. J. Milford, and M. Yagub (1965), p. 566.
- [96] M. R. Beasley, J. E. Mooij, and T. P. Orlando, Phys. Rev. Lett. **42**, 1165 (1979).
- [97] V. L. Pokrovskii and G. V. Uimin, Sov. Phys. JETP **38**, 847 (1974).
- [98] D. R. Nelson and J. M. Kosterlitz, Phys. Rev. Lett. **39**, 1201 (1977).
- [99] P. B. Wiegmann, J. Phys. C **11**, 1583 (1978).
-

-
- [100] I. Affleck, Phys. Rev. Lett. **46**, 388 (1981).
- [101] L. Landau and E. Lifschitz, Quantum Mechanics (Pergamon, Oxford, 1997).
- [102] R. Iengo and G. Jug, Phys. Rev. B **54**, 13207 (1996).
- [103] P. Ao, J. Low Temp. Phys. **89**, 543 (1992).
- [104] V. I. Goldanskii, Dokl. Acad. Nauk SSSR **124**, 1261 (1959).
- [105] B. I. Halperin and D. R. Nelson, J. Low Temp. Phys. **36**, 599 (1979).
- [106] S. Doniach and B. A. Huberman, Phys. Rev. Lett. **42**, 1169 (1979).
- [107] A. I. Larkin and Yu. N. Ovchinnikov, JETP Lett. **37**, 382 (1983).
- [108] E. M. Chudnovsky, Phys. Rev. A **46**, 8011 (1992).
- [109] A. I. Larkin and Yu. N. Ovchinnikov, Sov. Phys. JETP **59**, 2 (1984).
- [110] A. O. Caldeira and A. J. Leggett, Phys. Rev. Lett. **46**, 211 (1981).
- [111] S.-Y. Lee, H. Kim, D. K. Park, C. S. Park, and J. K. Kim, Phys. Rev. B **60**, 308 (1999).
- [112] P. W. Anderson, Phys. Rev. B **109**, 1492 (1958).
- [113] E. Abrahams, P. W. Anderson, D. C. Licciardello, and T. V. Ramakrishnan, Phys. Rev. Lett. **42**, 673 (1979).
- [114] A. D. Finkel'stein, Z. Physik B **56**, 189 (1984).
- [115] T. Nattermann, T. Giamarchi, and P. Le Doussal, Phys. Rev. Lett. **91**, 56603 (2003).
- [116] A. Glatz and T. Nattermann, Phys. Rev. Lett. **88**, 256401 (2002).
- [117] M. V. Feigelman and V. M. Vinokur, Phys. Rev. Lett. **87A**, 53 (1981).
- [118] M. M. Fogler, Phys. Rev. Lett. **88**, 186402 (2002).
- [119] B. Rosenow and T. Nattermann, Phys. Rev. B **73**, 085103 (2006).
- [120] B. I. Shklovskii, Fiz. Tekh. Poluprovodn. (S. Peterburg) **6**, 2335 (1972).
- [121] N. F. Mott, Journal of Non-Crystalline Solids **1**, 1 (1968).
-

-
- [122] N. F. Mott, *Philos. Mag.* **17**, 1259 (1968).
- [123] N. F. Mott, *Metal-Insulator Transitions* (Taylor and Francis, London, 1990).
- [124] V. J. Emery, in *Highly Conducting One-Dimensional Solids* (Plenum, New York, 1979).
- [125] J. Sólyom, *Adv. Phys.* **28**, 209 (1979).
- [126] K. Maki, *Phys. Rev. Lett.* **39**, 46 (1977).
- [127] M. Ma, *Phys. Rev. B* **26**, 5097 (1982).
- [128] H. Pang, S. Liang, and J. F. Annett, *Phys. Rev. Lett.* **26**, 4377 (1993).
- [129] E. Orignac, T. Giamarchi, and P. Le Doussal, *Phys. Rev. Lett.* **83**, 2378 (1999).
- [130] T. Giamarchi, P. Le Doussal, and E. Orignac, *Phys. Rev. B* **64**, 245119 (2001).
- [131] T. Nattermann, A. Petković, Z. Ristivojevic, and F. Schütze, *Phys. Rev. Lett.* **99**, 186402 (2007).
- [132] F. D. M. Haldane, *Phys. Rev. Lett.* **47**, 1840 (1981).
- [133] P. Nozieres, in *Solids Far from Equilibrium*, edited by C. Godreche (Cambridge University Press, Cambridge, 1992).
- [134] W. Kohn, *Phys. Rev.* **133**, A171 (1964).
- [135] A. Rivero, arxiv:0209072 (2002).
- [136] S. Fujimoto and N. Kawakami, *Phys. Rev. B* **54**, R11018 (1996).
- [137] I. F. Herbut, *Phys. Rev. B* **57**, 13729 (1998).
- [138] B. I. Shklovskii and A. L. Efros, *Sov. Phys. JETP* **54**, 218 (1981).
- [139] M. P. A. Fisher, P. B. Weichman, G. Grinstein, and D. S. Fisher, *Phys. Rev. B* **40**, 546 (1989).
- [140] T. Emig and T. Nattermann, *Phys. Rev. Lett.* **81**, 1469 (1998).
- [141] J.-P. Bouchaud and A. Georges, *Phys. Rev. Lett.* **68**, 3908 (1992).
-

Acknowledgements

- I would like to thank Prof. Dr. Thomas Nattermann for supervising this thesis and sharing his ideas and views of physics and of life with us, his students.
 - I would like to thank Dr. Thorsten Emig for a fruitful collaboration.
 - I would like to thank Prof. Dr. V. M. Vinokur for helpful discussions on the topic studied in Chapter 3.
 - My special thanks goes to Friedmar Schütze for a friendly atmosphere, many discussions and a critical reading of parts of this thesis.
 - I thank Dr. Gianmaria Falco, Dr. Leiming Chen and Dr. Christophe Deroulers for a nice ambiance and pleasant lunch breaks.
 - And, of course, I thank Zoran Ristivojevic for his patience, innumerable discussions and everything else.
-

Abstract

This thesis investigates three different topics related to transport and order in type-II superconductors and Luttinger liquids.

In the main part of this thesis, in Chapter 2, we study the influence of randomly distributed point impurities and planar defects on the static and dynamic properties of type-II superconductors. It is shown that the phase resulting from weak point impurities, the so-called Bragg glass phase, is unstable with respect to planar defects. Even a single weak defect plane oriented parallel to the magnetic field as well as to one of the main axis of the Abrikosov flux line lattice is a relevant perturbation in the Bragg glass phase. We examine the effect of a finite density of randomly distributed parallel planar defects aligned to the magnetic field and find that the system exhibits a new glassy phase, which we call planar glass. The planar glass is characterized by a transverse Meissner effect and by resistance against shear deformations. We also obtain sample to sample fluctuations of the longitudinal magnetic susceptibility and an exponential decay of translational order in the direction perpendicular to the defects. The flux creep perpendicular to the defects leads to a nonlinear resistivity and a new creep exponent $\mu = 3/2$. We find that strong planar defects enforce edge dislocations located at the defects, with a Burgers vector parallel to the defects, in order to relax shear strain.

In Chapter 3, we study voltage-current characteristics occurring in a thin superconducting film at different temperatures and in the absence of an external magnetic field. Below the Berezinskii-Kosterlitz-Thouless transition vortices and antivortices are bound into pairs. In the presence of a transport current, that tends to separate a pair, there is a finite energy barrier that has to be overcome in order to break a vortex pair and produce free vortices. Hence, thermally activated pairs can dissociate yielding a nonlinear power law voltage-current relation. We find that at sufficiently low temperatures the quantum tunneling of vortices through the barrier turns out to be more probable than the thermal activation over the barrier, leading to a different voltage-current relation than the above mentioned classical one. We study the crossover from purely quantum to purely classical behavior.

In Chapter 4, we investigate the competition between the Mott and the

Anderson insulating state in a one-dimensional disordered fermionic system. Contrary to some studies, tracing back both a finite compressibility and a nonzero ac conductivity to vanishing kink energy of the electronic displacement field, we exclude the existence of an intermediate Mott Glass phase in systems with short-range interaction. The phase diagram is constructed from combining the information from the renormalization group flow, the kink energy, and simple scaling arguments.

Zusammenfassung

Die vorliegende Arbeit untersucht drei verschiedene Problemfelder, die sich mit Transport- und Ordnungsphänomenen in Supraleitern 2. Art und in Luttingerflüssigkeiten befassen.

Im Hauptteil dieser Arbeit, in Kapitel 2, wird der Einfluß zufällig verteilter Punktstörstellen sowie planarer Defekte auf die statischen und dynamischen Eigenschaften von Supraleitern 2. Art studiert. Es wird gezeigt, daß die von schwachen Punktstörstellen erzeugte Phase, die sogenannte Bragg-Glas-Phase, instabil gegenüber planaren Defekten ist. Sogar eine einzige schwache Defektebene stellt eine relevante Störung im Bragg-Glas dar, wenn sie parallel zum Magnetfeld oder zu einer der Hauptachsen des Flußliniengitters (Abrikosowgitter) ausgerichtet ist. Wir untersuchen den Effekt einer endlichen Dichte zufällig verteilter paralleler planarer Defekte, die parallel zum Magnetfeld ausgerichtet sind, und finden, daß das System eine neue glasartige Phase, die wir planares Glas nennen, aufweist. Das planare Glas ist charakterisiert durch einen transversalen Meißnereffekt, sowie eine hohe Widerstandskraft gegenüber Scherungsdeformationen. Darüberhinaus erhalten wir Fluktuationen der longitudinalen magnetischen Suszeptibilität unter den verschiedenen Proben (Unordnungskonfigurationen) und es ergibt sich ein exponentieller Zerfall der Translationsordnung senkrecht zu den Defekten. Das Kriechen der Flußlinien senkrecht zu den Defekten führt zu einem nichtlinearen spezifischen Widerstand und einem neuen Kriechexponenten $\mu = 3/2$. Weiter finden wir, daß starke planare Defekte zum Auftreten von Versetzungsfehlstellen an den Defektebenen führen, wobei der Burgersvektor parallel zu den Defekten ausgerichtet ist, um die Scherungen kleinzuhalten.

In Kapitel 3 werden Spannungs-Strom-Charakteristika dünner supraleitender Filme bei verschiedenen Temperaturen in Abwesenheit externer Magnetfelder untersucht. Unterhalb des Berezinskii-Kosterlitz-Thouless-Übergangs sind Wirbelkonfigurationen (Vortizes) entgegengesetzter Orientierung paarweise gebunden (Vortexpaare). In Gegenwart eines Transportstromes, der sich destabilisierend auf die Vortexpaare auswirkt, gibt es eine endliche Energiebarriere, die überwunden werden muß, um die Vortexpaare aufzuspalten und freie Vortizes zu erzeugen. Durch thermische Anregung können Vortexpaare somit dissoziieren und es ergibt sich ein Potenzgesetz für die

Spannungs-Strom-Beziehung. Bei hinreichend kleinen Temperaturen erweist sich das Quantentunneln der Vortizes durch die Energiebarriere hindurch als maßgeblich im Vergleich zur thermischen Anregung. Dies führt zu einer Spannungs-Strom-Beziehung, die sich von der oben erwähnten klassischen unterscheidet. Darüberhinaus untersuchen wir die Überleitung vom Quanten- zum klassischen Verhalten.

In Kapitel 4 befassen wir uns mit dem Gegenspiel von Mott- und Andersonisolator in eindimensionalen ungeordneten fermionischen Systemen. Indem wir sowohl die endliche Kompressibilität, als auch die endliche ac-Leitfähigkeit auf eine verschwindende Kinkenergie des elektronischen Verzerrungsfeldes zurückführen, können wir in Systemen mit kurzreichweitiger Wechselwirkung die Existenz einer intermediären Mottglasphase ausschließen. Das Phasendiagramm kann durch das Zusammenführen der Informationen über den Renormierungsgruppenfluß und der Kinkenergie, sowie durch einfache Skalenargumente konstruiert werden.

Erklärung

Ich versichere, dass ich die von mir vorgelegte Dissertation selbständig angefertigt, die benutzten Quellen und Hilfsmittel vollständig angegeben und die Stellen der Arbeit - einschließlich Tabellen, Karten und Abbildungen -, die anderen Werken im Wortlaut oder dem Sinn nach entnommen sind, in jedem Einzelfall als Entlehnung kenntlich gemacht habe; dass diese Dissertation noch keiner anderen Fakultät oder Universität zur Prüfung vorgelegen hat; dass sie - abgesehen von unten angegebenen Teilpublikationen - noch nicht veröffentlicht worden ist sowie, dass ich eine solche Veröffentlichung vor Abschluss des Promotionsverfahrens nicht vornehmen werde. Die Bestimmungen der Promotionsordnung sind mir bekannt. Die von mir vorgelegte Dissertation ist von Prof. Dr. Thomas Nattermann betreut worden.

Köln, 10. Mai 2009

Aleksandra Petković

Teilpublikationen

1. T. Nattermann, A. Petković, Z. Ristivojevic, F. Schütze, "Absence of the Mott Glass Phase in 1D Disordered Fermionic Systems", Phys. Rev. Lett. **99**, 186402 (2007).
 2. A. Petković and T. Nattermann, "Order and Creep in Flux Lattices and CDWs Pinned by Planar Defects", Phys. Rev. Lett. **101**, 267005 (2008).
 3. A. Petković, T. Emig and T. Nattermann, "Pinning of Flux Lines by Planar Defects", Phys. Rev. B **79**, 224512 (2009).
-

Curriculum vitae

Personal data

Date of birth 21. February 1981
Place of birth Kragujevac, Serbia
Nationality Serbian
Marital status Single

Education

- 1988–1996** Elementary school, Kragujevac, Serbia.
GPA: 5.00 (out of 5)
The best student in generation.
- 1996–2000** Gymnasium, Kragujevac, Serbia.
GPA: 5.00 (out of 5)
The best student in generation.
- 2000–2005** Undergraduate studies, section Theoretical and Experimental Physics, Faculty of Physics, University of Belgrade, Belgrade, Serbia.
GPA:10.00 (out of 10)
Valedictorian.
- Diploma thesis: Spin configurations of quantum dot in high magnetic field. Thesis advisor: Prof. Milica Milovanović.
- 2006–2009** Doctoral studies, Institute of Theoretical Physics, University of Cologne, Cologne, Germany.

Significant awards and scholarships

- 2006** Award from the Government of Republic of Serbia for 100 best postgraduate Serbian students studying abroad.
Amount: 15000 Euro (declined).
-

- 2005** Award "Ljubomir Ćirković" for **the best diploma thesis** at the Faculty of Physics, Belgrade.
- 2005** **Student of generation** at the Faculty of Physics, award from the University of Belgrade.
- 2002–2005** Scholarship from the Serbian Republic Foundation for Development of Scientific and Art Youth.
- 2003** Royal Norwegian Government Award for one of 500 best students in Serbia.
- 1994–2000** Numerous awards at Federal and Republic level student competitions in physics (problem solving) including four first prizes.

Employment and summer schools

- Oct 2009–** Argonne National Laboratory, Argonne, USA.
- 2006–Sep 2009** Institute of Theoretical Physics, University of Cologne, Germany.
- July 2008** The Boulder School in Condensed Matter and Materials Physics: Strongly Correlated Materials.
- Aug 2004** Exchange Student, Department of Applied Physics, University of Ghent, Ghent, Belgium.
- Aug–Sep 2003** Summer student, Hahn-Meitner Institute, Berlin, Germany.

Publications from the diploma thesis

1. A. Petković and M.V. Milovanović, "Fractionalization into Merons in Quantum Dots", Phys. Rev. Lett. **98**, 066808 (2007).
-